Understanding loss of consciousness under general anaesthesia using multimodal neuroimaging

Jostein Holmgren

Keble College

University of Oxford

A thesis submitted for the degree of

Doctor of Philosophy

Michaelmas 2021

for Mum & Dad

Acknowledgements

I have sometimes likened my experience doing a DPhil to climbing a mountain. It has been an exciting and wondrous journey to the peak, but along the way there have been setbacks and steep climbs where the end goal seemed unreachable. I am very fortunate that I did not have to climb this mountain alone.

First and foremost, I would like to thank Katie Warnaby. As my supervisor, she has been an inspiration and a guidance throughout my DPhil. Without her experience, tenacity, and know-how this thesis would never have seen the light of day. Under her wings, I have grown, as an academic and as a human being. I thank her for her encouragement when I was discouraged and her instruction when I was uninformed. Above all, I thank her for being kind when I needed it most.

I owe a debt of gratitude to Saad Jbabdi, who has generously and freely given much of his time and expertise so that I could learn. I never thought myself as much of an engineering type before he showed me the way. I am immensely thankful to Irene Tracey, who somehow found time between running first a department, then a college to give me valuable inspiration and feedback. She helped me see the value in my work when I could only see the flaws.

As I have progressed through my DPhil, I have seen the Anaesthesia Neuroimaging Group grow from being a duo of Katie and me into a thriving and stimulating research group. Lara Prisco working with you has been a joy. Without your enthusiasm, my DPhil would have been a sorry affair. After all, I could not

have collected such an exciting dataset for my project without you to deliver the anaesthetic. Marco Fabus, James Wilsenach, Di Zang, and Minh Tran, thank you all for valuable feedback and inspiring discussions.

Finally, I owe the world to my family and friends. My parents, Anne and Tor, and my siblings, Rune and Faiza, are the foundation that I could grow from. The curiosity and drive that led me to embark on my DPhil can inevitably is traced back to them. I thank my friends in Oxford and elsewhere, that I am fortunate are too numerous to list, for the continuous love, support, and banter. I am eternally grateful to Aisling, who has stood by me and brought me light and joy through some of the darkest moments of this endeavour.

Abstract

Despite major advancements in consciousness science over the past few decades, how anaesthesia causes loss of consciousness remains incompletely understood and the translation from basic science to clinical practice has been limited. Recent concurrent electroencephalography (EEG) and functional magnetic resonance imaging (FMRI) evidence indicates that a state of complete perception loss is achieved under general anaesthesia when slow wave activity in the brain reaches saturation. Slow wave activity saturation (SWAS) is therefore a potentially clinically relevant end point for titration of anaesthesia.

We have developed a prototype system for titrating anaesthesia to SWAS within an individual. The system features EEG and anaesthesia data input, modelling of slow wave power and detection of SWAS, and visualisation of the model output in a graphical user interface. The prototype system was applied in a patient pre-surgery study (Study 1) which focused on clinical translation of SWAS, and a healthy volunteer EEG-MRI study (Study 2) which focused on experimental validation of SWAS.

We successfully applied the prototype SWAS system in twelve patients (Study 1) and twenty-three healthy volunteers (Study 2). No subjects in either Study 1 or Study 2 were behaviourally responsive when held at SWAS and none had recall of events from when they were held at SWAS.

In Study 2, we also acquired measures of cerebral blood flow (CBF), and resting and task-related FMRI data during wakefulness and when held at SWAS. When held at the SWAS state, CBF was significantly elevated compared to wakefulness. Furthermore, we found that the brain was unresponsive to external stimulation when held at SWAS even when controlling for the observed CBF changes. Finally, we found that this was accompanied by disruption of functional connectivity in the thalamocortical system and in known resting state networks. Our findings provide further evidence that SWAS is a state of perception loss and a clinically relevant target for surgical anaesthesia.

Table of Contents

1 Introduction 1

1.1 Current clinical practice 2

1.2 Pharmacological properties of anaesthesia 4

1.3 Spectral changes during general anaesthesia 5

1.4 Slow wave activity saturation 8

1.5 Clinical translation of SWAS 9

1.6 Overview of chapters 11

2 Development of the prototype SWAS system 14

2.1 Introduction 14

2.2 Overview of the prototype system and its application 17

2.2.1 Real time data input 19

2.2.2 SWAS real-time detection model 22

2.2.3 Graphical user interface (GUI) 27

2.2.4 Additional system features 29

2.3 Discussion and future directions 31

3 Real-time titration to SWAS in practice 35

3.1 Introduction 35

3.1.1 Predicting anaesthesia requirement to SWAS 38

3.2 Methods 41

3.2.1 Ethical approval 41

3.2.2 Study 1 41
3.2.3 Study 2 46
3.2.4 Data analysis 51
3.3 Results 54
3.3.1 Study 1 54
3.3.2 Study 2 59
3.3.3 Factors predicting susceptibility to anaesthesia 65
3.4 Discussion 67
3.4.1 Time to achieve SWAS 67
3.4.2 Accuracy of SWAS titration 68
3.4.3 Lack of behavioural responsiveness at SWAS 70
3.4.4 Relationship between responsiveness and SWAS 73
3.4.5 Susceptibility to anaesthesia 73
3.4.6 Informing SWAS model initiation for real-time operation 74
4 Altered cerebral blood flow at SWAS 77
4.1 Introduction 77
4.2 Materials and methods 79
4.2.1 Data acquisition 79
4.2.2 Data analysis 81
4.2.3 Statistical testing 84
4.3 Results 85
4.3.1 Changes in cerebral CBF with sevoflurane anaesthesia 86
4.3.2 Relationship between cerebral CBF and EEG power 90
4.4 Discussion 90

5 Disruption of pain- and auditory processing at SWAS 99

5.1 Introduction 99

5.2 Methods 102

5.2.1 MRI data acquisition 103

5.2.2 Pain stimulation and modified isolated forearm paradigm 103

5.2.3 Physiological data acquisition 105

5.2.4 Pre-processing of BOLD-FMRI data 106

5.2.5 Whole-brain task FMRI analysis 107

5.2.6 Task FMRI region of interest analysis 108

5.2.7 Heart rate variability analysis 109

5.3 Results 110

5.3.1 Pain- and IFT-evoked brain activity disrupted at SWAS 110

5.3.2 Heart rate variability reduced at SWAS 115

5.4 Discussion 116

5.4.1 Altered CBF cannot explain lack of stimulus-evoked BOLD response 117

5.4.2 Negative stimulus-evoked BOLD responses are absent at SWAS 119

5.4.3 Disruption of pain and auditory processing under general anaesthesia 119

5.4.4 Inconclusive results on pain-evoked HRV changes 123

6 Breakdown of large-scale brain networks at SWAS 125

6.1 Introduction 125

6.1.1 Anaesthetic effects on thalamocortical connectivity 125

6.1.2 Anaesthetic effects on connectivity in large-scale brain networks 126

6.2 Methods 128

6.2.1 Data acquisition 128

6.2.2 Resting state FMRI preprocessing 129
6.2.3 Thalamocortical functional connectivity analysis 130
6.2.4 Within-network functional connectivity analysis 133
6.3 Results 134
6.3.1 Thalamocortical connectivity at SWAS 134
6.3.2 Within-network connectivity at SWAS 135
6.4 Discussion 138
6.4.1 Thalamocortical connectivity at SWAS 138
6.4.2 Higher order network connectivity at SWAS 139
6.4.3 Visual, auditory, and sensorimotor network connectivity at SWAS 142
6.4.4 Thalamus connectivity to default mode and sensory motor networks 144
7 Concluding remarks 146
8 Bibliography 151

List of Abbreviations

A2	Secondary auditory cortex
ACC	Anterior cingulate cortex
AEPs	Auditory evoked potentials
AP	Anterior-posterior
APAIS	Amsterdam Preoperative Anxiety and Information Scale
ASA	American Society of Anesthesiology
ASL	Arterial Spin Labelling
BASIL	Bayesian Inference for Arterial Spin Labeling MRI
BIS	Bispectral Index
BOLD	Blood Oxygen Level Dependent
CBF	Cerebral blood flow
CHEPs	Contact heat evoked potentials
CI	Confidence interval
CO_2	Carbon dioxide
COG	Centre of gravity
DC	Direct current
dwMRI	Diffusion-weighted MRI
ECG	Electrocardiogram
EEG	Electroencephalography
EPI	Echo-planar imaging
ESSS	Embodied sense of self scale
ET	End-tidal
FEAT	FMRIB's Expert Analysis Tool
FIRST	FMRIB's Integrated Registration and Segmentation Tool
FLAME	FMRIB's Local Analysis of Mixed Effects
FLIRT	FMRIB's Linear Image Registration Tool
FMRI	Functional Magnetic Resonance Imaging
FNIRT	FMRIB's Non-linear Image Registration Tool
FOV	Field of view
FSL	FMRIB Software Library
FWHM	Full-width half-maximum
$GABA_A$	Gamma-aminobutyric acid type A
GLM	General linear model
GUI	Graphical user interface
GWH	Global workspace hypothesis
HRF	Haemodynamic response function
HRV	Heart rate variability
ICA	Independent component analysis
IFT	Isolated forearm test
IIT	Integrated information theory
IQR	Inter-quartile range
ISI	Inter-stimulus interval

LOBR	Loss of behavioural responsiveness
LOC	Locus of control
MAC	Minimum alveolar concentration
MAPE	Mean absolute percentage error
MCFLIRT	Motion Correction using FMRIB's Linear Image Registration Tool
MELODIC	Multivariate Exploratory Linear Optimized Decomposition into Independent Components
MH	Metropolis-Hastings
MHLC	Multidimensional Health Locus of Control
MNI	Montreal
MRI	Magnetic resonance imaging
MRS	Magnetic resonance spectroscopy
NHS	National Health Service
NIRS	Near-infrared spectroscopy
NMDA	N-methyl-D-aspartate
NuDESC	Nursing Delirium Scale
O_2	Oxygen
OUH	Oxford University Hospitals
PA	Posterior-to-anterior
PAC	Primary auditory cortex
PASL	Pulsed arterial spin labelling
pcASL	Pseudo-continuous arterial spin labelling
PD/PK	Pharmacodynamic/pharmacokinetic
PET	Positron Emission Topography
PNM	Physiological noise modelling
PSQI	Pittsburgh Sleep Quality Index
RDA	Remote Database Access
REM	Rapid eye movement
RMSSD	Root mean squared successive differences
ROI	Region of interest
rsFMRI	Resting state FMRI
S1	Primary somatosensory cortex
S2	Secondary somatosensory cortex
SCA	Seed-based connectivity analysis
SD	Standard deviation
STAI	State and Trait Anxiety Index
SWAS	Slow wave activity saturation
TAS	Tellegen Absorption Scale
TCD	Transcranial Doppler flowmetry
TCP	Transmission Control Protocol
TE	Echo time
TFCE	Threshold-free cluster-enhancement
TIVA	Total intravenous anaesthesia
TR	Repetition time
Xe113	Xenon113

List of Figures

Figure 2.1 Schematic of the prototype SWAS system

Figure 2.2 Flow chart of real-time SWAS model operations

Figure 2.3 Illustration of SWAS sigmoid function

Figure 2.4 Main SWAS prototype system GUI

Figure 2.5 SWAS prototype system initiation menu

Figure 2.6 SWAS prototype system settings menu

Figure 3.1 Overview of Study 2 procedures

Figure 3.2 Study 1 offline SWAS sigmoid curve fits

Figure 3.3 Study 1 SWAS sigmoid parameter variability

Figure 3.4 Example EEG spectrogram of Study 2 anaesthesia session

Figure 3.5 Study 2 offline SWAS sigmoid curve fits

Figure 3.6 Interindividual variability in C_{LOBR} and C_{SWAS} in Study 2

Figure 3.7 Study 2 SWAS sigmoid parameter variability

Figure 3.8 Bland-Altman and MAPE analysis of Study 2 titration accuracy

Figure 3.9 Study 1 correlation between age and slow wave power at SWAS

Figure 4.1 Schematic of the novel EEG compatible PASL sequence

Figure 4.2 Mean absolute CBF for the room air, O_2, and SWAS conditions

Figure 4.3 Alterations in CBF due to sevoflurane and oxygen delivery

Figure 4.4 Regional % increases in grey matter CBF due to sevoflurane

Figure 4.5 End-tidal CO_2 changes and their relationship with CBF

Figure 4.6 Relationship between CBF and slow wave power at SWAS

Figure 5.1 Flow chart of task FMRI stimulation paradigm

Figure 5.2 Stimulus-evoked brain activity when awake and at SWAS

Figure 5.3 Overlap between awake negative BOLD and SWAS > awake

Figure 5.4 ROI stimulus-locked BOLD percent signal change

Figure 5.5 Effects of sevoflurane on HR and HRV during pain stimulation

Figure 6.1 Flow chart of thalamocortical functional connectivity analysis pipeline

Figure 6.2 Thalamocortical functional connectivity at SWAS vs. awake

Figure 6.3 Group ICA resting state networks used for within-network analyses

Figure 6.4 Within-network functional connectivity changes at SWAS vs. awake

1 Introduction

Consciousness is intimately familiar to everyone, yet simultaneously it is a mysterious phenomenon that has eluded scientific explanation. How physical matter can give rise to rich, subjective experience has intrigued philosophers and scientists for centuries. However, it is only in the past few decades that a science of consciousness has emerged (Mashour & Hudetz, 2018; Seth, 2010).

This modern scientific pursuit of consciousness has yielded a common framework for approaching the problem of objectively studying this inherently subjective phenomenon. A distinction now exists between the so-called “hard problems” of why and how conscious experience can arise from physical matter and the “easy problems” that can be approached using conventional neuroscientific research methods where phenomena can be explained through computational or neural mechanisms (Chalmers, 1995). The hard problems remain elusive, but much progress has been made in addressing a range of “easy” problems.

Over the past thirty years, formal theories of consciousness have been formulated in an effort to the provide frameworks for investigating consciousness and generate testable hypotheses. Two leading theories of consciousness are Integrated Information Theory (IIT) (Tononi, 2004, 2012; Tononi et al., 2016) and the Global Workspace Hypothesis (GWH) (Baars, 1997, 2005). The IIT takes phenomenological subjective experience as a starting point to propose a set of

axioms that testable hypotheses about consciousness can be derived from. In contrast, the GWH frames consciousness in terms of a cognitive architecture comprised of a set of parallel, specialised processes or resources (e.g., sensory processes, memories, etc.) that are unconscious unless and until they are integrated in working memory.

1.1 Current clinical practice

The science of consciousness has important implications for humane care in modern medicine. Whether preventing the agony of surgery or optimising care for disorders of consciousness patients, the patient's subjective phenomenological experience is a vitally important factor that remains exceedingly difficult to measure. Despite the progress that has been made in the scientific understanding of consciousness, the translation of our improved understanding to clinical practice has been slow.

As hundreds of thousands of anaesthetics are administered worldwide each day (Pandit et al., 2014), consciousness science has wide-ranging potential to inform and improve care. Surgical anaesthesia aims to achieve three main goals, often called the triad of anaesthesia, which are the prevention of awareness, prevention of pain, and prevention of voluntary and reflexive movement (Rees & Gray, 1950). These goals are achieved through the administration of a hypnotic agent, an analgesic agent, and muscle relaxants, respectively.

There is considerable heterogeneity in modern anaesthetic practice, with procedures varying between patient characteristics, types of surgeries, individual

hospital policies, and anaesthetist preferences. In general, clinical anaesthesia goes through three phases: induction, maintenance, and recovery. During induction, the patient is rendered unconscious by the anaesthetic drug and prepared for the surgery, including the management of airways. Anaesthetic maintenance refers to the ongoing management of the anaesthetic agent during the surgical procedures. Finally, recovery refers to the process of halting the anaesthetic delivery and allowing the patient to wake after the end of surgery.

Despite the brain being the site of consciousness, only a small minority of surgeries are performed with any type of brain-based monitoring. In the United Kingdom, brain-based depth of anaesthesia monitors were only used in 2.8% of general anaesthetics (Pandit et al., 2014). Instead, the majority of surgeries rely on drug dosing based on population-calibrated dose-response models and monitoring of non-brain vital signs to prevent awareness.

Under-dosing of anaesthesia can result in the patient not being rendered fully unaware of the surgical procedures, including perceiving painful surgical stimulation. Accidental intra-operative awareness is very likely to result in long-term psychological disorder such as post-traumatic stress disorder (Leslie, Chan, et al., 2010). Anaesthetists commonly administer elevated anaesthetic doses to ensure loss of awareness, and consequently the incidences of intra-operative awareness with recall are relatively low. However, there has been increased acknowledgement of the risks of adverse effects associated with over-anaesthesia, particularly in vulnerable patient groups such as neonates and

elderly (Leslie, Myles, et al., 2010; Monk et al., 2005; Sessler et al., 2012). These include elevated risk of prolonged recovery, post-operative delirium in the immediate post-operative recovery period, and long-term effects on cognitive abilities.

1.2 Pharmacological properties of anaesthesia

Remarkably, general anaesthesia can be achieved with a wide range of pharmacological agents that vary considerably in their molecular properties and how they interact with the brain. On the molecular level, anaesthetic agents can be classified according to which receptors they bind to in the brain (Franks, 2008). Broadly speaking, there are two receptor sites that most commonly used anaesthetic agents have affinity for: γ-aminobutyric acid type A ($GABA_A$) and N-methyl-D-aspartate (NMDA) receptors. $GABA_A$-ergic anaesthetic agents include propofol and the ether-derivatives sevoflurane, isoflurane, and desflurane (Garcia et al., 2010). Ketamine, nitrous oxide, and xenon are NMDA antagonists (Franks et al., 1998; Jevtović-Todorović et al., 1998; MacDonald et al., 1987). There are also examples of hypnotic agents outside these two groups, for example the α2-adrenergic receptor agonist dexmedetomidine (Bloor et al., 1992).

Another property by which anaesthetic agents are categorised according to is their mode of delivery. For example, whether the agent is delivered intravenously or vaporized into an inhaled gas mixture. Intravenous hypnotic agents include propofol, dexmedetomidine, and ketamine. Inhalational anaesthetics, also known as volatile anaesthetics, include sevoflurane, isoflurane, and desflurane, nitrous

oxide, and xenon. In clinical practice, it is common to use an intravenous agent for the induction phase and use a volatile anaesthetic for anaesthetic maintenance. Using an intravenous anaesthetic for both induction and maintenance, a practice known as total intravenous anaesthesia (TIVA) is also frequently used. Finally, anaesthetic induction with volatile agents can be performed, although patient tolerance of the anaesthetic can vary.

Considerable and important research on the pharmacological properties of different anaesthetic agents has been performed over the past several decades, demonstrating the existence of multiple modes of anaesthetic action (Franks, 2008). This has enabled the development of novel anaesthetic agents that are suitable for different clinical purposes and contribute to the relative safety of modern surgical anaesthesia (Brown et al., 2018). However, this general line of research has not alone been able to explain how such a diverse group of pharmacological agents have the common effect of disrupting connected consciousness (Brown et al., 2011; Mashour & Hudetz, 2018).

1.3 Spectral changes during general anaesthesia

More recently, the focus has shifted to electrophysiological and neuroimaging approaches to investigate anaesthetic action on large-scale brain networks (Mashour & Hudetz, 2018). The brain transfers information via electrical signals that, on aggregate, are detectable non-invasively on the scalp using electroencephalography (EEG). During induction to general anaesthesia, neuronal firing patterns are profoundly altered compared to wakefulness (Purdon, Sampson,

et al., 2015). The spectral characteristics of anaesthetic agents commonly used in clinical anaesthesia have been well described in several studies. During induction to propofol anaesthesia, the spectral content changes in multiple frequency bands, including increases in power in the beta (15-30Hz), theta (4-8Hz), and gamma (>30Hz) bands, whereas at higher doses the most dominant increases in power are in the alpha (8-15Hz) and slow wave (0.5-1.5Hz) frequency bands (Mhuircheartaigh et al., 2013; Purdon et al., 2013; Purdon, Sampson, et al., 2015). Sevoflurane anaesthesia is characterised by decreases in beta and gamma bands and increases in slow and alpha bands, with increasing theta activity at high doses (Akeju et al., 2014; Purdon, Sampson, et al., 2015). Isoflurane and desflurane have been found to have similar spectral characteristics as sevoflurane (Purdon, Sampson, et al., 2015). Finally, dexmedetomidine is characterised by activity in the slow wave and alpha frequencies (Purdon, Sampson, et al., 2015).

Several anaesthetic agents, including propofol, sevoflurane, and dexmedetomidine, have been found to cause short bursts (1-2 seconds) of oscillations in a narrow frequency range in the alpha band (Akeju et al., 2014; Huupponen et al., 2008). These are sometimes called spindles due to their similarity to alpha spindles commonly observed in EEG of sleep (Sleigh et al., 2011).

Among the most consistent spectral change observed across most anaesthetic agents is a strong increase in the slow wave (0.5-1.5Hz) frequency band at clinically relevant concentrations. This observation has received considerable

research attention because slow waves are a common feature of a range of states of unconsciousness, including slow wave sleep (Brown et al., 2010; Franks, 2008; Murphy et al., 2011) and disorders of consciousness (Husain, 2006; Kaplan, 2004; Sutter & Kaplan, 2012).

The neurophysiological generators of slow waves have been well characterised on the single neuron level. Under general anaesthesia, thalamic and cortical neurons oscillate between an “on state” of neuronal activity and an “off state” of neuronal silence at a rate of approximately 1 Hz (Steriade, Nuñez, et al., 1993). Slow waves can persist after thalamic and callosal lesions (Steriade, Nuiiez, et al., 1993), be expressed in deafferented cortical slabs (Timofeev et al., 2000), and in *in vitro* cortical slice preparations (Sanchez-Vives & McCormick, 2000), suggesting that the slow waves can be generated in the cortex without sub-cortical input. However, *in vivo* the thalamus likely plays an important role in the slow oscillation, particularly in initiating up states and determining the oscillatory period (Neske, 2016). Crucially, slow waves measured on the scalp represent large neuronal populations synchronously oscillating between the on and off states. Slow waves have been found to propagate across the cortex, most prominently in an anterior to posterior direction (Massimini et al., 2004).

A common feature of both the IIT and the GWH is that they predict that unconscious states are characterised by low levels of integration of neuronal signals from different cortical regions (Baars, 2005; Tononi et al., 2016). Slow waves provide a potential mechanistic explanation for how such disruption of

integration could occur under general anaesthesia. If consciousness is supported by the propagation of complex neuronal signals in diverse networks of brain regions, the neuronal silence during the “off state” of the slow oscillation might prevent this propagation from occurring (Pigorini et al., 2015).

1.4 Slow wave activity saturation

Previously, using an ultra-slow induction to propofol anaesthesia (48 min duration), our lab discovered that the increase in slow wave power reached saturation prior to peak anaesthetic dose (Mhuircheartaigh et al., 2013). Importantly, this slow wave activity saturation (SWAS) occurred at higher propofol concentrations than loss of responsiveness. Moreover, they found that slow wave power at SWAS was correlated with frontal grey matter volume. This indicates that with increasing dose of anaesthesia, there is an increased recruitment of cortical neurons to the slow oscillation. This further implies that the maximal recruitment of cortical neurons occurs at SWAS, and any further anaesthesia delivered past this point has no additional benefit.

Simultaneous EEG and functional magnetic imaging (FMRI) recordings revealed that, while reduced, pain- and auditory-evoked responses in primary sensory cortices and the thalamus persisted past loss of responsiveness. At propofol concentrations at and in excess of SWAS, however, stimulus-evoked brain activation in primary sensory and thalamic regions was significantly reduced. This was argued to indicate that the thalamocortical system had become isolated from external sensory stimulation at SWAS and that SWAS might be a state of

perception loss under general anaesthesia. Importantly, stimulus-evoked activation persisted in a set of cortical regions including in the precuneus, parietal, and prefrontal regions. Mhuircheartaigh et al., (2013) suggested this might represent a basic mode of brain funcitoning and indicate that SWAS is a state of perception loss under general anaesthesia.

While conscious processing of sensory information may be disrupted in the SWAS state, this does not necessarily preclude unconscious processing that may have lasting effects after return to consciousness. Pain chronification is known to be affected by both peripheral sensitisation, i.e., increased sensitivity of nociceptive primary sensory neuros, and central sensitisation, i.e., increased sensitivity to pain in the central nervous system (Pak et al., 2018; Woolf & Chong, 1993). It is possible that unconscious nociceptive and pain processing in peripheral nerves and the central nervous system during surgical procedures is related to the development of post-operative pain chronification through peripheral and central sensitisation (Pak et al., 2018). Therefore, if SWAS indeed is a state of complete loss of conscious perception of external stimulation, co-administration of analgesics will nevertheless remain a vital component of the anaesthetic care.

1.5 Clinical translation of SWAS

In order for SWAS to be a viable endpoint for clinical anaesthesia, it must occur and be detectable in less controlled clinical environments. Since its initial discovery, SWAS has been parameterised by fitting a parametric sigmoid curve to single-channel slow wave power (in EEG recorded during anaesthetic induction)

as a function of anaesthetic concentration (Warnaby et al., 2017). SWAS was formally defined as the slow wave power (P_{SWAS}) and anaesthetic concentration (C_{SWAS}) that corresponded to 95% of the posterior distribution of slow wave activity around the slow wave plateau. The formal mathematical definition is discussed in more detail in Chapter 2 (Section 2.2.2.3). Applying this post-hoc model, SWAS has been identified in both propofol and sevoflurane anaesthesia, and during induction and emergence. SWAS was identified in 92% of 393 individual EEG datasets from both experimental and clinical inductions to anaesthesia. Failed fits were primarily attributable to artefacts, as some individuals who did not receive a sufficiently high dose to achieve SWAS. Importantly, these datasets were not acquired for the purpose of modelling SWAS. The high success rate yields considerable confidence that SWAS can be reliably detected even in datasets acquired in noisy, clinical environments.

Importantly, SWAS was also identified in the clinical anaesthesia datasets where co-induction agents including opioids and neuromuscular blockers were used. Interestingly, co-administration of opioids potentiated the anaesthetic action and reduced the concentration of the anaesthetic agent required to achieve SWAS, without affecting the slow wave power at SWAS. Meanwhile, presence of neuromuscular blockers did not affect either the concentration required to achieve SWAS or the slow wave power at SWAS. This indicates that SWAS as a clinical target for anaesthesia titration is robust to interactions with other drugs forming the triad of anaesthesia.

These foundational studies of SWAS indicate that SWAS has great potential, both as a phenomenon that can help expand our understanding of anaesthesia-induced loss of consciousness and as a clinical target for titration of anaesthesia. Nevertheless, key challenges and questions remain to be addressed regarding SWAS. First and foremost, as previous investigations of SWAS did not target the SWAS state specifically, it is currently unknown whether it is feasible to titrate anaesthesia to the SWAS end point. Furthermore, is remains an open question whether the thalamocortical isolation observed at propofol concentrations at and in excess of SWAS can be demonstrated in individuals held at the SWAS endpoint, and whether this holds true for other anaesthetic agents. The primary aim of this thesis is therefore to expand on the foundational investigations of SWAS with a view of improving our understanding of anaesthesia-induced loss of consciousness and moving towards the clinical translation of SWAS to optimise anaesthetic dosing.

1.6 Overview of chapters

In order to investigate the SWAS brain state, it is crucial to be able to titrate anaesthesia for a particular individual to their SWAS end point. In Chapter 2, I describe the design and development of such a prototype system for titrating anaesthesia to the SWAS endpoint in an individual.

In Chapter 3, I describe the application of the SWAS prototype system in a pre-surgery study in a patient population, and a laboratory EEG-MRI study in healthy volunteers. The pre-surgery study was more focused on the clinical translation of

the prototype SWAS depth of anaesthesia monitor. It also allowed a number of practical teething problems to be solved before the prototype system was applied in the EEG-MRI study in healthy volunteers. The latter study allowed a more thorough investigation of the SWAS endpoint using multiple MRI modalities, including arterial spin labelling (ASL) and FMRI acquired during rest and task activity. These will be discussed in subsequent chapters.

Anaesthetic agents are known to influence cerebral blood flow (CBF), but this is rarely measured and incorporated in FMRI studies of anaesthetic effects on neuronal processes. This is problematic because the FMRI signal is derived from changes in blood oxygenation, and therefore effects of the anaesthetic agent on CBF could confound FMRI analyses. As part of the neuroimaging acquisitions in Study 2, we measured CBF when subjects were awake breathing room air, breathing oxygen, and when anaesthetised and held at the SWAS end point. The results from statistically comparing CBF in each condition are reported in Chapter 4.

A primary goal of surgical anaesthesia is rendering patients unaware of the surgical stimulation and the external world more generally. It is therefore crucial for the clinical usefulness of SWAS to demonstrate that individuals held at the SWAS end point are disconnected from the external world. In Chapter 5, I will report analyses of pain and auditory-evoked brain responses at SWAS and discuss the implications for SWAS as a state of perception loss under general anaesthesia.

Leading theories of consciousness suggest that consciousness may be supported by interconnected brain networks including the thalamocortical system and large-scale cortical networks. In Chapter 6, I will report analyses of functional connectivity within the thalamocortical system and known cortical networks from resting state FMRI data acquired when subjects were awake and held at SWAS.

In the final chapter, the results from the preceding chapters are considered as a whole in the context of current literature on anaesthesia-induced unconsciousness, as well as overarching theories of consciousness. The implication of the results for clinical anaesthesia are discussed.

2 Development of the prototype SWAS system

2.1 Introduction

EEG-based depth of anaesthesia monitoring is only used in about 2.8% of general anaesthetics delivered in the UK (Pandit et al., 2014). There are several commercially available EEG based depth of anaesthesia monitors, including Bispectral Index (BIS; Covidien, Mansfield, MA, USA), E-Entropy module (GE Healthcare, Medical Diagnostics, Amersham, UK), NeuroSENSE (NeuroWave B.V., Amsterdam, The Netherlands), and Narcotrend monitor (MonitorTechnik, Bad Bramstedt, Germany). While the specifics of how each system operates varies considerably, all of these systems attempt to quantify depth of anaesthesia using quantitative EEG measures that identify reductions in the power of high frequency oscillations and increases in the power of lower frequencies (Voss & Sleigh, 2007). These systems typically quantify anaesthetic depth on a numerical scale (BIS, E-Entropy, and NeuroSENSE) or in stages (Narcotrend), with a recommended range of values or stages to ensure loss of awareness during general anaesthesia. For instance, the BIS ranges from 100, indicating wakefulness, to 0, indicating absence of brain activity, with a recommended range of 40 to 60 for surgery (Avidan et al., 2011; Myles et al., 2004). However, systematic reviews indicate that current brain-based monitoring systems are no more effective in preventing accidental awareness than conventional vital signs monitoring (Ag et al., 2016; Shepherd et al., 2013). Moreover, current depth of anaesthesia monitors rely on population-based calibration as opposed to

individualised measures (Rampil, 1998), which inherently introduces some error when they are applied to individual patients.

By contrast, as introduced in Chapter 1 (Section 1.4), early evidence indicates that SWAS has direct neurophysiological underpinnings and can be identified within an individual without reliance on population-calibration. Therefore, SWAS is potentially an individualised measure of depth of anaesthesia (Mhuircheartaigh et al., 2013; Warnaby et al., 2017). Several factors suggest that SWAS is a viable clinical target for titration of anaesthesia. SWAS has been identified for several intravenous and volatile anaesthetic agents (Warnaby et al., 2017). Moreover, SWAS has been identified in data recorded during routine clinical anaesthesia in the presence of co-administered opioids and neuromuscular blockers (Warnaby et al., 2017).

Beyond clinical applications, SWAS also has promise as a target for titration of anaesthesia in research. Many studies target a pre-defined concentration of anaesthesia that is the same for all participants (e.g. Huang et al., 2016; Mhuircheartaigh et al., 2013; Palanca et al., 2015). However, since susceptibility to anaesthesia differs considerably between individuals, this approach inevitably leads to different participants being taken to different brain states under general anaesthesia. Other studies on anaesthesia rely on loss of a behavioural marker such as loss of responsiveness (e.g. Blain-Moraes et al., 2015; Huang et al., 2018; Jordan et al., 2013). While this approach does target a common brain state, loss of responsiveness does not necessarily imply loss of consciousness (Sanders et al.,

2012). Finally, some studies use commercial depth of anaesthesia monitors in an attempt to standardise anaesthetic depth (e.g. Conti et al., 2006; Law et al., 2014; Mirkheshti et al., 2020). However, as in clinical applications, this approach is limited by the inherent error introduced by relying on population calibration to infer depth of anaesthesia in an individual. SWAS overcomes these shortcomings by being a marker of a specific brain state under deep general anaesthesia that is identifiable on an individual basis.

However, titrating anaesthesia to the SWAS endpoint is not a trivial undertaking. Unlike existing commercial depth of anaesthesia monitors that rely on processing of the EEG signal alone, SWAS by definition requires identification of a plateau in slow wave power as a function of concentration (Warnaby et al., 2017). Therefore, when titrating to SWAS in an individual, one needs to track changes in slow wave power and anaesthetic concentration during the induction period. The concentration of volatile anaesthetics can be measured as an end-tidal concentration, with the caveat that the concentration in the brain will be delayed compared to the concentration measured in the lungs. In the case of intravenous anaesthetics, the concentration in the brain (i.e. the effect site concentration) is estimated using pharmacodynamic/pharmacokinetic (PD/PK) modelling (Kiang et al., 2012).

There are a number of additional challenges in the application of SWAS to clinical practice. Firstly, clinical practice often involves a mixture of anaesthetic agents, such as using propofol for induction of anaesthesia and a volatile anaesthetic for

maintenance. Additionally, opioids that are commonly co-administered as part of the triad of anaesthesia are known to potentiate anaesthetic action, effectively reducing the hypnotic concentration required to achieve SWAS (Warnaby et al., 2017). Accounting for the inputs of a variety of different anaesthetic agents and also the time-varying synergistic interaction of opioids is a key challenge in the development of a SWAS-based depth of anaesthesia monitor. Finally, there is also some early evidence that after reaching SWAS, slow wave power gradually decreases over time despite the anaesthetic concentration being kept constant (Warnaby et al., 2017), which could poses challenges for tracking SWAS during maintenance of anaesthesia.

The initial prototype system was developed to be suitable for later application in the pre-surgery and EEG-MRI studies. To that end, I reduced the scope of this initial prototype system to allow induction and maintenance of anaesthesia at SWAS using a single hypnotic agent without co-administration of opioids. However, crucially, the prototype system was developed with view to these future scenarios, so that subsequent development of the SWAS system can build on this initial prototype.

2.2 Overview of the prototype system and its application

The prototype system has dedicated hardware for acquiring EEG and anaesthesia concentration data and software for modelling SWAS in near real time (Figure 2.1). The prototype software was implemented in Matlab 2018a (The MathWorks Inc., USA). It consists of 1) a module for real-time sampling of EEG and

anaesthesia monitor data, 2) a mathematical model for tracking slow wave power as a function of concentration and detection of saturation, and 3) a graphical user interface (GUI) for visualising input data and the SWAS model output. Two different prototype systems have been developed that use either the 24-channel TMSi Porti 7 (Twente Medical Systems International B.V., The Netherlands) or the 32-channel BrainAmp MRplus (BrainVision GmbH, Germany) EEG systems. These systems were implemented in the pre-surgery patient and the EEG-MRI healthy volunteer studies respectively.

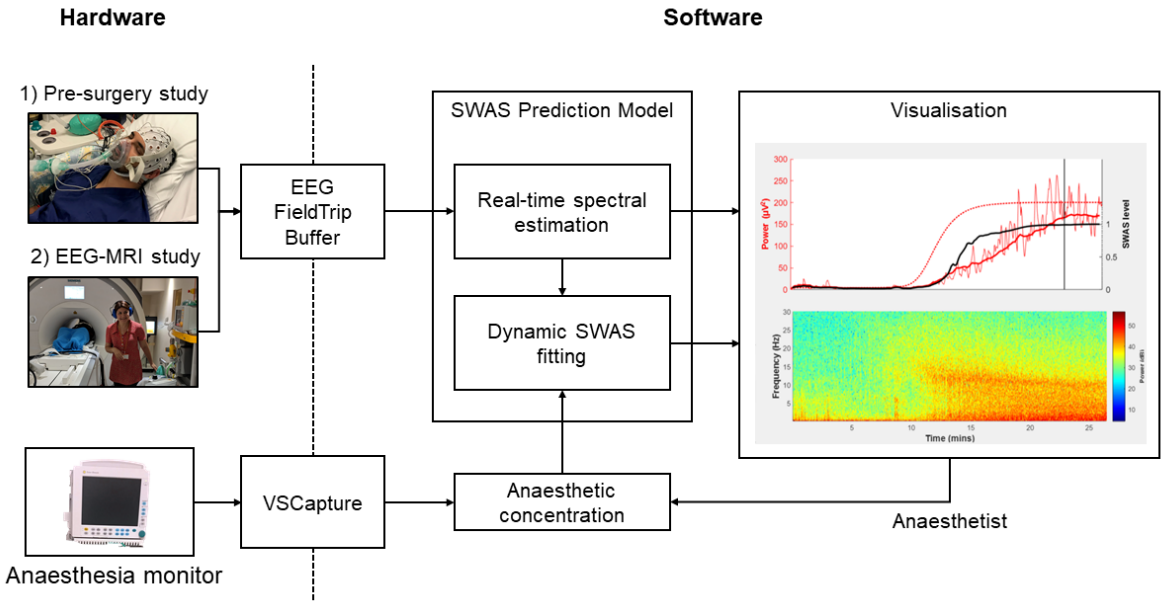

Figure 2.1: Schematic of the prototype SWAS system. Data from two separate EEG hardware systems used in each of the pre-surgery and EEG-MRI studies is interfaced with the SWAS model in software using the FieldTrip toolbox for Matlab. End-tidal anaesthesia concentration is imported from an anaesthesia monitor to the SWAS real-time model using the VSCapture software. In the case of intravenous agents, anaesthetic concentration is manually entered into the model. The prototype system then performs dynamic modelling of slow wave power as a function of concentration. Finally, EEG spectral estimates and SWAS model output is visualised.

2.2.1 Real time data input

2.2.1.1 Sampling EEG data

The FieldTrip toolbox (Oostenveld et al., 2011) was used to provide an EEG hardware-software interface for the two different EEG hardware systems. For the Porti 7 system, EEG data was read directly to Matlab using the tmsi2ft.exe FieldTrip tool. This tool interfaces with the the FieldTrip Matlab function ft_read_data.m to read data from the FieldTrip buffer into Matlab once per second. Only data that has been acquired by the EEG system since the last data read is sampled from the FieldTrip buffer. This new data segment is then appended to the stored EEG data resulting in an EEG channel $\times$ datapoints data structure. As SWAS is evaluated at a particular electrode, EEG from the Fz electrode is passed on as input to the SWAS real-time model.

When using the BrainAmp MRI-compatible MRplus EEG system to record data in the MRI scanner, some additional pre-processing was required compared to traditional EEG. EEG recorded during MRI acquisitions is affected by large artefacts caused by the switching of the magnetic gradients and from the subject's pulse moving the electrodes within the magnetic field (Allen et al., 1998, 2000). Correction of these MRI artefacts will be covered in detail in Chapter 3 (Section 3.2.3.2.1). For this use case, raw EEG data acquisition and MRI-specific pre-processing is performed on one computer and the real-time SWAS modelling is performed on a second computer to ensure that the computational load of running the real-time model does not interfere with the raw data acquisition.

The EEG data acquired at 5kHz is initially read into the BrainVision Recorder (BrainProducts GmbH, Germany) software and written to disk for offline analysis. At this point, the EEG data is also simultaneously forwarded to BrainVision RecView (BrainProducts GmbH, Germany) via the in-built Remote Database Access (RDA) protocol where the MRI artefacts are corrected in real time. After correction of the high-frequency MR gradient artefacts, data is downsampled to 500Hz to reduce the computational load in the subsequent data processing and model application.

Next, artefacts related to the subjects' pulse causing movement of the EEG artefacts within the magnetic field are detected and corrected for. At this point, the downsampled data is forwarded to the SWAS modelling computer via cross-over Ethernet cable. In software, the forwarding is performed via an RDA protocol to the FieldTrip tool rda2ft.exe and the FieldTrip buffer. The BrainAmp MRplus system can also be used as part of the SWAS prototype system outside of the MRI environment. In this case, the MRI artefact correction steps are not needed but it would still be necessary to reduce the EEG sampling rate before passing the data to FieldTrip.

When using the TMSi Porti 7 system, some system-specific pre-processing is also required in Matlab. Firstly, as the Porti 7 system does not remove any direct current (DC) offset in the signal, a DC blocking filter is applied to remove any signal offset prior to further processing. Secondly, the Porti 7 EEG signals are acquired as a common reference so are re-referenced to the Cz electrode to allow

the SWAS model to be applied at this electrode location. This is also more comparable to the FCz reference that is used by the BrainAmp MRplus system.

2.2.1.2 Sampling or manual entry anaesthesia data

Anaesthetic and other physiological data is acquired from either a Carescape B650 (General Electric Company Inc., USA) or a Datex-Ohmeda S/5 (GE Healthcare Finland Oy, Finland) anaesthesia monitor that is fitted with a gas analyser module. Data is acquired at a sampling rate of 0.2 Hz on a separate computer that is connected to the monitor via a RS232-to-USB interface. The software program VSCapture version v1.005 (Karippacheril & Ho, 2013) is used to write the inspired and expired anaesthesia data to a .csv file. VScapture also allows the real-time data acquisition of other physiological signals, including end-tidal carbon dioxide (CO_2), inspired oxygen (O_2), and respiration rate. The resulting .csv file is then read into Matlab by a custom text file import function that was automatically generated by the Matlab Import Tool.

For inhalational agents (e.g., sevoflurane, desflurane or isoflurane), end-tidal anaesthetic gas concentrations are used as input into the real-time SWAS detection model. Specifically, the model takes as input a time series of successive measurements of end-tidal concentration. A smoothed moving minimum of the measured end-tidal concentrations is calculated to eliminate spikes. The smoothed moving minimum is calculated for each time point by taking a moving minimum of ±6 seconds around the datapoint (movmin.m), then a moving maximum of ±4 seconds of that minimum (movmax.m). Finally, smoothing is applied by robust

local regression using weighted linear least squares and a 2st degree polynomial model (smooth.m).

The prototype system is also capable of accepting manually entered concentrations of intravenous anaesthetics in the form of a bolus, continuous infusion, or a combination of the two. The current version of the prototype system accepts input of propofol and ketamine intravenous anaesthetics. The input boluses of both drugs are entered as the dose in mg and continuous infusion as the dose per hour (i.e., mg/hr). The effect site concentration of the anaesthetic is then estimated through PD/PK modelling. Propofol and ketamine PD/PK modelling is performed using parameters from Wiczling et al. (2012) and Sigtermans et al. (2009) respectively.

2.2.2 SWAS real-time detection model

The pre-processed EEG and anaesthetic concentration data are used as inputs to the SWAS real-time detection model (Figure 2.2). Firstly, pre-processing is applied to the EEG and real-time spectral estimation is performed to obtain the power in the slow wave frequency band. Next, slow wave power is dynamically estimated as a function of anaesthetic concentration. Finally, model parameters are updated based on the new data and model output is passed on for visualisation purposes.

Portions of the work reported in this section (Section 2.2.2) were performed by other people. The SWAS sigmoid function has been previously published in Warnaby et al., (2017). The dynamic module was developed by Prof. Myles Allen and an offline implementation of the SWAS model was developed by Prof. Saad

Jbabdi. My contribution was making significant modifications to the offline implementation to accept input and produce output in real time.

2.2.2.1 Spectral estimation

EEG slow wave power (0.5-1.5Hz) from the Fz electrode is extracted using a real-time spectral estimation method applied to 16 second raw EEG time windows, updated every 3 seconds. A tanh function that saturates if the current EEG activity exceeds ±3 standard errors of the preceding 8 seconds, is applied to each time window to minimise the impact of artefactual EEG spikes.

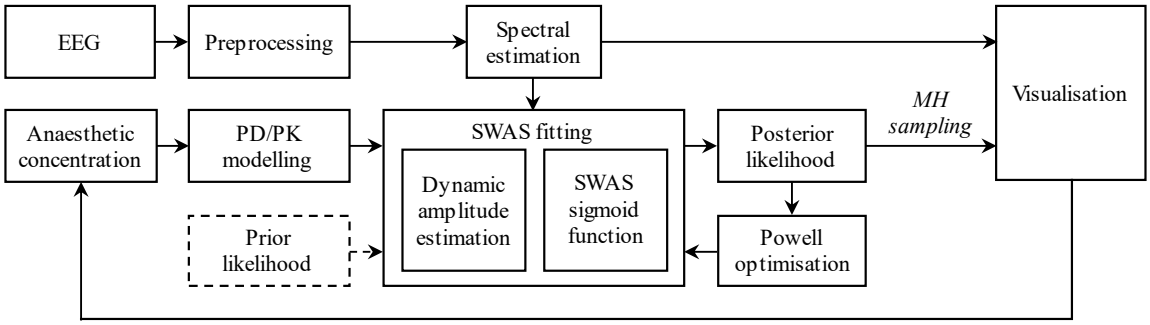

Figure 2.2: Flow chart illustrating the real-time SWAS model processing pipeline. EEG = electroencephalography, PD/PK = pharmacodynamic/pharmacokinetic, MH = Metropolis-Hastings.

To weight more recent data, a half-Hamming window is applied to the demeaned EEG data in each 16s window. The MATLAB fft.m function was then applied to each time window, and the relevant bins for the slow wave activity in 0.5-1.5Hz frequency band extracted. The spectrum is estimated for each window assuming a 30s adjustment time. The weight of the current window is calculated as $1 -$

$exp(-f/T_{adjust})$ where f is the time between successive spectral estimations in seconds and T_{adjust} is the adjustment time. This approach allows for the rate of spectral estimation or the adjustment time to be changed independently of each other. The slow wave power for a given time is then calculated using the weighted sum of $1 - exp(-3/30) = 0.095$ of the current window and 0.905 times the preceding one.

2.2.2.2 Dynamical modelling of slow wave power

The dynamical estimation of slow wave power is a Kalman filter. It comprises of a first order differential equation, where the amplitude A of frequency i varies as a linear relaxation to amplitude S_i at a rate of time-constant τ_i. Additionally, a non-linear interaction term, W_{ij}, modulates A_i by allowing for a cross-frequency coupling between frequencies i and j.

$$\tau_i \frac{dA_i}{dt} = S_i(C) - A_i + \sum_j W_{ij} C A_j \qquad (1)$$

In this implementation, the cross-frequency coupling has been set to zero.

2.2.2.3 SWAS sigmoid function

Changes in amplitude S_i of frequency band i are modelled as a parametric sigmoid function of the anaesthetic concentration C(t) (see Figure 2.3). $S_i(C)$ is defined as a logistic function of the initial amplitude r_i and the amplitude at saturation s_i, which is given by

$$S_i(C) = \frac{s_i - r_i}{1 + exp\left(\frac{-(C - t_i)}{u_i}\right)} + r_i \qquad (2)$$

The rate of change per unit increase in C is determined jointly by the parameters t_i, defined as the concentration at half saturation, and u_i, which defines the gradient of the curve at this point. Specifically, the steepness of the gradient of the curve is calculated as $tan^{-1}[(s-r)/4u\,]$ in degrees, meaning the value of u_i is inversely related to the steepness of the curve. A flat prior distribution is defined by initial values for the free parameters r, s, t, and u. A posterior probability distribution is calculated from the prior and a likelihood function that assumes while Gaussian noise of unknown variance. A Jeffrey's prior on the variance allows for analytical integration. The free parameters are estimated using the Metropolis-Hastings algorithm. The Metropolis-Hastings algorithm is a randomised sampling method (Markov Chain Monte Carlo), allowing us to sample the joint posterior probability distribution of the free parameters.

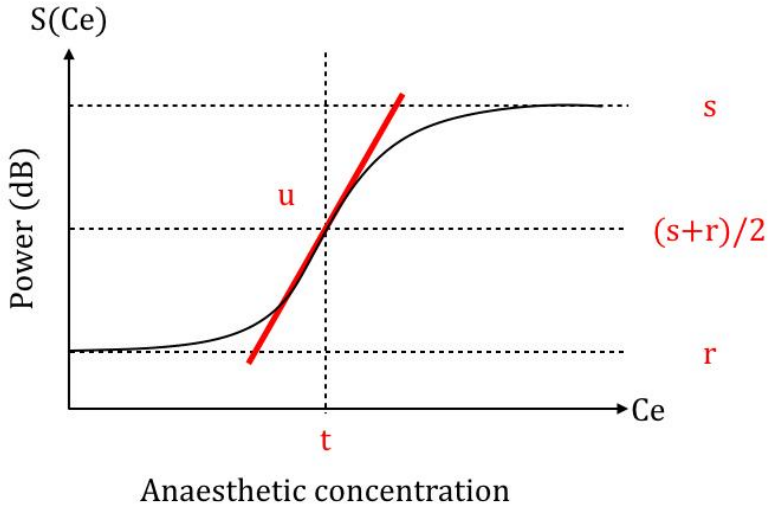

Figure 2.3: Illustration of the sigmoid curve modelled in Equation 2. r is slow wave power at baseline and s is slow wave power at SWAS. t is the anaesthetic concentration at half-saturation, defined as the mean of s and r, and u is inversely related to the steepness of the gradient of the curve at that point.

When applied in real-time, the free parameters from Equation (1) and (2) are dynamically updated at user-specified intervals using Powell maximisation of the posterior likelihood with log-normal priors and an exponentially weighted fit with decay-time of 7.5 minutes. Finally, the saturation level of frequency band i is defined as

$$SWAS\ level = \frac{A_i}{s_i} \quad (3)$$

where A_i and s_i are extracted from Equation 1 and 2. SWAS is defined as when the SWAS level is ≥0.99.

The SWAS sigmoid function can also be applied in isolation offline to previously acquired full anaesthesia induction datasets. If applied post-hoc in this manner, the concentration of slow wave activity saturation (C_{SWAS}) is defined as the concentration that contains 95% of the posterior distribution around SWAS where C_{SWAS} = SWA(Ce) > SWAS – 1.65σ, and SWAS (±σ) is the estimate of the location and precision of SWAS. Slow wave power at SWAS (P_{SWAS}) is the absolute slow wave power at C_{SWAS} and 95% of the distribution around the slow wave activity plateau.

2.2.3 Graphical user interface (GUI)

The prototype system features a GUI that displays input data and SWAS model output in real time (updating every second) (Figure 2.4). Firstly, visualisation of input EEG and anaesthetics data is included for the purpose of monitoring signal quality and troubleshooting potential issues. A spectrogram of the input EEG is generated by the Matlab function spectrogram.m that has been modified for real-time application (window width = 4s, overlap = 3s, frequency bin size = 0.25Hz, frequency range = 0.25 to 30Hz). Secondly, the GUI features a visualisation of the real-time SWAS model output, including estimated slow wave power, model fit to that spectral estimation (A_i in Equation 2 and 3), and SWAS level (Equation 3). Additionally, a dose-response curve of slow wave power as a function of anaesthetic concentration is plotted. Finally, the GUI displays numerical summaries of slow wave power, anaesthetic concentration, and SWAS level.

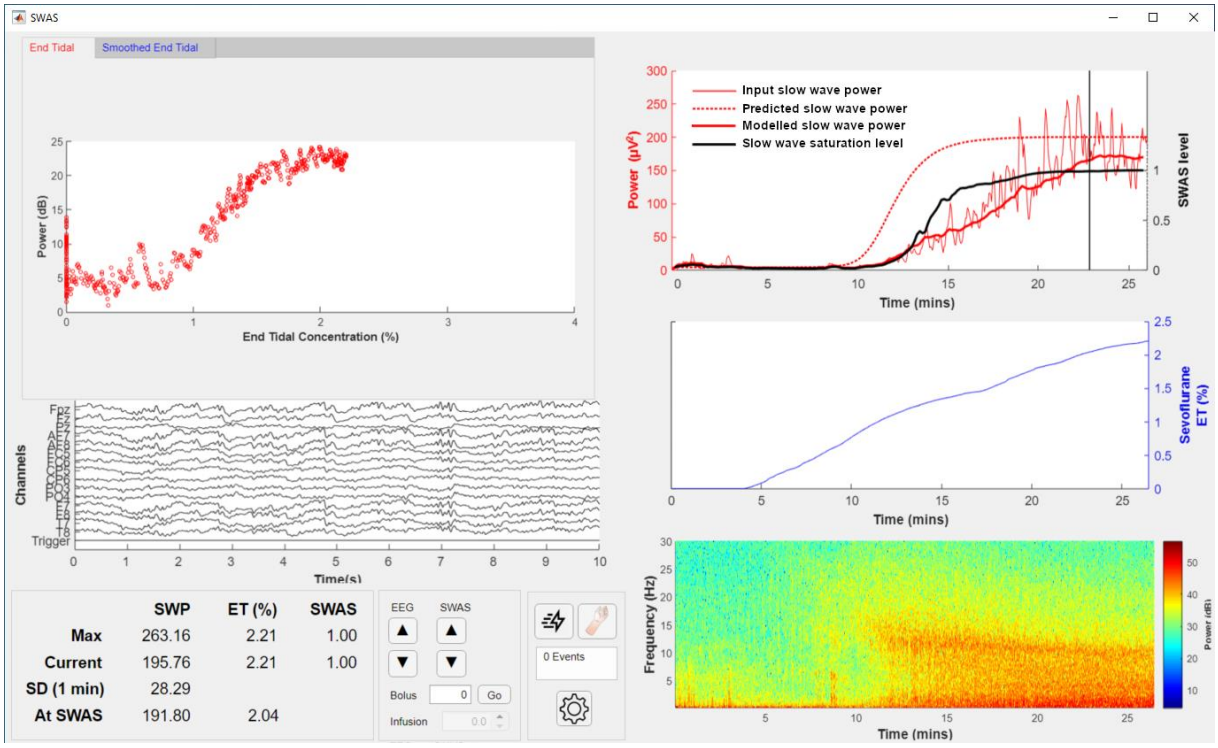

Figure 2.4: Screen capture of the GUI used to titrate anaesthesia to SWAS. Top right: Visualisation of the SWAS real time model output. Against the left y-axis, modelled slow wave power (thick red line; A_i in Equations 1 and 3) is plotted over the input slow wave power (thin red line; estimation described in Section 2.2.2.1) and predicted slow wave power based on initial r, s, t, u, and τ parameter values (dotted red line). Against the right y-axis, the slow wave saturation level (Equation 3) is plotted in black, with a vertical black line indicating the point SWAS was reached. Middle right: Smoothed anaesthetic concentration plotted as a function of time. Bottom right panel: Spectrogram of the raw EEG used as input to the SWAS model. Top left panel: Slow wave power plotted as a function of anaesthetic concentration. Middle left: Most recent 10s of raw EEG. Bottom left: Numerical summary values for slow wave power, anaesthetic concentration, and SWAS level. Bottom middle: Panels for user input during model operation, including plot scaling, intravenous anaesthetic concentration entry, and inserting event time stamps.

The user is able to customise the visualisation during system operation, including changing scaling of data axes and choosing to plot all or only the most recent X minutes of data, where X is a user-configurable number. When taking intravenous anaesthetic concentrations as input, the GUI also includes an interface to input anaesthetic concentration data.

When initialising the model, the user is first prompted to enter some basic session information (Figure 2.5). Secondly, the user is able to set initial values for the r, s, t, u, and τ parameters and whether each parameter is allowed to dynamically update or not. Thirdly, some additional fixed parameters used outside the model fitting itself are user configurable. These are the rate of spectral estimation (estimation period), the window width of the Powell estimation, the evolution time which determines the weighting of the current and previous spectral estimation windows, and the half-width of the spectral estimation window. Finally, the user can configure where to write the model output.

2.2.4 Additional system features

In some situations, it may be desirable to change initial model parameters during model operation. Therefore, the GUI includes a menu where new model parameters can be entered, and recalculation of model parameters can be initiated (Figure 2.6). Doing this will purge previously calculated model output and the altered model parameters are applied to all data acquired in the recording session. Both EEG and anaesthetics data from anaesthetic monitor are continuously sampled during model recalculation. However, the prototype system is not capable of accepting changes to intravenous anaesthetic concentration while the model is recalculated. This is not such a problem as these changes in anaesthetic concentration tend to change more slowly.

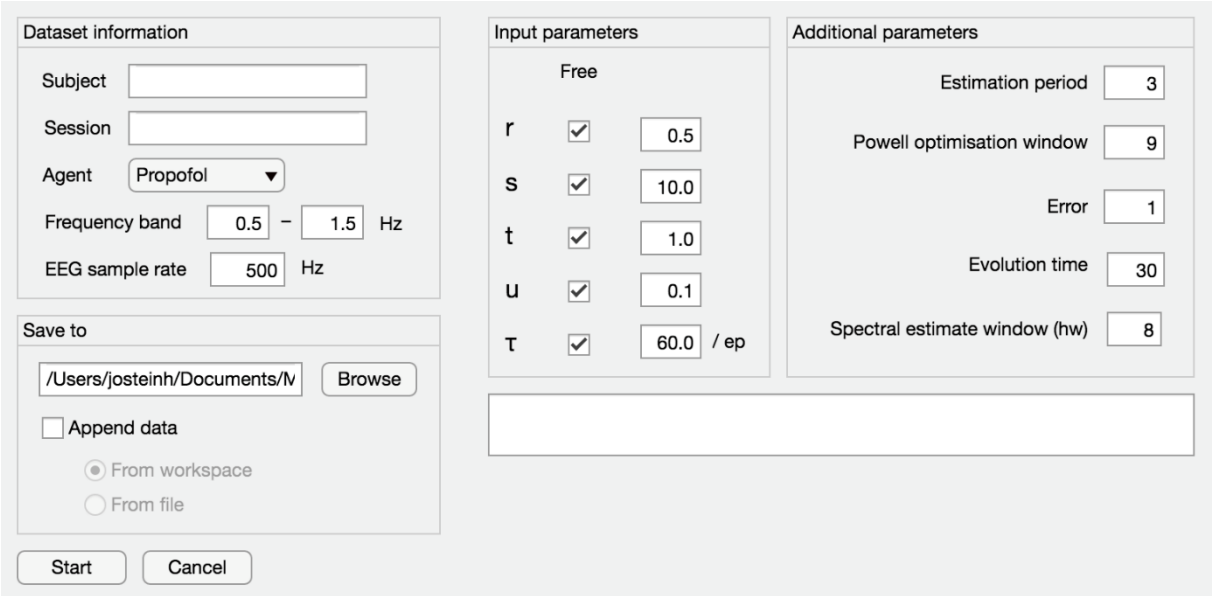

Figure 2.5: GUI used to initialise the SWAS prototype system. Top left: User-configurable fields for generating meta-data for the recording session, and select anaesthetic agent, frequency band, and EEG sample rate. Top middle: User-configurable initial values for the r, s, t, u, and τ parameters with individual toggles for freeing or fixing parameters. Top right: Additional user-configurable

parameters. Bottom left: User-configurable settings for writing output, as well as the option to resume an ongoing session by appending new data to either data in the workspace or loaded in from a file. Bottom right: Text box displaying error messages in case of invalid parameter values.

The prototype system includes some features to allow for recovery in the event of system crashes. Firstly, the model is cancelled or crashes, but the Matlab instance remains running, the model is able to append data to the variables and data structures stored in the Matlab workspace. This includes both input data and model output, only requiring the model to be applied to any new data that has been acquired since the model stopped. Secondly, if the Matlab environment itself goes down, the prototype system can read in EEG and anaesthetic data that was written to disk up to the point of the system failure. If the session is recovered in this way, the model has to be applied to the data from the beginning, similar to when the user initialises a recalculation of the model as described above.

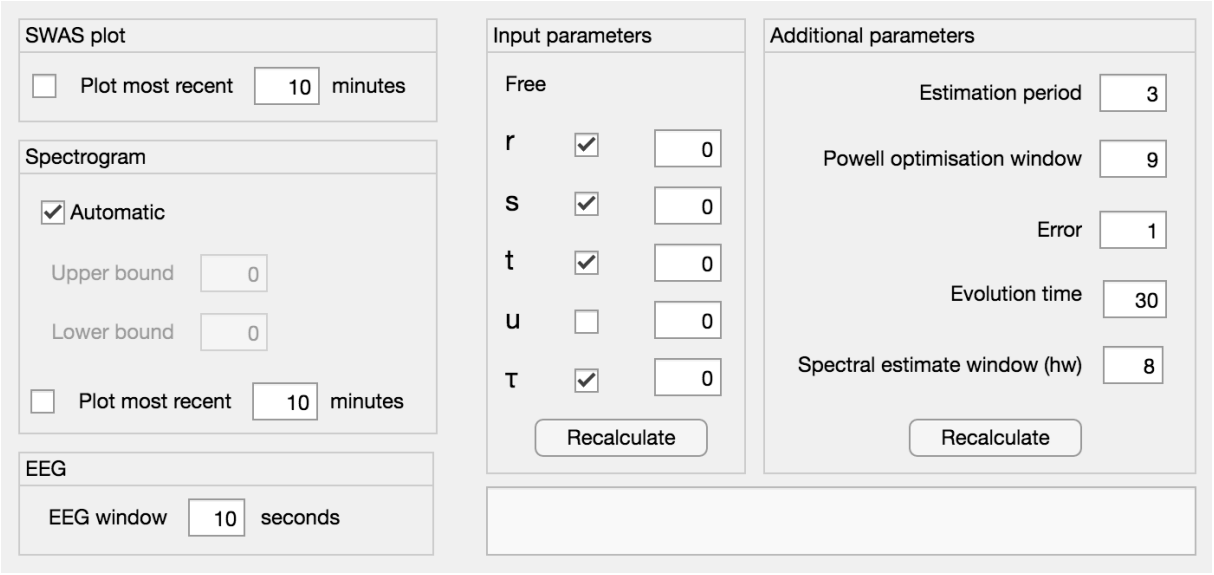

Figure 2.6: Settings menu that can be opened from cog icon in the main GUI (Figure 2.4). Left panels: Options for data visualisation in the main GUI. Top

middle and right: Options for recalculating the real-time SWAS model with altered parameters. Bottom right: Text box displaying error messages in case of invalid parameter values.

2.3 Discussion and future directions

I have developed a prototype system for guiding anaesthesia delivery to an individual's SWAS endpoint. The prototype system has all the core functionality required to titrate anaesthesia to SWAS in a research context and serves as a stepping-stone for further development of a clinical depth of anaesthesia monitor.

There are some limitations of this first iteration that will need to be overcome in the future development of the SWAS prototype system. The current iteration of the prototype system is only capable of modelling one anaesthetic agent at a time. However, the current implementation is flexible to be able to add additional anaesthesia input options, including combinations of different agents. The simplest case is a mixture of different volatile anaesthetics. Concentrations of volatile anaesthetics can be expressed as minimum alveolar concentration (MAC), which is the concentration at sea level at which movement in response to a surgical stimulus is absent in 50% of subjects (Eger et al., 1965; Quasha et al., 1980). MAC remains the gold standard for comparing potency of volatile anaesthetics and is widely used in clinical practice (Aranake et al., 2013). When expressing volatile concentrations as MAC they are additive, meaning the combined effect of the drugs is equal to the sum of the individual effects of each drug (Hendrickx et al., 2008). For example, a mixture of 1MAC sevoflurane and 0.3 MAC nitrous oxide has a combined MAC of 1.3. A caveat to this is that the propensity of these agents to cause slow waves may not be strictly additive, and may governed by a more

complex relationship. SWAS has previously been modelled offline in terms of volatile anaesthetic concentrations expressed as MAC (Warnaby et al., 2017). As MAC calculated from end-tidal concentration in a straightforward manner, it would be feasible to implement a combined MAC as input to the prototype SWAS system.

Implementing input of a combination of multiple intravenous or intravenous and volatile anaesthetics is less straightforward, as there is significant heterogeneity in how these drugs interact (Hendrickx et al., 2008). Many anaesthetic drug combinations are either synergistic or infra-additive, meaning the combined effect either exceeds or is less than the sum of the individual drug effects (Hendrickx et al., 2008). However, for some common anaesthetic drug combinations, such as propofol and sevoflurane, the drug effects does appear to be additive (Harris et al., 2006).

Similarly, co-administered opioids potentiate anaesthetic action (Bouillon, 2008; Hendrickx et al., 2008), giving an example of synergistic drug interaction. In line with this, opioids have been found to reduce the anaesthetic concentration required to achieve SWAS (Warnaby et al., 2017). Modelling the effect of different types and doses of opioids on the SWAS curve will be a key challenge in developing the prototype further for clinical applications. The influence of opioid can already be taken into account by the SWAS model by changing the initial values for the t and u parameters (i.e., reducing the expected concentration at half saturation and the steepness of the curve at that point), but this solution has not

yet been sufficiently tested. One important caveat is that we currently do not know how much to change the initial values to account for different doses of opioids.

Furthermore, the current iteration of the prototype system only has fairly rudimentary artefact correction. Specifically, the prototype system features a tanh filter that saturates spikes in slow wave power. While the tanh filter is effective at suppressing transient artefacts, sustained periods of artefacts will still cause the modelled slow wave power to be significantly overestimated. However, more sophisticated artefact correction is not trivial to implement. Firstly, artefacts that are problematic at baseline and during early induction can be of higher amplitude than slow wave power at SWAS. This makes it challenging to detect artefacts without falsely flagging genuine increases in slow wave power. This is particularly challenging when artefactual waveforms resemble slow waves, such as artefacts from eye blinks. Secondly, as the SWAS real-time model in its current iteration assumes a continuous input, it would not be possible to simply discard artefactual data segments. Therefore, the model would either have to be adjusted to handle missing data segments, or the slow wave power for the rejected segments would have to be interpolated.

Burst suppression is a pattern of electrical brain activity characterised by alternating periods of high-amplitude activity (bursts) and isoelectricity (suppression) observed in abnormal brain states such as coma and hypothermia, as well as deep general anaesthesia. Sustained periods of burst suppression have been suggested to potentially be predictive of post-operative delirium, though

evidence regarding causality is mixed (Shanker et al., 2021). Burst suppression occurs at deeper levels of anaesthesia than is required to achieve SWAS (Warnaby et al., 2017). Therefore, while not essential to titration of anaesthesia to SWAS, a system for detecting burst suppression would provide additional information to anaesthetists that they have gone past SWAS. Severity of burst suppression can be quantified as the ratio of time spent in high-amplitude bursts and isoelectric suppression (Rampil & Laster, 1992), and several methods of detecting burst suppression have been proposed (Leistritz et al., 1999; Lipping et al., 1994, 2007; Särkelä et al., 2002; Y. Wang & Agarwal, 2007). There is also precedence for existing depth of anaesthesia metrics to include burst suppression ratio in their algorithms, including BIS (Bruhn et al., 2000) and Narcotrend (Kreuer & Wilhelm, 2006) monitors. Therefore, it is feasible to implement burst suppression detection in future development of the SWAS titration system.

In this chapter I have described the implementation of a prototype system for titrating anaesthesia to the SWAS endpoint within an individual. Finally, I have discussed some limitations of the current implementation and proposed future directions of development with a view towards commercialisation and adoption into routine clinical practice.

3 Real-time titration to SWAS in practice

3.1 Introduction

In the previous chapter, I described the development of a prototype system for titrating anaesthesia to individual SWAS levels. SWAS had previously only been characterised offline in healthy volunteer and clinical datasets using post-hoc application of the sigmoid response function (Mhuircheartaigh et al., 2013; Sleigh et al., 2019; Warnaby et al., 2017). During the development of the SWAS prototype system, an inherent limitation was that the mathematical model and the prototype system could only be tested in previously acquired observational data where the anaesthetic dose delivered was often far in excess of SWAS. Therefore, a key outstanding question was whether it is possible to use the SWAS prototype system to achieve and maintain an individual at their SWAS level.

Offline modelling of SWAS has the advantage of knowledge of the whole anaesthetic induction period, allowing for more thorough preprocessing and artefact correction. For these reasons, offline SWAS modelling is the current gold standard that the accuracy of the real-time SWAS titration can be compared to. Specifically, the concentration of SWAS (C_{SWAS}) as determined by offline SWAS modelling is the optimal dose, and the accuracy in obtaining this target can be quantified by the deviation from this value. Similarly, the slow wave power at SWAS (P_{SWAS}) as determined by offline SWAS modelling is the value that the real-time model should identify (i.e., the s parameter in Equation 2 and 3 in Chapter 2).

For clinical translation of SWAS, it is necessary to be able to titrate anaesthesia to SWAS within a timeframe that is compatible with other clinical considerations and constraints. In particular, operating theatre and anaesthetic room time is a limited resource (Koenig et al., 2011). Furthermore, unpredictable anaesthesia induction duration contributes to idle waiting times among anaesthetists and surgeons (Koenig et al., 2011). Ideally, anaesthesia titration to SWAS would be both fast and accurate, although in practice there will likely be a trade-off between the two concerns due to delays in anaesthetic action at the brain. Standard clinical induction of anaesthesia typically takes between approximately 10-45 minutes depending on the number and complexity of the required anaesthetic induction services (Koenig et al., 2011; Schuster et al., 2008). Simple cases requiring only airway management tend to be shorter than cases that require central venous catheters, arterial lines, and/or epidural catheters (Schuster et al., 2008). As these services come in addition to the administration of the anaesthetic drug, time of titration to SWAS should be towards the lower bounds of this range to be clinically viable.

Additionally, it is important to be able to relate SWAS to behavioural readouts of awareness under general anaesthesia. The gold standard for detecting connected consciousness monitoring during surgery is the isolated forearm test (IFT) (Linassi et al., 2018), which involves restricting blood flow to an arm during administration of neuromuscular blockers and giving the anaesthetised patient a verbal command to respond. A common criticism of existing depth of anaesthesia monitors is that they do not prevent positive IFT responses during surgery any more than

conventional vital signs monitoring when the recommended range of values is targeted (i.e., 40 to 60 for the BIS) (Linassi et al., 2018), indicating that they fail to reliably prevent at least some degree of connected consciousness. Therefore, a key outcome measure for SWAS as a target for clinical anaesthesia is whether individuals titrated to SWAS are unresponsive to the IFT. Furthermore, positive responses to the IFT in the SWAS state would challenge the interpretation that SWAS is a state of complete perception loss under general anaesthesia.

Crucially, however, positive IFT responses are many times more frequent than subsequent recall of intra-operative awareness (Linassi et al., 2018). Estimates of incidents of awareness with recall range from about 1:600 to 1:17,000 (Tasbihgou et al., 2018). Intra-operative awareness with recall are generally considered more clinically significant than awareness without recall, as long term psychological disorder is associated with recall of the awareness event (Ag et al., 2016). The Brice Awareness Questionnaire (Brice et al., 1970) is considered the gold standard for detecting intra-operative awareness with explicit recall (Mashour et al., 2013). For SWAS to be a viable target for clinical anaesthesia, it is of utmost importance that patients held at their SWAS end point during surgery have no explicit recall of surgical events. At the very least, rates of incidences of intra-operative awareness need to be comparable to or lower than current clinical standards. Due to the low incidence rates of intra-operative awareness with recall, any incidence during early SWAS investigations in comparatively low samples would be of great concern.

3.1.1 Predicting anaesthesia requirement to SWAS

In order to improve the speed and accuracy of SWAS titrations, it is useful to know factors that can impact anaesthetic susceptibility. Firstly, physiological factors such as body weight, sex, and age have been well established to affect susceptibility to a range of anaesthetic agents (Forrest et al., 1994; Mapleson, 1996). PD/PK models generally attempt to account for some of these factors when estimating effect site concentration. For instance, when estimating propofol PD/PK, the Marsh model incorporates weight and the Schneider model incorporates age, weight, height, and sex (Marsh et al., 1991; Schneider et al., 1998). In the case of volatile anaesthetics, MAC robustly decreases with age (Mapleson, 1996), and therefore age-adjusted MAC is often used to compare anaesthetic dose requirements at different ages (Aranake et al., 2013).

Relatedly, as SWAS may have a neurophysiological underpinning, it may be possible to predict the concentration and slow wave power at SWAS for an individual, i.e., C_{SWAS} and P_{SWAS}, respectively. Firstly, while Warnaby et al. (2017) found that the concentration of propofol required to reach SWAS during induction was not correlated with age, the MAC concentration at emergence was correlated with age. Secondly, slow wave power at SWAS was found to be negatively correlate with age (Warnaby et al., 2017). Additionally, although not SWAS *per se*, other studies have found a negative association between age and slow wave power during propofol and sevoflurane anaesthesia (Purdon, Pavone, et al., 2015) and during slow wave sleep (Ringli & Huber, 2011).

Beyond physiological factors, there may be personality traits that predict anaesthetic requirement to achieve SWAS. Locus of control is a psychological concept referring to the strength of an individual's belief that they are in control over their own situation and experience (Levenson, 1973). LOC has been extensively tied to heath, with the Multiple Health Locus of Control (MHLC) scale having been developed as a domain-specific version of the LOC scale for healthcare (Wallston et al., 1978). The original LOC scale (Levenson, 1973) has three sub-scales: Internal LOC, faith in powerful others, and chance. High internal LOC and low faith in powerful others have been found to predict increased requirement for anaesthesia in minor gynaecological surgery (Abbott & Abbott, 1995). We hypothesise that people who have a high trust in powerful others and low internal LOC will be more susceptible to the anaesthetic, and consequently requiring a lower anaesthetic concentration to lose behavioural responsiveness (C_{LOBR}), have a lower C_{SWAS}, or both.

It has been suggested that the personality trait absorption measures the openness to an altered sense of reality and the self (Tellegen & Atkinson, 1974) and has been found to be associated with hypnotic susceptibility (Glisky et al., 1991). Previous work in our lab suggests that people lose a sense of selfhood when they become unresponsive under general anaesthesia (Warnaby et al., 2016). We hypothesise that individuals who are open to an altered sense of the self might be more susceptible to entering an altered state of consciousness under general anaesthesia, particularly in the period around loss of responsiveness where the

anaesthetic may impair their sense of self. Specifically, we expect people who score high on the absorption trait will have a lower C_{LOBR}, C_{SWAS} or both.

Future surgery and anaesthesia can cause anxiety (Jawaid et al., 2007). Worry about receiving an anaesthetic was found to be negatively correlated with anaesthetic susceptibility (Abbott & Abbott, 1995). Negative views towards diagnosis, as well as severity of melancholic/vegetative depressive symptoms, were significantly associated with anaesthesia response as measured by BIS (Price et al., 2015). We hypothesise that people who are more anxious the day of the anaesthetic and in general will require more anaesthesia to lose responsiveness and achieve SWAS.

Finally, little is known about the effect of pre-anaesthetic sleep quality on anaesthesia in humans. However, one study showed that people with poor sleep quality required less propofol anaesthesia to maintain a BIS score within the recommended range (Mirkheshti et al., 2020). In the other direction, there is some evidence in animals (Jang et al., 2010; Nelson et al., 2010; Pick et al., 2011; Tung et al., 2004) and humans (Moote & Knill, 1988) that anaesthesia can interact with subsequent sleep. Based on this, it is possible that general sleep quality and sleep quality the night preceding an anaesthetic could predict anaesthetic requirement.

In this chapter, I report on the application of the real-time SWAS prototype system in two studies: a pre-surgery study in a patient population (Study 1) and a laboratory EEG-MRI experiment in healthy volunteers (Study 2). Here, I will assess the performance of the prototype system across the two studies, both in

terms of the speed and accuracy in which we could obtain SWAS. Finally, I analyse how individual psychological and behavioural measures relate to SWAS and discuss how such measures could be used to inform future model development.

3.2 Methods

3.2.1 Ethical approval

Studies 1 and 2 were jointly approved by the West Midlands - Coventry & Warwickshire Research Ethics Committee (ethics reference 18/WM/0030) and were designed and conducted in accordance with the Declaration of Helsinki. Written informed consent was obtained from all participants before participation. General exclusion criteria for both studies were: a history of tobacco or illicit drug use; high alcohol intake (>14 UK units/week); neurological or psychological pathology; pregnancy; conflicting prescription medication; clinical indication of risk of airway obstruction, adverse reaction to anaesthesia, or venous throbo-embolic event; or vulnerable group status. More specific criteria for each study are included below.

3.2.2 Study 1

3.2.2.1 Recruitment and screening

We recruited patients who were having general anaesthesia for elective plastic surgery or minor trauma surgery at the Oxford University Hospitals (OUH) NHS Foundation Trust. To be included in the study the patients had to be between 18 and 60 years old and to have an American Society of Anesthesiology (ASA) score

of 1 or 2. In addition to the general exclusion criteria listed in Section 3.2.1, patients were excluded if they were involved in litigation cases or were scheduled for a surgery to the head or neck or requiring the prone position. Participating surgical, anaesthetic, and peri-operative assessment teams identified patients who met the study inclusion criteria. The clinical teams performed an initial screening of patients on the basis of the primary inclusion criteria, the surgical exclusion criteria, and vulnerable group status. Additionally, we recruited patients who were scheduled second or later on a surgical list so as to avoid the potential of introducing delays to the surgical lists.

Suitable patients were invited to participate by the clinical team at either their out-patient or pre-operative assessment appointment. They were given a brief explanation of the study, an invitation letter, and a patient information sheet to take home. It was clearly explained to the patient that there was no obligation to participate and that non-participation would not influence their future medical care.

After the initial explanation of the study, participants were asked if they were happy to be contacted by the research team. The research team contacted interested patients at the pre-operative assessment appointment, by telephone or email to discuss the study further. At this time, they confirmed that the patient understood what the study involved. If the patients still expressed an interest in participating, a consultant grade anaesthetist that was part of the research team carried out a full eligibility assessment based on the study's inclusion and exclusion criteria. Written informed consent to participate in the study was

obtained either on the morning of surgery, or at the earlier pre-operative assessment clinic if the patient was happy to proceed at that time.

3.2.2.2 Study procedures

Patients were allocated to be titrated to SWAS using either sevoflurane or propofol anaesthesia. The allocation to each agent was not randomised. As Study 1 was in part intended to prepare the research team for titrating sevoflurane anaesthesia in the MRI environment in Study 2, initially patients were preferentially allocated to the sevoflurane group. We targeted a total sample of 20 patients, evenly divided so that there were ten patients in each group.

On the day of surgery, initial preparations were performed on the admission ward. Both the clinical anaesthetist and the study anaesthetists met with the patients to discuss the anaesthetic. Once the clinical anaesthetist was happy with the standard preoperative check in, and written informed consent had been obtained, the study personnel performed the study procedures.

On the out-patients ward, patients were asked to fill in a booklet of validated questionnaires: State-Trait Anxiety Inventory (STAI) trait component (Spielberger et al., 1983), Amsterdam Preoperative Anxiety and Information Scale (APAIS) (Moerman et al., 1996), Pittsburgh Sleep Quality Index (PSQI) (Buysse et al., 1989), and the Tellegen Absorption Scale (TAS) (Tellegen & Atkinson, 1974).

A 24-channel EEG cap fitted with Ag/AgCl cup electrodes (Twente Medical Systems International B.V., The Netherlands) was fitted to each patient. Each

electrode site was prepared with surgical alcohol and a conductive gel was applied between the electrode and the scalp to ensure good signal quality. EEG was recorded with a TMSi Porti 7 amplifier system at a sampling rate of 2048Hz.

In the anaesthetic room, patients were prepared for their surgery according to their clinical protocol by the clinical team and for the study procedures by the study anaesthetist. Recommended practices of patient monitoring and trained anaesthetist assistance was met for all patients as per the Royal College of Anaesthetists' Guidelines for the Provision of Anaesthetic Services 2016 (http://www.rcoa.ac.uk/node/21849). An anaesthetic nurse or operating department practitioner was present to aid the study anaesthetist throughout the anaesthetic induction.

Patients were fitted with a tight-fitting facemask used for delivery of 100% oxygen and, if allocated to the sevoflurane group, the anaesthetic agent at a flow rate of 5L/min. When clinically appropriate, the EEG cap was connected to the SWAS prototype system. At this point, EEG quality was reassessed and adjustments to individual electrodes were made as appropriate.

The patient was instructed to keep their eyes closed. This was done to limit EEG artefacts from eye blinks. The SWAS prototype system was initialised to obtain baseline slow wave power, i.e., the value used as the initial value of the r parameter. After adjusting the initial value for r, the model was reinitiated, and the delivery of the anaesthetic commenced. An experimenter held the patient's hand throughout the anaesthetic induction. Every two minutes, the modified isolated

forearm test (IFT) was performed by the experimenter saying “[PATIENT NAME], please squeeze my hand.” to assess behavioural responsiveness. In the standard IFT, blood flow is restricted to the forearm during administration of muscle relaxants so that the hand retains the ability to respond to the prompt. The modified IFT was modified in the sense that no muscle relaxants were administered, and therefore no restriction of blood flow to the forearm was done. Once SWAS was reached according to the real-time SWAS model, the concentration of the anaesthetic was held constant for 10 minutes. If time permitted with respect to not disrupting the surgical list schedule, the anaesthetic concentration was further increased after the 10-minute hold to extend the range of anaesthetic concentration to construct dose-response curves offline.

After the completion of the experimental protocol, the patient was handed over to the clinical team. From this point on the research team had no active role and imposed no restrictions on the clinical procedures, including which anaesthetic agent and concentration was used. However, EEG, anaesthetic and physiological data was recorded throughout the surgery and during recovery. Notable surgical events and the timings of administration of any medications were recorded. These included the time and dose of the various intravenous hypnotic and analgesic drugs, time of loss and recovery of behavioural response, time of insertion and removal of airway devices, and time of first surgical incision. Additionally, heart rate, blood pressure, end-tidal CO_2, end-tidal anaesthetic concentrations, and oxygen saturation levels of the patient were recorded. Upon recovering from the anaesthetic, an experimenter scored the Nursing Delirium Screening Scale

(NuDESC) and conducted the Brice Awareness Questionnaire. The NuDESC scoring and Brice Awareness Questionnaire was repeated 15 minutes after recovery. The Brice Awareness Questionnaire was also repeated by telephone 4 weeks after the operation.

3.2.3 Study 2

3.2.3.1 Recruitment and screening

We recruited 23 healthy volunteers between the ages of 18 and 50 through local and social media advertising. During an initial session, all participants were screened by a consultant anaesthetist to ensure that they met the general inclusion and exclusion criteria outlined in Section 3.2.1. Additionally, participants were excluded if they were left-handed, had contraindications to MRI, or facial hair that would prevent a tight mask seal.

3.2.3.2 Study procedures

The experiment took place over two sessions (Figure 3.1). The experiment was designed to include a multitude of measurements for different analyses, including EEG, MRI, behavioural, and questionnaire data. This chapter will detail the acquisition and analysis of the anaesthesia EEG, behavioural, and questionnaire data. Details regarding the MRI acquisitions and their subsequent analyses will follow in Chapters 4, 5, and 6.

During the first session, a series of baseline MRI images of the brain were acquired: 1) high resolution anatomical image (T_1-weighted MRI); 2) structural white matter pathway measurements, (diffusion-weighted MRI [dwMRI]; 3) resting

state FMRI; 4) cerebral blood flow measurements (arterial spin labelling [ASL]), and 5) neurotransmitter measurements (magnetic resonance spectroscopy [MRS]). Participants filled in a questionnaire booklet and had a sleep EEG-kit fitted (SomnoHD, SOMNOmedics GmbH, Germany). Participants were given instructions for fasting in preparation for the anaesthetic and sent home via taxi for a night of sleep EEG recording in their own bed.

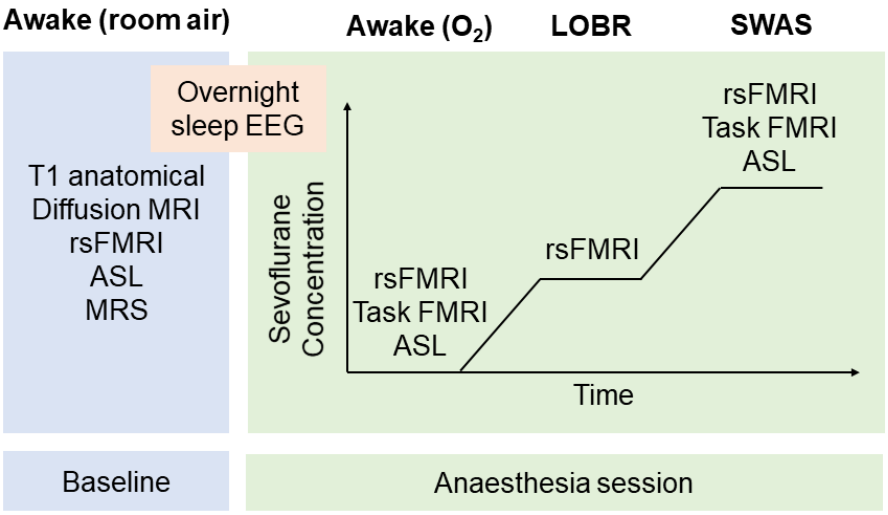

Figure 3.1: Overview of the study procedures in Study 2. The study was performed over two sessions: an evening baseline session and the main anaesthesia session.

Participants returned the following morning for the anaesthesia session. The sleep EEG-kit was removed, and an MRI-compatible EEG cap (BrainCap MR, Easycap GmbH, Germany) was applied. Participants were fitted with noise dampening earphones that were used for auditory stimulus delivery.

Anaesthesia was titrated in two stages. First, anaesthesia was titrated to loss of behavioural responsiveness (LOBR) to beeps of 1kHz frequency and 60ms duration delivered through the noise dampening earbuds, at which point anaesthetic concentration was held constant during steady-state FMRI measurements. Second, anaesthesia was titrated according to individual real-time EEG feedback from the Fz electrode using the prototype SWAS system. In cases where continuous real-time model fitting was not possible due to excessive artefacts from movement within the magnetic field, the research team gauged if SWAS had been achieved from a continuously populating concentration vs. slow wave power plot. At SWAS, the concentration was held constant during MRI acquisitions.

Resting state FMRI was acquired during wakefulness, the steady state hold at LOBR, the transition to SWAS and the hold at SWAS. Task FMRI and ASL data were acquired during wakefulness and at SWAS. A modified version of the IFT was administered as part of both task FMRI acquisitions. Finally, the participant was removed from the bore, the anaesthetic was turned off and the participant was allowed to wake up naturally while the EEG was recorded.

3.2.3.2.1 EEG data acquisition

EEG was acquired with a 32 channel EEG cap (BrainCap MR, Easycap GmbH, Germany) and MRI compatible amplifier system (MRplus, BrainVision GmbH, Germany) at a 5kHz sampling rate. Each electrode site was cleaned with surgical alcohol, and an abrasive electrolyte gel was applied between each electrode and

the scalp to keep impedances below 5kΩ. Electrocardiogram signals (ECG) were simultaneously recorded from a chest electrode integrated into the EEG cap. EEG and ECG data were recorded using BrainVision Recorder (BrainProducts GmbH), along with the onset timings of each ASL volume. To optimise the temporal accuracy of volume onset timers, the EEG clock was synchronised to the MRI scanner master clock (SyncBox, BrainProducts GmbH, Germany).

In addition to writing the raw EEG data to disk, they were transferred to RecView (BrainProducts Gmbh, Germany) for real-time MRI artefact clean-up. Artefacts resulting from the MRI gradient switching were firstly corrected using a real-time implementation of the template subtraction method (Allen et al., 2000), before the EEG was down-sampled to 500Hz. Heart beats detected from the ECG channel in real time were used to correct pulse-related artefacts in the downsampled EEG data using template subtraction (Allen et al., 1998). Generation of new templates for the gradient and cardioballistic artefact correction could be triggered by the experimenters if and when the artefact waveforms changed (e.g., due to gradual drift or participant movement). Finally, the MRI artefact corrected EEG was transferred via TPC in real time to a FieldTrip buffer running on a separate computer. The EEG was then read into MATLAB as part of the prototype SWAS system (as outlined in Section 2.2.1.1).

3.2.3.2.2 Anaesthetic delivery

Sevoflurane and O_2 gases were delivered through a tight-fitting face mask using an MRI compatible anaesthesia machine (Prima 451 MRI, Penlon Ltd., UK). In the

anaesthesia session, participants received 100% O_2 at 5L/min flowrate prior to anaesthesia delivery. During anaesthesia titration, participants received increasing levels of sevoflurane mixed with 100% O_2 at a flowrate of 5L/min until saturation of slow wave activity was identified using real-time EEG feedback (SWAS condition). The anaesthetic team, comprising a consultant anaesthetist and an anaesthetic assistant, had no other study responsibilities and could abort the experiment at any time if they had any concerns for participant safety.

Participants' vital signs, as well as the inspired and expired gas content, were monitored during anaesthesia delivery using either a Carescape B650 (General Electric Company Inc., USA) or Datex-Ohmeda S/5 (GE Healthcare Finland Oy, Finland) anaesthesia monitor. Blood pressure was monitored by a Tesla Duo MRI Patient Monitor (Mammendorfer Institut für Physik und Medizin GmbH, Germany) and oxygen saturation by a Nonin 7500FO pulse oximeter (Nonin Medical, inc. Plymouth, MN, USA). These vital signs and gas data were recorded from the monitor at a sampling frequency of 0.2Hz using VSCapture v1.005 (Karippacheril & Ho, 2013) and imported into MATLAB in real-time. Additionally, during both the baseline and anaesthesia sessions, pulse plethysmography and respiration bellows traces were recorded at a sampling rate of 200Hz using an MP150 system and Acknowledge software (BIOPAC Systems Inc., Goleta, CA, USA) for off-line analyses.

3.2.3.2.3 Questionnaires

Participants were asked to complete a series of validated questionnaires. During the evening baseline session, they completed questionnaires related to static traits. These were the State-Trait Anxiety Inventory (STAI) trait component (Spielberger et al., 1983), the Pittsburgh Sleep Quality Index (PSQI) (Buysse et al., 1989), the Tellegen Absorption Scale (TAS) (Tellegen & Atkinson, 1974), the Embodied sense of self scale (ESSS) (Asai et al., 2016), and the Locus of Control (LOC) (Levenson, 1973) questionnaires. On the morning of the anaesthesia session, the participants were asked to fill in two additional questionnaires: STAI state component (Spielberger et al., 1983) and the PSQI (Buysse et al., 1989) adapted to ask about the previous night's sleep. Finally, upon awakening the anaesthetist completed the NuDESC, and the Brice Awareness Questionnaire was administered. The NuDESC and interview was repeated after a short delay while the participant was recovering in an adjoining room.

3.2.4 Data analysis

3.2.4.1 Offline EEG processing

All offline EEG pre-processing and analyses were performed in MATLAB. For Study 1, the raw EEG was down sampled by a factor of 4 to 512 Hz and bandpass filtered with a 6^{th} order zero-phase Butterworth filter (0.1-45Hz). Slow wave power was estimated using short-time Fourier transform (spectrogram.m; 4s window, 3s overlap, 0.25Hz frequency bin size). The average of the frequency bins constituting the slow wave (0.5-1.5Hz) frequency band was calculated for each window.

For offline analyses for Study 2, MRI artefact correction was performed in BrainVision Analyzer version 2.1 (BrainProducts GmbH). EEG recorded during the FMRI acquisitions were cleaned for gradient artefacts using moving template subtraction (Allen et al., 2000). Separate moving templates were generated for each acquisition. Next, the EEG was downsampled to 1kHz prior to cardioballistic artefact correction, also using moving template subtraction (Allen et al., 1998). Further EEG preprocessing and analysis was performed in MATLAB (MathWorks Inc., USA).

As for Study 2, a 6th order zero-phase bandpass (0.1-45Hz) Butterworth filter was applied to each data segment prior to spectral decomposition (4 s window, 3 s overlap, 0.25Hz frequency bin size) using spectrogram.m. The average of the frequency bins constituting the slow wave (0.5-1.5Hz) frequency bands was calculated for each window.

3.2.4.2 Offline SWAS curve fitting

To assess the performance of the real-time SWAS model, the SWAS sigmoid curve (Equation 2 in Chapter 2) was fitted offline to slow wave power. For both Study 1 and Study 2, it was estimated at the Fz electrode from artefact-free EEG from the onset of anaesthesia delivery until the peak anaesthetic dose. For Study 1, up to 100 s of artefact-free EEG collected at baseline was included in the SWAS curve fitting to establish a baseline for slow wave power. Similarly, for Study 2, 100 s of EEG acquired during the resting state FMRI acquisition prior to onset of anaesthetic delivery was included in the SWAS curve fitting for the same purpose.

To visualise the variability in the SWAS sigmoid curve parameters across volunteers for each study and EEG system, the individual r, s, t, and u parameters values were plotted as boxplots. As the t parameter (concentration at half saturation) is dependent on the anaesthetic agent, the sevoflurane and propofol groups were plotted separately for Study 1.

3.2.4.2.1 Assessing accuracy of titration to SWAS

To assess the accuracy of titration to SWAS in Study 1, the anaesthetic concentration during the hold at SWAS (C_{hold}) was compared to C_{SWAS} estimated from the offline SWAS curve fitting. As the full 10-minute hold could not be completed for all patients due to time constraints on the surgical list, C_{hold} was calculated as the mean concentration of the first minute of the hold. Additionally, the time from anaesthetic onset to the beginning of the hold at SWAS (T_{hold}) was recorded for each patient.

As we anticipated that different individuals would reach SWAS at different concentrations, for both studies we calculated the mean absolute percentage error (MAPE) between the actual measured anaesthetic concentration that was achieved and C_{SWAS}. In this context, $MAPE = \frac{Measured\ concentration - C_{SWAS}}{Measured\ concentration}$.

Additionally, for Study 2 only, a Bland-Altman analysis was performed to assess the agreement between the measured anaesthetic concentration and C_{SWAS}.

3.2.4.2.2 Questionnaires

All questionnaires were scored according to their respective standard procedures. Correlation analyses were performed between each scale and sub-scale. To account for multiple testing, Benjamini-Hochberg false discovery rate correction was applied to C_{LOBR} and C_{SWAS} analyses separately.

3.3 Results

We successfully applied the real-time SWAS prototype in 12 patients in a clinical setting (Study 1) and 23 heathy volunteers in the MRI environment (Study 2). No subjects in either study responded to the IFT when held at SWAS. Furthermore, no subjects in either study reported recall of awareness of the surgical procedures (Study 1) or experimental procedures past loss of responsiveness (Study 2) as assessed by the Brice Awareness Questionnaire.

3.3.1 Study 1

3.3.1.1 Participants

The study was originally designed with a target of 20 patients. However, due to the COVID-19 pandemic, data collection had to cease before this target was reached. In total, twelve patients (eight in the sevoflurane group [age = mean±SD 44.5±11.6, four female] and four in the propofol group [age mean±SD 49.8±7.5, three female]) received an induction of anaesthesia guided by the real-time SWAS model. Nine of the patients underwent elective plastic surgery (seven in sevoflurane group) and four underwent surgery for minor trauma injuries (one in sevoflurane group). Three of the twelve patients had a NuDESC score indicating

delirium (≥2). An overview of the anaesthesia titration for each patient is given in Table 3.1.

Table 3.1: Overview over anaesthesia titration in each patient. T_{hold} = time from anaesthesia onset to the beginning of the hold at SWAS, C_{LOBR} = concentration at loss of behavioural response, C_{SWAS} = concentration at SWAS determined offline, C_{hold} = mean concentration in the first minute of the hold at SWAS, MAPE = mean average percentage error between C_{SWAS} and C_{hold}, sevo = sevoflurane, prop = propofol.

	Agent	T_{hold} (min)	C_{LOBR}	C_{SWAS}	C_{hold}	C_{SWAS}-C_{hold}	MAPE (%)	NuDESC
Subject 1	Sevo	-	2.1 %	-	-	-	-	0
Subject 2	Sevo	13.5	1.0 %	2.5 %	2.6 %	0.1 %	4.1	0
Subject 3	Sevo	-	-	1.7 %	-	-	-	7
Subject 4	Sevo	22.5	1.3 %	2.1 %	2.3 %	0.2 %	8.0	1
Subject 5	Sevo	20.4	1.1 %	1.8 %	2.3 %	0.6 %	25.5	0
Subject 6	Sevo	31.9	0.9 %	1.6 %	1.5 %	0.1 %	3.8	0
Subject 7	Sevo	20.5	1.2 %	1.9 %	2.2 %	0.4 %	15.8	0
Subject 8	Sevo	10.4	-	1.6 %	2.8 %	1.3 %	44.2	1
Subject 9	Prop	-	1.6 µg/ml	1.8 µg/ml	-	-	-	0
Subject 10	Prop	-	1.6 µg/ml	3.5 µg/ml	-	-	-	3
Subject 11	Prop	15.7	-	1.3 µg/ml	3.0 µg/ml	1.8 µg/ml	58.1	2
Subject 12	Prop	25.4	1.8 µg/ml	2.2 µg/ml	2.9 µg/ml	0.7 µg/ml	24.5	0

3.3.1.2 Real-time estimation of SWAS

With regard to the real-time titration, a stable hold at SWAS was achieved in six of the eight patients in the sevoflurane group. In addition to Subject 1, who did not reach SWAS at all, computer failure during the titration to SWAS in Subject 3 precluded identification of SWAS in real time. For the remaining six, the time from the onset of the anaesthesia to the hold at SWAS, i.e., T_{hold}, was mean±SD 20.0±6.9 minutes. The concentration during the first minute of the hold at SWAS, i.e., C_{hold}, was 2.3±0.5% (mean±SD) end-tidal sevoflurane.

In the propofol group, a stable hold at SWAS was achieved in two of the four patients. The failure to stabilise the propofol concentration at SWAS that occurred in the first two patients was due to the delay in the drug effect and difficulty targeting a specific effect site concentration without the use of target-controlled infusion.

3.3.1.3 Post-hoc estimation of SWAS

Post hoc SWAS fits using the Bayesian sigmoid function (Equation 1 in Chapter 2) for the 12 patients are shown in Figure 3.2. This off-line curve fitting showed that SWAS was achieved in all patients, except Subject 1. This was due to an insufficient concentration of sevoflurane (2.7% peak end-tidal concentration) being achieved despite reaching the maximal output from the anaesthetic machine. This was thought to be due to a mask leak. In that case, the end-tidal readings would also be unreliable. While SWAS was not achieved in this patient, the expected increase of slow wave power after loss of responsiveness did occur. For the remaining seven patients in the sevoflurane group, C_{SWAS} was achieved at sevoflurane end-tidal concentration of 1.6±0.7%. In the propofol group, the mean±SD effect site concentration of C_{SWAS} was 2.2±1.0µg/ml. P_{SWAS} was mean±SD 13.2±4.9dB in the sevoflurane group, 8.6±3.4dB in the propofol group, and 11.5±4.8dB when combining the groups.

In the sevoflurane group, the MAPE of C_{hold} relative to C_{SWAS} was 16.9±13.3% (mean±SD). In the propofol group, the MAPE was 58.1% and 24.5% in each of the two patients who established a hold.

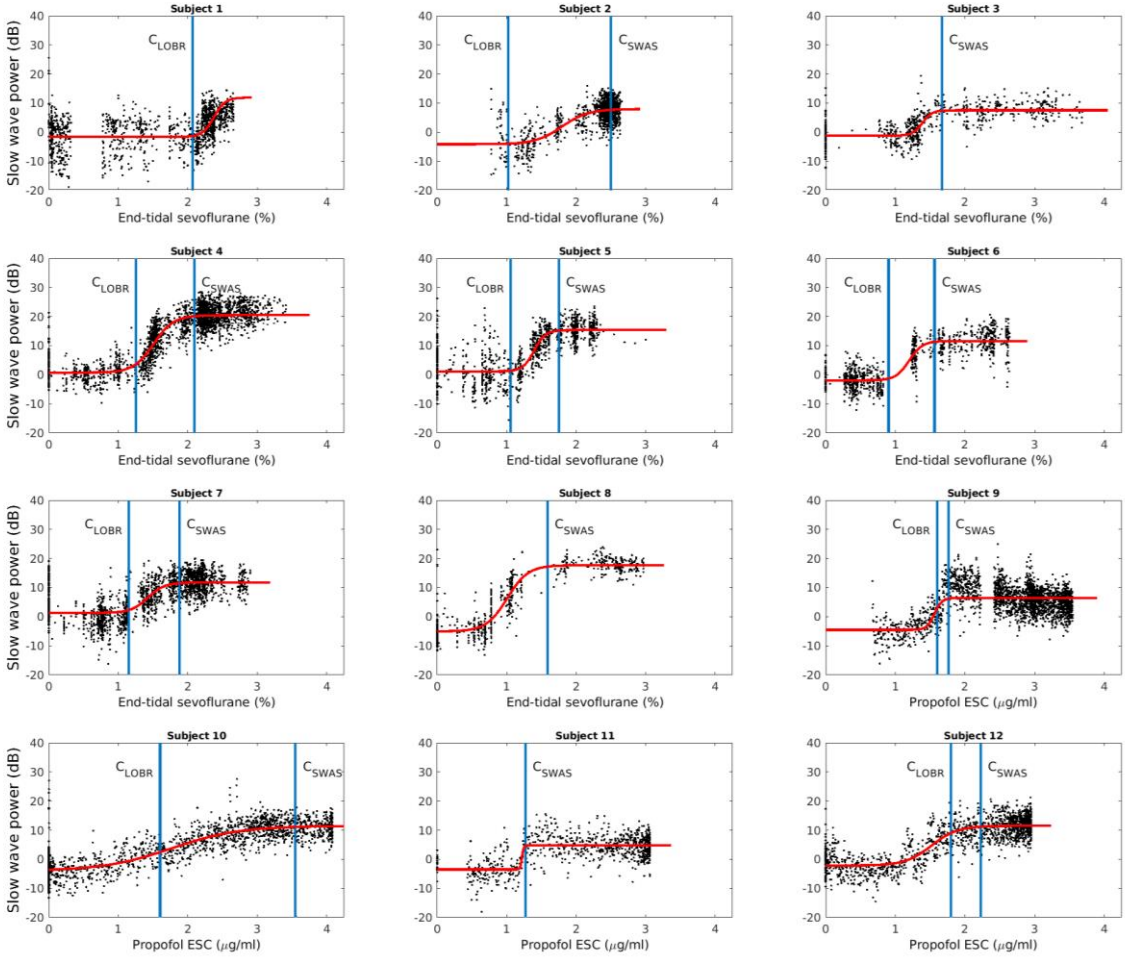

Figure 3.2: Slow wave power plotted as a function of anaesthetic concentration, with offline fits of the SWAS Bayesian sigmoid function (Equation 2). C_{LOBR} is the concentration at which each patient lost responsiveness to the modified IFT (first negative response). C_{SWAS} is the concentration at SWAS defined as the 95% of the plataeu of slow wave power.

Importantly, no patients responded to the IFT prompt after SWAS was achieved. In three patients (subjects 3, 8, and 11), an accurate concentration of loss of responsiveness could not be determined as the gap in concentration between the last positive and the first negative response was too high (>0.5% sevoflurane or

>0.5µg/ml propofol). The mean±SD concentration for loss of responsiveness, C_{LOBR}, was 1.2±0.4% end-tidal sevoflurane and 1.6±0.1µg/ml of propofol.

A boxplot visualising the variability of the parameters that describe the SWAS sigmoid curve, r, s, t, and u, is shown in Figure 3.3. In the sevoflurane group, mean±SD values for each parameter were: r = -1.3±2.6dB, s = 13.2±4.9, t = 1.4±0.3% end-tidal, u = 0.12±0.04. In the propofol group, the mean±SD parameter values were r = -3.6±1.0dB, s = 8.6±3.4dB, t = 1.5±0.2µg/ml, u = 0.19±0.21.

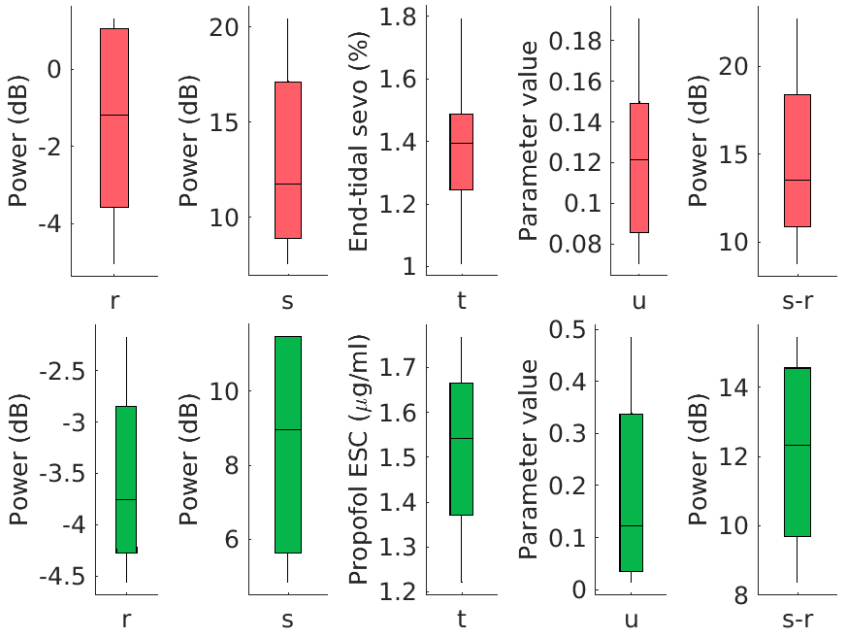

Figure 3.3: Study 1 SWAS sigmoid parameter variability for the sevoflurane group (top) and the propofol group (bottom). r is the initial slow wave power and s is the slow wave power at saturation, t is the anaesthetic concentration at half-saturation, and u is inversely related to the steepness of the sigmoid curve. The steepness of the curve is calculated as $tan^{-1}[(s-r)/4u\,]$ *in degrees. s-r is the change in slow wave power.*

3.3.2 Study 2

3.3.2.1 Participants

In total, 24 participants attended all three sessions. Two EEG-MRI sessions were aborted prior to onset of anaesthetic delivery due to computer failure; one participant was re-enrolled and completed participation in the study at a later date. Thus, 23 participants in total were administered sevoflurane guided by the SWAS prototype system in the MRI scanner. An annotated spectrogram of the EEG for an example subject is shown in Figure 3.4 to illustrate a typical anaesthesia EEG-MRI session.

3.3.2.2 Real-time titration to SWAS

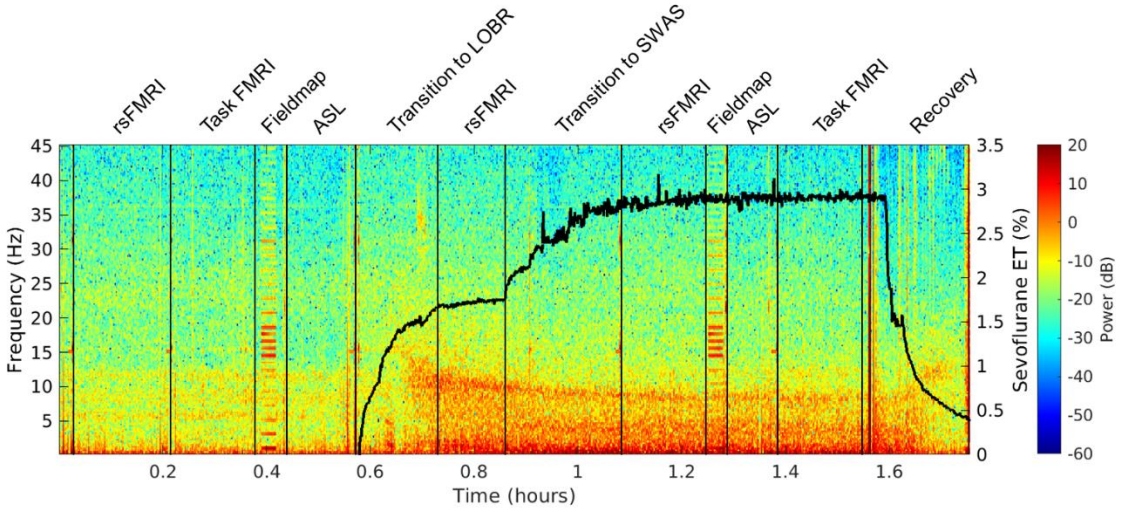

Figure 3.4: Annotated spectrogram of the cleaned EEG acquired over the course of the anaesthesia session from an example subject. Vertical black lines indicate the beginning and end of each acquisition. Above each section is the label for the corresponding acquisition. End-tidal sevoflurane concentration is plotted as the thick black line against the right y-axis.

Four sessions were aborted prior to the participants reaching deep levels of sedation; three of these were due to excessive hyperexcitability around loss of responsiveness and one due to airway obstruction.

One additional participant reached deep sedation, but excessive artefacts due to snoring-induced movements within the magnetic field made slow wave power estimates unreliable. For one further participant (Subject 13), the Cz electrode was used to identify SWAS instead of the Fz electrode due to poor signal quality. This participant was included in subsequent analyses involving C_{SWAS}, but not in analyses of P_{SWAS} or the r, s, t, and u parameters.

Finally, in one participant end-tidal gas measurements were of insufficient quality to model SWAS. In total, deep sedation and EEG signal quality sufficient to model SWAS post-hoc was achieved in 18 participants (Figure 3.5). One session was aborted due to concerns about the participant's CO_2 levels after reaching SWAS, but before neuroimaging at SWAS could be completed.

All participants lost behavioural responsiveness to beeps at a lower concentration of sevoflurane than the concentration required to achieve SWAS. Furthermore, no participants responded to the IFT when held at the SWAS end point.

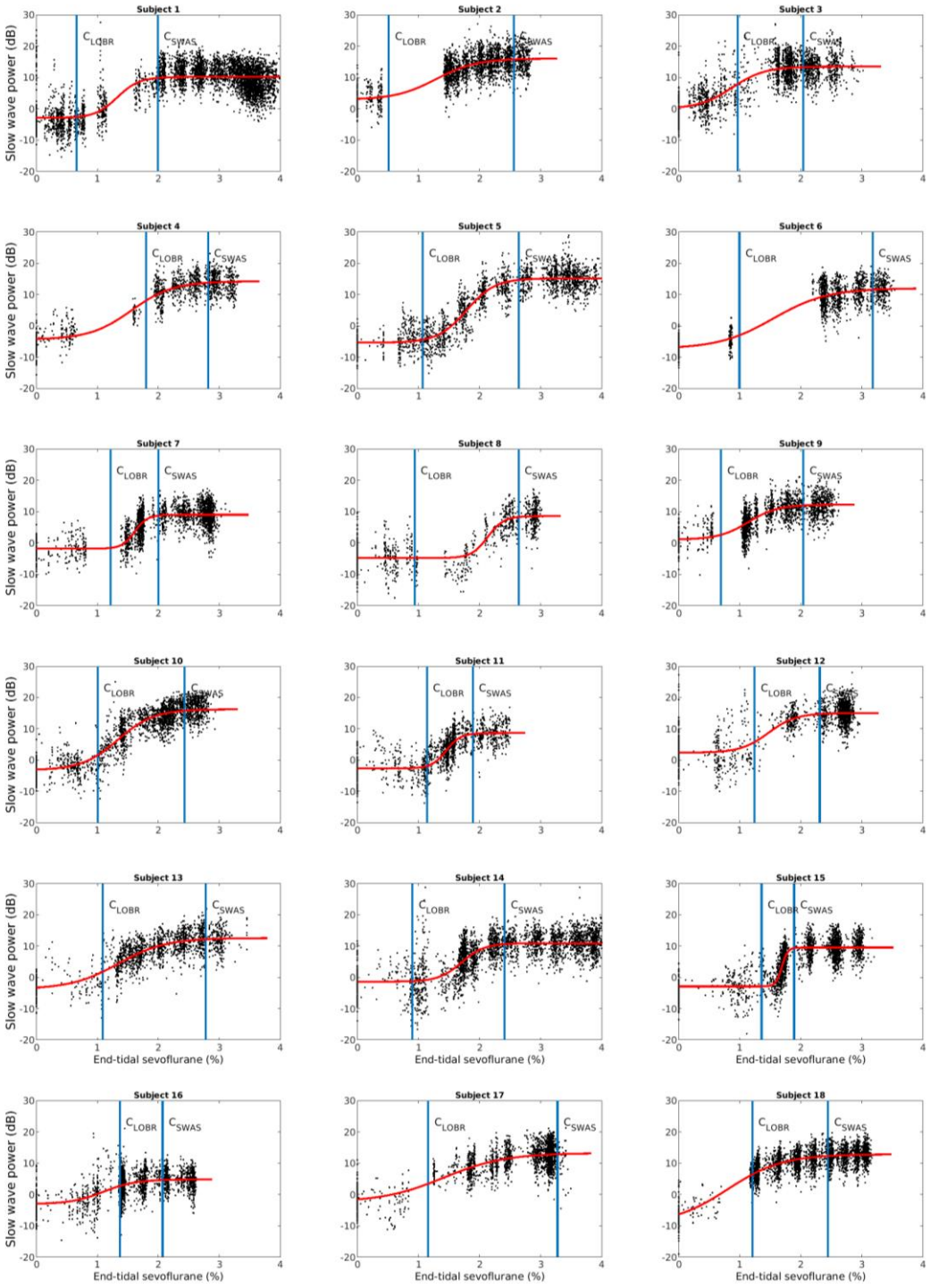

Figure 3.5: Slow wave power plotted as a function of anaesthetic concentration, with offline fits to the SWAS Bayesian sigmoid function (Equation 2). C_{LOBR} is the concentration each participant lost responsiveness to beeps. C_{SWAS} is the concentration of SWAS defined as the 95% of the plataeu of slow wave power.

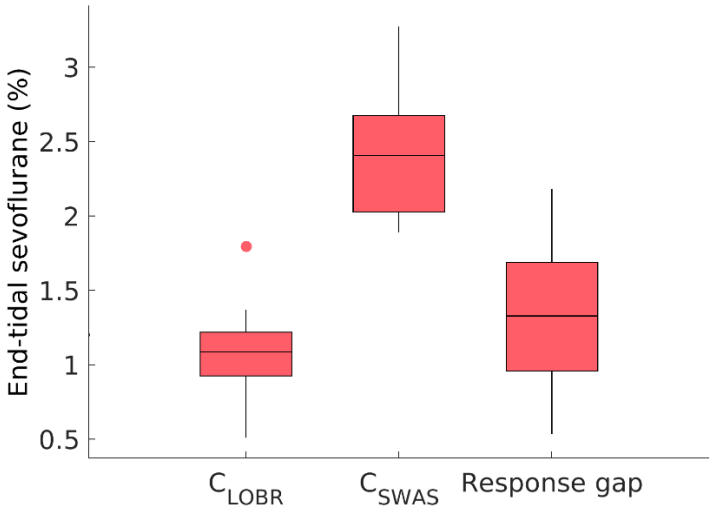

Figure 3.6: Interindividual variability in C_{LOBR}, C_{SWAS}, and the SWAS response gap (difference between C_{SWAS} and C_{LOBR}) in Study 2.

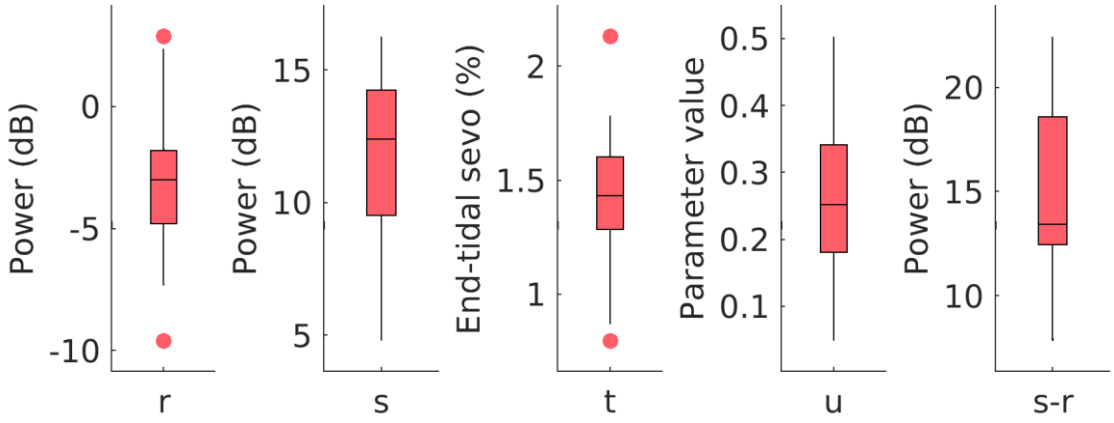

Figure 3.7: Study 2 SWAS sigmoid parameter variability. r is the initial slow wave power and s is the slow wave power at saturation, t is the anaesthetic concentration at half-saturation, and u is inversely related to the steepness of the sigmoid curve. The steepness of the curve is calculated as $tan^{-1}[(s-r)/4u]$ in degrees. s-r is the change in slow wave power.

3.3.2.3 Post-hoc identification of SWAS

Individual post-hoc model fits for each participant are shown in Figure 3.5. C_{LOBR} was mean±SD 1.09±0.31 and C_{SWAS} was 2.38±0.44, with a SWAS response gap of 1.30±0.51 (see Figure 3.6). A boxplot visualising individual SWAS sigmoid parameter values is shown in Figure 3.7. Mean parameter values were r = -2.8±3.4dB, s = 11.8±3.1dB, t = 1.4±0.3% end-tidal, u = 0.27±0.1.

3.3.2.4 Ability to hold participants at SWAS

A Bland-Altman analysis was performed to assess the agreement between C_{SWAS} and the actual measured concentration during the ASL (Figure 3.8A), task FMRI (Figure 3.8B), and resting state FMRI (Figure 3.8C) acquisitions. These were used to inform inclusion in subsequent neuroimaging analyses reported in Chapter 3, 4, and 5. As a whole, participants were held at a concentration that was higher than that required to reach SWAS, as indicated by the 95% confidence interval around the bias line (solid line) not overlapping with the line of agreement (dotted line). From the Bland-Altman plot there is no apparent proportional bias, i.e., the degree of agreement does not change over the range of measurements. The relative deviation of the sevoflurane concentration measured during each MRI acquisition and C_{SWAS}, calculated as the mean average percentage error (MAPE) is shown in Figure 3.8D.

Overall, 15 of the 17 participants who completed neuroimaging at SWAS were determined to be held at SWAS during the ASL and task FMRI acquisitions and 14

of 17 during the resting state FMRI acquisition. This was defined as MAPE < 35% if overshooting SWAS and MAPE < 10% if undershooting SWAS.

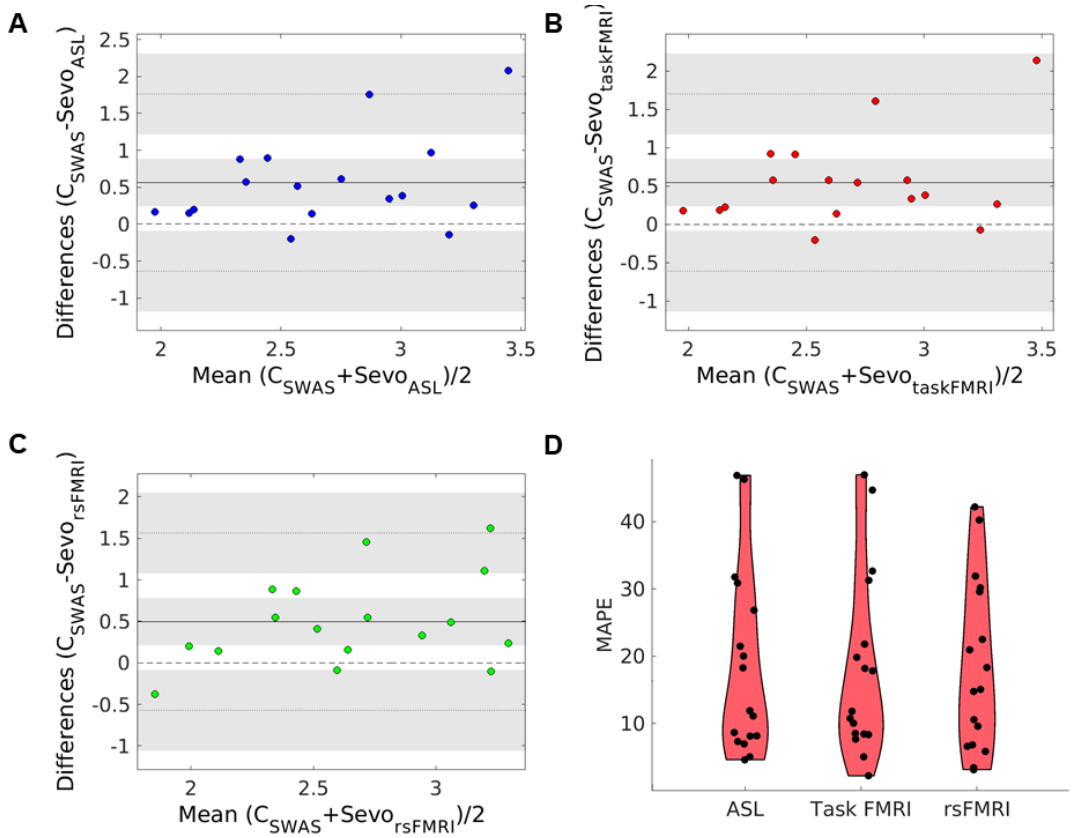

Figure 3.8: Bland-Altman plots comparing C_{SWAS} estimated offline to the end-tidal sevoflurane concentration measured during the ASL (A), task FMRI (B), and resting state FMRI (C) acquisitions at SWAS. Bland-Altman plots visualise agreement between two methods. In this case, the measured sevoflurane concentration is compared to target concentration, i.e., C_{SWAS}. The line of equality (dashed line) indicates perfect agreement between the methods. The bias (solid line) indicates the mean deviation from the line of equality. The lines of agreement (dotted lines) around the bias encompass 95% of measurements (±1.96 standard deviations). The 95% confidence intervals (CIs) around the lines of agreement and the bias are shown in grey. When the line of equality is outside the 95% CI around the bias, the measures are significantly different. D: Violin plots showing individual mean average percentage error between the end-tidal sevoflurane concentration measured during the ASL, task FMRI, and resting state FMRI acquisitions at SWAS.

3.3.3 Factors predicting susceptibility to anaesthesia

We assessed the association between different individual factors and the SWAS parameters (C_{SWAS} and P_{SWAS}) calculated post-hoc.

3.3.3.1 Age

In study 1, we found a significant negative correlation between age and P_{SWAS}, i.e., absolute slow wave power at SWAS, when analysing both groups together (r = -0.76, p<0.05; Figure 3.9). There was no significant correlation between age and C_{SWAS}. In study 2, there was no significant correlation between age and either P_{SWAS} or C_{SWAS} (r = -0.35, $p > 0.05$).

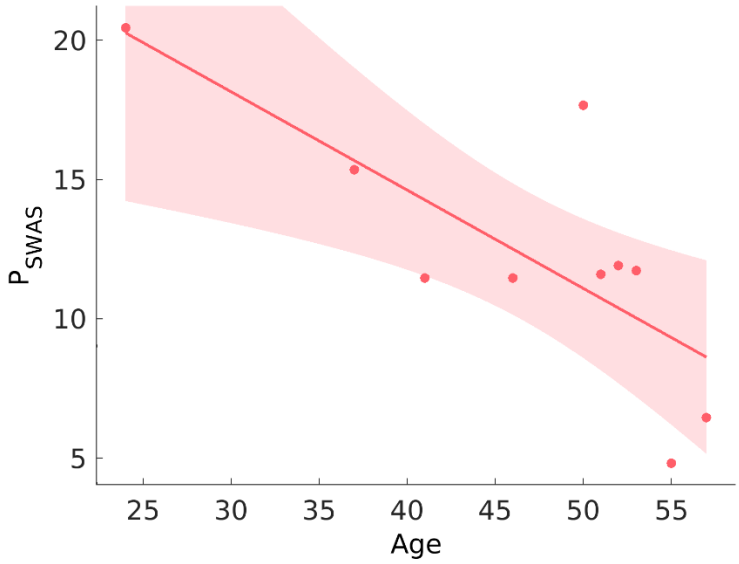

Figure 3.9: Correlation between age and slow wave power at SWAS (P_{SWAS}) in Study 1 (sevoflurane and propofol group combined; r = -0.76, p<0.05).

3.3.3.2 Personality traits

In Study 1, there were no questionnaire measures that were significantly correlated with either C_{LOBR} or C_{SWAS} when adjusting for multiple testing (Table 3.2). However, when not correcting for multiple testing, C_{SWAS} was significantly correlated with the STAI trait component ($p = 0.03$).

Table 3.2: Summary of correlation analyses between each Study 1 questionnaire scale or sub-scale (rows) and C_{LOBR} (left column) and C_{SWAS} (right column). APAIS = The Amsterdam Preoperative Anxiety and Information Scale, STAI Trait = State and Trait Anxiety Inventory – trait component, PSQI = Pittsburgh Sleep Quality Index, TAS = Tellegen Absorption Scale. P-values adjusted for Benjamini-Hochberg false discovery rate.

	C_{LOBR}		C_{SWAS}	
	r	*p*	*r*	*p*
APAIS Anxiety	-0.04	0.93	0.28	0.49
APAIS Need For Information	0.62	0.44	0.44	0.34
APAIS Last Night Sleep Quality	0.38	0.87	0.36	0.41
STAI Trait	-0.14	0.87	0.65	0.19
PSQI	0.20	0.87	0.45	0.34
TAS	-0.15	0.87	0.16	0.63

In Study 2, we found that there was a significant correlation between C_{LOBR} and the “powerful others” subscale of the LOC inventory (Table 3.3). No other questionnaire scales were significantly correlated with either C_{LOBR} or C_{SWAS} when correcting for multiple testing. However, if not correcting for multiple testing, there

were significant correlations between C_{SWAS} and both the LOC internal control (p = 0.02) and chance (p = 0.02) subscales.

Table 3.3: Summary of correlation analyses between each Study 2 questionnaire scale or sub-scale (rows) and C_{LOBR} (left column) and C_{SWAS} (right column). STAI = State and Trait Anxiety Inventory, PSQI = Pittsburgh Sleep Quality Index, TAS = Tellegen Absorption Scale, LOC = Locus of Control scale. P-values adjusted for Benjamini-Hochberg false discovery rate.

	C_{LOBR}		C_{SWAS}	
	r	*p*	*r*	*p*
STAI Trait	0.01	0.69	0.04	0.88
STAI State	-0.17	0.36	0.40	0.26
PSQI	0.07	0.69	0.21	0.64
TAS	0.26	0.69	-0.17	0.64
LOC Internal Control	0.00	0.58	-0.53	0.08
LOC Powerful Others	-0.66	0.03	0.26	0.57
LOC Chance	-0.01	0.69	0.54	0.08

3.4 Discussion

3.4.1 Time to achieve SWAS

On average it took 20 minutes from anaesthetic onset to the hold at SWAS. By comparison, surveys of anaesthesia inductions have reported approximately half that time from anaesthetic onset to being surgically ready in cases of tracheal intubation and laryngeal mask placement (Koenig et al., 2011; Schuster et al., 2008). While this is a substantial time difference, it is reasonable to expect that first time application of a prototype will yield suboptimal performance, and that improvements in technique and to the SWAS titration system itself can bring down the time to SWAS. Nevertheless, as titrating to a brain-based endpoint is

inherently more complex than current clinical practice, some added induction time is to be expected even in an ideal scenario.

Anaesthetic room and operating theatre time is limited by economic constraints, and therefore making efficient use of this time is a high priority for hospital administrations. However, it has been noted that 5 to 15 minute changes to the time spent in the anaesthetic room has a very small effect on operating room efficiency (Dexter & Wachtel, 2006; Overdyk et al., 1998; Schuster et al., 2008). Moreover, operating room costs are not the only costs associated with a surgery (Macario et al., 1995). If approximately half of patients receive twice as much anaesthesia as necessary, assuming complete perception loss at SWAS (Warnaby et al., 2017), some costs could be recuperated by reducing the amount of anaesthesia used. Furthermore, as over-anaesthesia has been found to predict increased time to discharge, titrating to SWAS could reduce hospital costs associated with post-operative recovery (Dexter et al., 1999). To properly assess costs associated with titrating anaesthesia to SWAS compared to standard clinical practice, a much more extensive clinical trial is needed.

3.4.2 Accuracy of SWAS titration

In Study 1, five of the six patients in the sevoflurane group that were held at SWAS were held within 35% of SWAS, indicating relatively high accuracy. As approximately 50% of patients receive twice as much anaesthesia as is required to reach SWAS (Warnaby et al., 2017), this constitutes a significant improvement over current clinical practice, assuming the dose required to reach SWAS is

optimal. It is worth noting that the patient who had the largest overshoot, Subject 8, also had the shortest induction time. While anecdotal, it may be an indication of a trade-off between time to SWAS and accuracy.

Comparatively, titrating propofol to SWAS proved more challenging. A stable hold was achieved in only two of the four patients in the propofol group. Furthermore, the MAPE for those two patients was higher than the average for the sevoflurane group. The primary cause of this issue was the delay in anaesthetic action making it challenging to prevent increased effect site concentration past the point of SWAS, as opposed to a failure to detect SWAS. It is probable that this issue was in part exacerbated by the decision to perform a manually-controlled infusion with propofol PD/PK modelling within the prototype SWAS system instead of using target-controlled infusion. However, due to the COVID-19 pandemic preventing completion of the study, we were unable to explore improvements to the way we titrated propofol to SWAS. This will now be the focus of a much larger clinical study.

In Study 2, anaesthesia was titrated to SWAS so that neuroimaging could be performed in the brain state of interest as opposed to a pre-determined anaesthetic concentration. Therefore, it was crucial to ensure that the end-tidal concentration measured during each MRI acquisition was close to SWAS. The Bland-Altman analysis performed for each acquisition showed that participants were on average at a slightly higher concentration than was required to achieve SWAS. This was anticipated in advance, as one can only confirm saturation by

seeing an increase in concentration with no increase in slow wave power. Nevertheless, a total of 15 participants were within the threshold for inclusion in analyses of the ASL and task FMRI acquisitions and 14 participants for the resting state FMRI analyses.

3.4.3 Lack of behavioural responsiveness at SWAS

In Study 2, all participants lost responsiveness to beeps prior to reaching SWAS (N=18). Moreover, in Study 1, no patients gave a positive IFT response after reaching SWAS (N=11), and in Study 2 no participants responded to the IFT when held at SWAS (N=15). This is in line with the study where SWAS was initially discovered (Mhuircheartaigh et al., 2013), in which all participants lost responsiveness to a word discrimination task at lower concentrations of propofol than SWAS (N=16 and N=12).

While altogether these studies still represent a relatively small number of subjects, and assessments of IFT responsiveness at SWAS in a larger sample is needed, it is notable that in studies using commercial depth of anaesthesia monitors in comparable samples fail to discriminate IFT responders and non-responders (Linassi et al., 2018). A recent meta-analysis of studies assessing intraoperative awareness using the IFT found across studies that 76 of 124 (61.2%) of patients receiving brain monitor-guided anaesthesia responded to the IFT at any time during anaesthesia, compared to 269 of 542 patients (49.6%) (Linassi et al., 2018). One caveat is that almost all the included studies that used brain monitoring used the BIS.

Furthermore, it is worth noting that all except one of the studies in the meta-analysis that included a BIS monitor had a target range within the recommended range for preventing awareness under general anaesthesia (i.e., 40 to 60), with reported incidences of positive IFT responses even towards the lower end of the range. While targeting values below this range is possible, there is likely a trade-off between preventing positive IFT responses and risking over-anaesthesia. The anaesthetic concentrations required to achieve SWAS in the present studies are considerably higher than those reported in studies included in Linassi et al. (2018). However, all of the studies included an opioid co-induction agent, with the exception of Zand et al. (2014), where the sevoflurane concentration used was comparable to our studies. As opioids were not administered as part of the titration to SWAS in the present studies, the effect of anaesthetic potentiation of the opioid likely accounts for this difference, although a direct comparison of dosages is not possible.

The BIS has been found to decrease below levels recommended to prevent intraoperative awareness during administration of a neuromuscular block in fully conscious individuals (Messner et al., 2003; Schuller et al., 2015). Beyond implying that the BIS index doesn't completely discriminate between conscious and unconscious states, this is particularly problematic as neuromuscular blockers are routinely co-administered alongside anaesthetic agents.

However, it should be noted that while the IFT is commonly interpreted to indicate at least some degree of connected consciousness, it has been argued that the IFT

doesn’t require consciousness equivalent to a fully conscious person (Pandit et al., 2015). IFT responders often show no spontaneous movement, leading some to argue IFT responses in absence of spontaneous movement to represent a distinct brain state (“dysanaesthesia”) (Pandit, 2013, 2014).

Nevertheless, the IFT remains a gold standard for detecting intraoperative awareness, particularly in the presence of neuromuscular blockers (Linassi et al., 2018). However, cases of intraoperative awareness with recall are much more prevalent than without recall, and whether intraoperative awareness without recall is a clinical problem is controversial (Mashour & Avidan, 2015). It has been argued that intraoperative awareness might have psychological sequalae such as PTSD even in the absence of recall (M. Wang et al., 2012). Besides clinical considerations, there is also a philosophical question whether intraoperative awareness without recall is ethically tenable (Mashour & Avidan, 2015).

The clear dissociation of loss of responsiveness and SWAS suggests that SWAS either meets or exceeds these clinical and ethical requirements for loss of awareness, and therefore further supports SWAS as a clinical target for titration of anaesthesia. However, behavioural responsiveness at SWAS has yet to be assessed while maintaining anaesthetic concentrations to individual SWAS levels during surgical procedures in the presence of opioids and neuromuscular blockers. This will be a key clinical outcome measure in future development of the SWAS metric as a clinical endpoint for anaesthesia delivery.

3.4.4 Relationship between responsiveness and SWAS

Interestingly, there was no correlation between C_{LOBR} and C_{SWAS} in either study. This implies that the concentration of anaesthesia required at each stage in the transition from wakefulness through loss of responsiveness to SWAS is not proportional from individual to individual. If SWAS indeed constitutes a state of perception loss under general anaesthesia, this further emphasises the distinction between loss of responsiveness and loss of consciousness (Sanders et al., 2012). Loss of responsiveness has previously been linked to loss of stimulus-evoked activity in the dorsal anterior insula (Warnaby et al., 2016), from which the authors hypothesised that anaesthesia induces loss of responsiveness from a loss of selfhood. Moreover, this has implications for what is meant by susceptibility to anaesthesia, as one's relative susceptibility to becoming unresponsive may be different from one's relative susceptibility to loss of consciousness.

3.4.5 Susceptibility to anaesthesia

Different individuals require different doses of anaesthesia in order to lose conscious perception of the outside world. This is partly due to different amounts of anaesthesia being required to achieve the same effect site concentration. However, even when accounting for this, some individuals are more susceptible to anaesthesia than others.

We found that having low faith in powerful others was associated with requiring a higher anaesthetic dose to lose responsiveness to beeps. This is in line with a previous study in women undergoing minor gynaecological surgery, where low

faith in powerful others predicted increased requirement of propofol anaesthesia dose to induce loss of consciousness (operationalised as loss of eyelash reflex) (Abbott & Abbott, 1995). Although not significant after correcting for multiple testing, we found an indication that people who had low internal locus of control may require a higher dose of sevoflurane to reach SWAS. This goes against our hypothesis and is in contrast to Abbott and Abbott (1995), who found that high internal locus of control predicted increased requirement of anaesthesia. However, we found no association between internal loss of control and loss of behavioural response, which may be a closer analogue to the loss of eyelash reflex definition used in their study.

No other questionnaire measures in our study were significantly correlated with either loss of responsiveness or SWAS. However, we note that if not correcting for multiple testing, C_{SWAS} was positively correlated with the STAI trait component in Study 1 and the state component in Study 2. Considering the relatively low sample size with respect to questionnaire data, and as there has previously been found a relationship between anaesthetic susceptibility and worry about anaesthesia (Abbott & Abbott, 1995), anxiety remains a trait of interest for future development of SWAS in larger samples.

3.4.6 Informing SWAS model initiation for real-time operation

Inherent to the Bayesian formulation of the SWAS model is that initial values for each of the r, s, t, u, and τ parameters have to be set (i.e., the priors). The model includes an error term that determines the degree to which the model trusts the

data versus the prior, which allows dynamic compensation of imperfect initial values. Regardless of this, any improvement that can be made in accurately defining the initial state of the model is key to more efficiently titrating anaesthesia to SWAS.

The r parameter simply reflects slow wave power at baseline and can therefore be measured before onset of anaesthesia delivery without requiring extra equipment. This was shown to be viable in practice in both Study 1 and Study 2, where baseline measures of slow wave power were acquired and used as the initial value for r.

The s parameter reflects slow wave power at SWAS, i.e., P_{SWAS}. Therefore, factors that influence or are predictive of individual P_{SWAS} can be used to inform the initial value of the s parameter. We found a strong negative correlation between P_{SWAS} and age in Study 1 ($r = -76$). This finding replicates previous work in our lab, in which a similarly strong relationship was found ($r \approx 0.6$) (Warnaby et al., 2017). Although it was trending in the same direction, no significant correlation between P_{SWAS} and age was found in Study 2. However, this could be explained by the age range in Study 2 being much narrower (age range 19 to 35, mean±SD 24.5±4.8) compared to Study 1 (24 to 57, mean±SD 46.6±10.1) and Warnaby et al. (2017) (age range 18 to 90). Therefore, age is an easily obtainable variable that could improve initialisation of s. However, slow wave power at baseline was not significantly correlated with slow wave power at SWAS and is therefore unlikely to be useful for setting the initial value for s.

We can also theorise further predictions that could not be assessed in the present studies. Firstly, co-administered opioids are known to potentiate anaesthetic action so that a lower concentration of the hypnotic agent is required to achieve loss of responsiveness (Bouillon, 2008). Similarly, co-administration of opioids have been found to reduce the anaesthetic concentration required to reach SWAS (Warnaby et al., 2017). Consequently, the concentration at half-saturation, t, is proportionally reduced. Additionally, as P_{SWAS} is not different with and without co-administration of opioids (Warnaby et al., 2017), the slope of the sigmoid curve would likely also increase. Therefore, in future application of the model with co-administration of opioids, the initial values of t and u should be adjusted.

In conclusion, the real-time SWAS prototype system for titrating anaesthesia to SWAS was successfully applied in a pre-surgery study and a laboratory EEG-MRI study. No patients or participants were responsive when held at their SWAS endpoint or had any recollection of events that occurred after being titrated to SWAS. When corrected for multiple comparisons in this small sample, faith in powerful others was the only personality trait that correlated with measures of anaesthetic susceptibility. However, internal control and chance LOC subscales, as well as state and trait anxiety, stood out as traits of interest to investigate in larger samples. Finally, it was discussed how initialisation of the real-time SWAS model could be improved by measuring baseline slow wave power, predicting slow wave power at SWAS from age, and accounting for co-administered opioids.

4 Altered cerebral blood flow at SWAS

4.1 Introduction

Anaesthetic agents differ significantly in their pharmacological properties and their influence on the body's physiology. FMRI has been used to study anaesthesia-induced loss of consciousness, either at rest (e.g. Palanca et al., 2015) or in response to stimulation (e.g., Mhuircheartaigh et al., 2013). Changes in the FMRI blood oxygenation level dependent (BOLD) signal are used as a proxy for changes in neuronal activation (or deactivation) due to anaesthesia (Logothetis & Wandell, 2004). However, alterations in cerebral blood flow (CBF) of non-neuronal origin can potentially confound these resting-state or task-based FMRI analyses (Aksenov et al., 2015; van Alst et al., 2019). Accounting for these non-neuronal CBF changes is therefore important for the study of anaesthesia-induced loss of consciousness. It also has additional relevance for the field of animal neuroimaging where anaesthesia is often used for sedation (Austin et al., 2005).

Several different techniques have been used to assess changes in CBF due to anaesthesia, including transcranial Doppler flowmetry (TCD) (Conti et al., 2006; Matta et al., 1999), near infrared spectroscopy (NIRS) (Kondo et al., 2016), and positron emission tomography (PET) (Kaisti et al., 2002, 2003). Comparing across techniques, it is clear the various anaesthetic agents have differential effects on CBF. Furthermore, in the case of volatile (inhalational) anaesthetics, there are complex dose-dependent interactions due to direct and indirect drug effects (Matta

et al., 1995, 1999). Arterial spin labelling (ASL) is a non-invasive MRI technique that allows the quantification of cerebral CBF on conventional MRI scanners without the need for specialised hardware. It is, therefore, an ideal choice to be used alongside FMRI to quantify changes in cerebral vasculature due to anaesthesia. Despite this, ASL has seen only limited application in the study of anaesthesia in humans (Qiu et al., 2008; Ramani et al., 2007; Saxena et al., 2019) and rarely at anaesthetic doses that would be used to during surgery (Makki et al., 2019; Qiu et al., 2017).

As discussed in Chapter 1 (Section 1.3), anaesthesia and other altered states of consciousness induce profound changes in the spectral content of the brain's electrical activity, as can be measured non-invasively using electroencephalography (EEG) (Purdon, Sampson, et al., 2015). However, the neurophysiological relationship between electrical activity and cerebral blood flow has not been fully explored, especially under anaesthesia. During wakeful resting, a frequency-specific coupling between EEG power and CBF has been found, with lower frequencies being negatively correlated with CBF (O'Gorman et al., 2013). Slow waves during sleep have also been found to be negatively associated with CBF in the prefrontal cortex and positively correlated with CBF in the lingual gyrus (Tüshaus et al., 2017).

As part of our combined EEG-MRI study in healthy volunteers undergoing sevoflurane anaesthesia, we developed a novel pulsed arterial spin labelling (PASL) sequence that was compatible with concurrent EEG recordings to assess

changes in the global and regional CBF under sevoflurane anaesthesia. As mentioned earlier, anaesthesia was titrated to the SWAS endpoint on an individual basis using real-time EEG feedback. This controls for inter-individual differences in anaesthetic susceptibility and allows us to identify dose-dependent CBF effects in a common brain state. Finally, we assessed the relationship between EEG slow wave power at SWAS and changes in cerebral blood flow during sevoflurane anaesthesia.

4.2 Materials and methods

All data that are analysed in this chapter were acquired as part of Study 2, as described in Chapter 3 (Section 3.2.3). The data presented here were acquired in three conditions over the two sessions. In the evening baseline session, ASL data were acquired while the participants were awake breathing room air (awake air condition). In the anaesthesia session, ASL data were collected when participants were breathing 100% oxygen (awake O_2 condition) and anaesthetised with a sevoflurane and 100% O_2 mix delivered to the SWAS EEG endpoint (SWAS condition).

4.2.1 Data acquisition

4.2.1.1 MRI

All MRI data were acquired in a Siemens 3T Prisma MR scanner with a 64-channel head coil. For both sessions, subjects were positioned with the isocentre shifted 4cm axially towards the feet relative to the standard inion position. This is in line with current best practices for concurrent EEG-MRI (Mullinger et al., 2013).

We developed a new EEG compatible, single-delay pulsed arterial spin labelling (PASL) sequence, which is compliant with the current White Paper recommendations (Alsop et al., 2015). This contribution was made by Prof. Mark Chiew. PASL sequences magnetically label blood water travelling through brain-feeding arteries by inverting the blood magnetisation using a relatively short radio frequency pulse. In our sequence, the duration of this inversion pulse is extended relative to a standard inversion pulse so that the peak radio frequency voltage is reduced (see Figure 4.1). This results in lower power deposition to the EEG electrodes and amplifier, reducing the likelihood of amplifier saturation resulting in data loss, as well as electrode heating and damage to the amplifier.

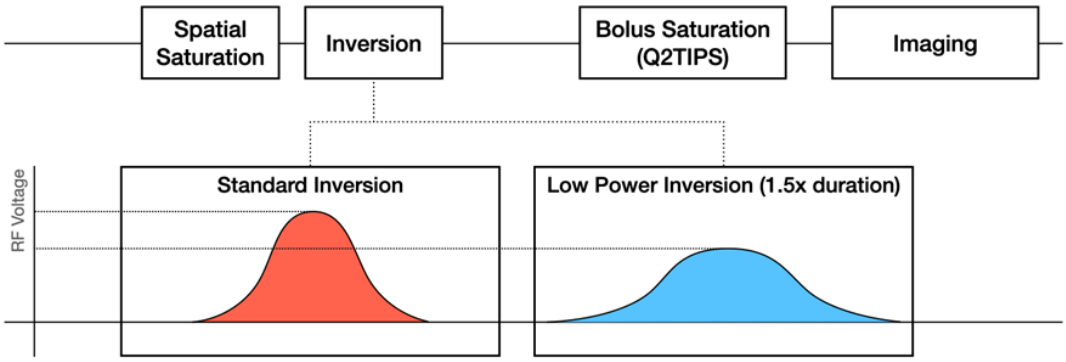

Figure 4.1: Schematic of the novel EEG compatible pulsed arterial spin labelling (PASL) sequence. The sequence uses a longer duration (1.5×) but lower power inversion pulse compared with standard PASL techniques to ensure that radio frequency (RF) voltage is kept within safe limits and does not cause unnecessary tissue heating at the EEG electrode sites.

The 5 minute PASL sequences had the following parameters: bolus duration = 0.8s, inversion time = 1.8s, single shot echo planar imaging (EPI), repetition time (TR) = 3s, echo time (TE) = 56ms, 6/8 partial Fourier, FOV = 224 × 224, matrix

size = 64 × 64, 20 ascending slices, slice thickness = 6mm, slice gap = 10%, slice acquisition time = 46.5ms, 50 tag-control pairs. The bolus duration was fixed using QUIPSSII. An initial proton-density-weighted calibration image without labelling or background suppression, but otherwise identical parameters to the PASL images, was also acquired.

A T_1-weighted structural image was acquired in the baseline session for the purpose of registration and tissue-type segmentation with the following parameters: TR = 2500ms, TE = 4.7ms, flip angle = 8°, voxel size = 1mm^3. Gradient-echo field map images for correction of B_0 distortions were acquired before each PASL acquisition using the following parameters: TR = 482ms, TE = 4.92/7.38ms, voxel size = 2mm^3, 49 interleaved ascending slices, flip angle = 46°.

4.2.2 Data analysis

4.2.2.1 Quantification of absolute CBF

For each subject, a high resolution T_1-weighted structural image was skull-stripped and tissue-type segmented using fsl_anat (Woolrich et al., 2009). Pre-processing of the ASL tag-control images for each condition was performed in BASIL (Chappell et al., 2009). A brain mask in ASL space was generated by linearly registering each subject's brain-extracted structural image to the ASL data. Corrections were applied for motion and EPI distortions (Jenkinson et al., 2002). Finally, pair-wise subtraction of tag-control image pairs was performed to generate CBF-weighted images.

Kinetic modelling of the labelled blood-water was applied to the tag-control subtracted images was performed for quantification of regional CBF. BASIL default parameter values for PASL data acquired at 3T were used (arterial transit time = 0.7s, $T1_{tissue}$ = 1.3s). For the scans acquired awake breathing room air, a $T1_{blood}$ = 1.65s was used (Zhang et al., 2013). For the acquisitions awake with O_2 delivery and at SWAS, a $T1_{blood}$ = 1.49s was used (Siero et al., 2015). Since QUIPSSII was used to fix the bolus duration, automatic estimation of bolus duration was not performed. As is appropriate with single-delay ASL data, correction for macro-vascular contamination was not applied nor was the arterial transit time estimated from the data.

Equilibrium magnetisation of arterial blood was estimated from the cerebrospinal fluid using a ventricle reference region in the calibration image. Lateral ventricle masks were generated from individual T_1-weighted images and transformed into ASL space. Where automated mask generation failed, ventricle masks were drawn in ASL space manually. To account for the PASL images being acquired with a non-zero echo time, corrections for T_2 decay was applied using BASIL default parameters ($T2_{CSF}$ = 750ms, $T2_{blood}$ = 150ms). Coil sensitivity was corrected for using bias field maps generated from individual T_1-weighted images. Finally, quantification of CBF in absolute units was performed, assuming an inversion efficiency of 0.98.

To increase accuracy of voxel-wise grey matter CBF estimates for calculation of whole-brain median grey matter CBF, partial volume correction was applied

(Chappell et al., 2011). Partial volume estimations from individual T_1-weighted images were generated with fsl_anat and transformed to ASL space by BASIL.

4.2.2.2 Offline EEG processing and analysis

EEG data recorded during the ASL acquisitions were cleaned up offline for gradient artefacts using moving template subtraction (Allen et al., 2000) in BrainVision Analyzer version 2.1 (BrainProducts GmbH), as was done for the EEG recorded during the transition from awake to SWAS reported in Chapter 3 (Section 3.2.4.1). Separate moving templates were generated for tag and control ASL images. The EEG data was then downsampled to 1kHz and cardioballistic artefact correction was also applied using moving template subtraction (Allen et al., 1998)

Further off-line EEG analysis was performed in MATLAB (MathWorks Inc.). The same processing steps that were applied to the EEG used for SWAS sigmoid curve fitting (see Section 3.2.4.1) was used for the EEG recorded during the ASL acquisition. In summary, A 6^{th} order zero-phase bandpass (0.1-45Hz) Butterworth filter was applied to each data segment prior to spectral decomposition using spectrogram.m (4s window, 3s overlap, 0.25Hz frequency bin size). The average of the frequency bins constituting the slow wave (0.5-1.5Hz) frequency bands was calculated for each window. Finally for each subject, the average slow wave power over all windows was calculated for time periods corresponding to the awake breathing O_2 and at SWAS ASL data acquisitions.

4.2.2.3 Physiological data

Peaks in the pulse and respiratory traces were identified using FSL's PNM tool (Brooks et al., 2008) and used to calculate mean heart rate and respiration rate for each subject and all conditions. Mean fractional inspired O_2 (FIO_2) and end-tidal CO_2 ($ETCO_2$) values for the awake breathing O_2 and at SWAS conditions were calculated for each subject. For each physiological parameter, statistical testing was performed using paired t-tests.

4.2.3 Statistical testing

4.2.3.1 Quantification of CBF changes

Absolute CBF maps were generated in native ASL space for the awake air, awake O_2, and SWAS conditions for each subject. These were transformed from native space to structural and Montreal Neurological Institute (MNI) space for group analyses using FNIRT (Andersson et al., 2007).

Median grey matter CBF was calculated for each individual from partial volume-corrected grey matter CBF maps. As CBF estimates are more accurate in voxels with one predominate tissue type, only voxels with >80% grey matter were included (BASIL default threshold). Paired t-tests for each pairing of the three conditions were run using permutation testing in FSL's randomise ($N_{permutations}$ = 5000). Correction for multiple testing was achieved using Threshold-Free Cluster Enhancement (TFCE) with default parameters (H = 2, E = 0.5, and C = 6) and a corrected voxel-wise significance threshold of $p<0.05$. Voxel-wise percentage

change in CBF from awake O_2 to SWAS was also calculated for each subject in standard space and averaged to generate a group map.

4.2.3.2 Correlations with slow wave power

Correlation analyses between individual EEG slow wave power estimates and whole-brain voxel-wise CBF estimates were performed for the O_2 and SWAS conditions. An additional correlation analysis between the change in slow wave power and change in CBF between the two conditions was also performed. Statistical testing was carried out using permutation testing ($N_{permutations}$ = 5000) with TFCE for cluster-based correction and a significance threshold of $p<0.05$.

4.3 Results

A total of 15 participants (age mean±SD 24.5±4.8; nine female) were included in the final group level analyses. The mean slow wave power (±SD) across subjects during ASL data acquisitions rose significantly from 2.8 (± 3.4) dB before anaesthesia delivery to 11.8 (± 3.1) dB at SWAS ($p<0.001$).

There was no significant difference in the measured inspired oxygen between wakefulness (mean±SD = 88.46±15.91%) and at SWAS (mean±SD = 91.51±6.89%, $p>0.05$). However, end-tidal CO_2 ($ETCO_2$) levels at SWAS (mean±SD = 50.04±16.33 mmHg) were significantly elevated compared to awake breathing O_2 (mean±SD = 37.46±3.74 mmHg, $p<0.001$). The respiration rate was significantly elevated at SWAS (mean±SD) compared to awake O_2 (mean±SD, $p<0.001$), but there was no significant difference in heart rate due to the

sevoflurane anaesthesia (awake O_2 mean±SD 59.8±12.2 beats/min vs. SWAS 65.8±14.5 beats/min, p>0.05).

4.3.1 Changes in cerebral CBF with sevoflurane anaesthesia

Whole-brain cerebral blood CBF maps for the three conditions (awake room air, awake O_2 and SWAS) are shown in Figure 4.2A. The median grey matter CBF was significantly decreased when awake breathing O_2 (median = 40.5 ml/min/100g, IQR = 13.8) compared to awake breathing room air (median = 53.2 ml/min/100g, IQR = 10.3, p<0.05). Conversely, the median grey matter CBF at SWAS (median = 72.7, IQR = 14.7) was significantly elevated above both the O_2 (p<0.001) and room air conditions (p<0.001). Median values were used because the distribution of grey matter CBF values was non-normally distributed (Figure 4.2B).

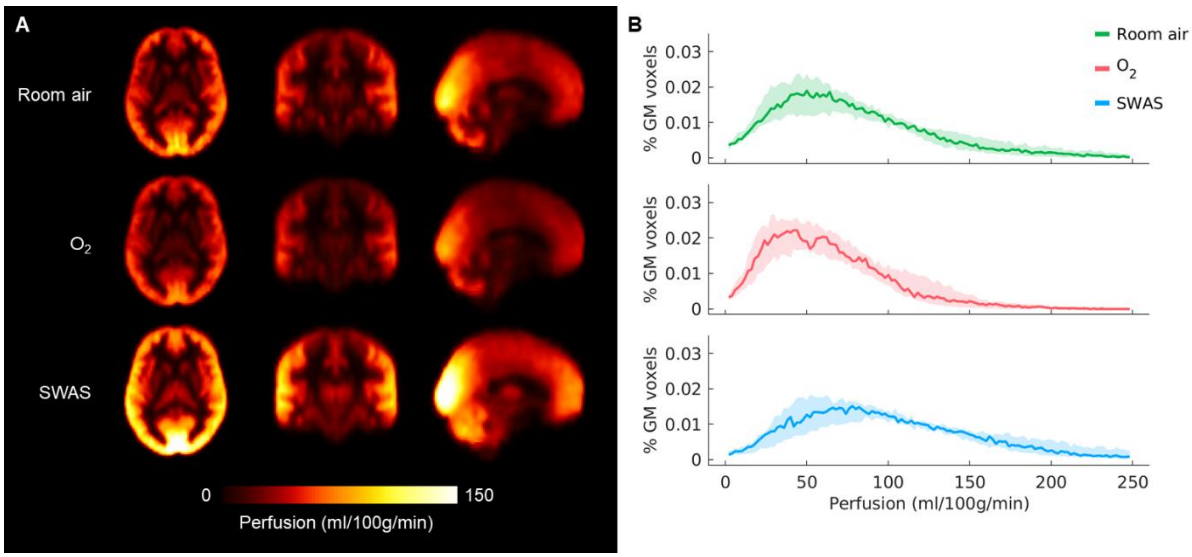

Figure 4.2: Mean absolute blood CBF for the room air, O_2, and SWAS conditions A) Voxel-wise group mean absolute CBF. Whole-brain absolute CBF maps are not corrected for partial volume effects by convention. B) Distribution of voxel-wise

grey matter CBF corrected for partial volume effects, with voxels with <10% grey matter excluded from the histograms. The solid line indicates the group median, and the shaded area indicates the inter-quartile range.

Voxel-wise statistical testing revealed significant regional alterations in CBF between conditions (Figure 4.3A). When awake breathing oxygen, there was reduced grey matter CBF in several localised regions when compared with breathing air. In particular, reduced CBF was observed in the bilateral medial occipital cortices, the parietal lobe, the posterior cingulate gyrus, the thalamus, and the lateral frontal cortex including the precentral gyrus (Figure 4.3A).

When comparing the wakeful breathing room air to the SWAS contrasts, some regional increases in grey matter CBF were apparent at SWAS (Figure 4.3B). These included CBF increases in the bilateral occipital and temporal cortices, the cingulate cortex, the supplementary motor cortex, the inferior prefrontal cortex, the cerebellum, the thalamus and the brainstem. While the CBF increases were largely bilateral, there were more widespread CBF increases in the left hemisphere. For example, CBF increases were present in the left primary somatosensory cortex, the motor cortex, and the premotor cortex were absent in the corresponding regions in the right hemisphere.

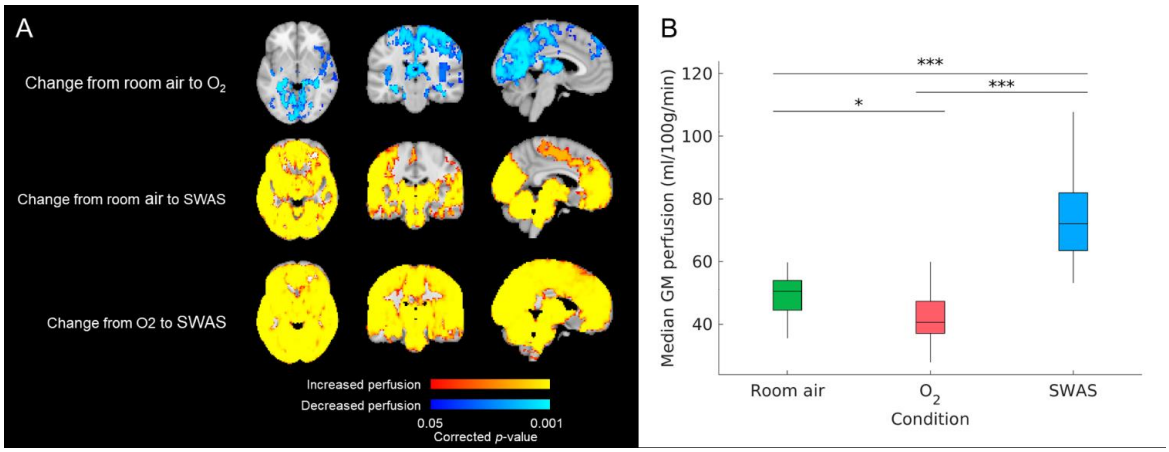

Figure 4.3: Alterations in cerebral blood flow due to sevoflurane and oxygen delivery. A) Group averaged statistical maps showing statistically significant changes in median grey matter CBF values ($p<0.05$) between contrasts. Only the contrast displayed here showed significant changes. B) Between-subject median grey matter CBF values corrected for partial volume effects. Individual grey matter CBF means were calculated from pure grey matter voxels which were defined as voxels with >80% grey matter.

When comparing wakeful breathing O_2 to SWAS (i.e., exploring the effect of sevoflurane), there were widespread increases in CBF at SWAS across all cortical and subcortical grey matter regions. Furthermore, no brain regions displayed any significant decreases in CBF. The largest regional percentage increases in grey matter CBF due to sevoflurane anaesthesia were found in the thalamus and the cerebellum Figure 4.4.

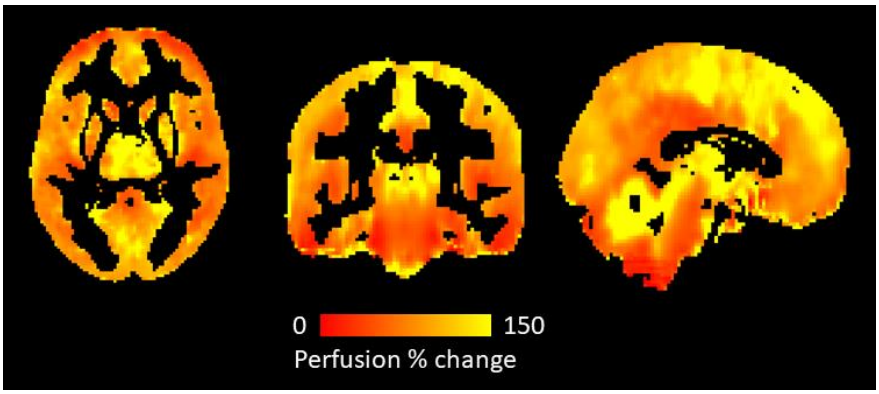

Figure 4.4: Regional percentage increases in grey matter CBF due to sevoflurane anaesthesia. The figure shows the group average voxel-wise percentage change in CBF from the O_2 to SWAS conditions in MNI space.

As noted above, end-tidal CO_2 was significantly elevated at SWAS compared to awake O_2 (Figure 4.5A). However, there was no significant correlation between the median grey matter CBF percentage change and the change in end-tidal CO_2 between the conditions across subjects (Figure 4.5B).

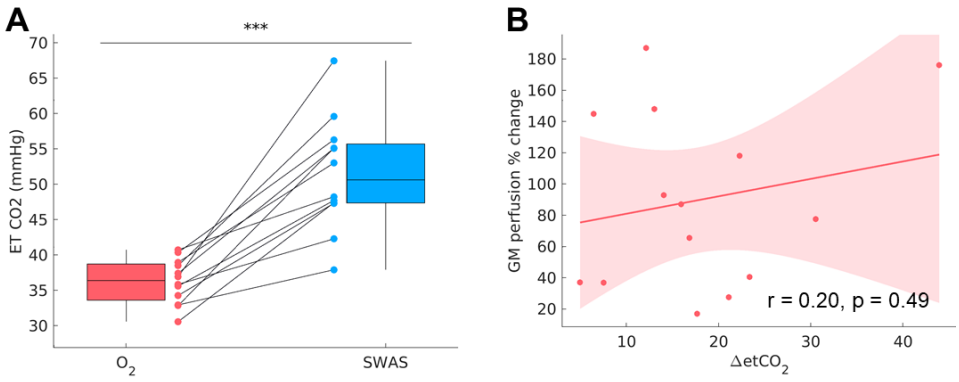

*Figure 4.5: End-tidal CO_2 changes and their relationship with grey matter CBF increases under anaesthesia. A) Boxplots showing the significant change in end-tidal CO_2 due to the sevoflurane anaesthesia where *** indicates p<0.001. B) Scatterplot showing the relationship between percentage change in grey matter CBF and the change in end-tidal CO_2 levels between the O_2 and SWAS conditions.*

4.3.2 Relationship between cerebral CBF and EEG power

At SWAS, slow wave power was significantly negatively correlated with CBF in several brain regions (Figure 4.6). These included the bilateral medial frontal cortices, the paracingulate gyrus, the frontal pole, the middle temporal gyrus, the right temporal occipital fusiform cortex, the right superior frontal gyrus, and the right lingual gyrus. In contrast, there were no significant correlations found between slow wave power and CBF while participants were wakeful breathing O_2.

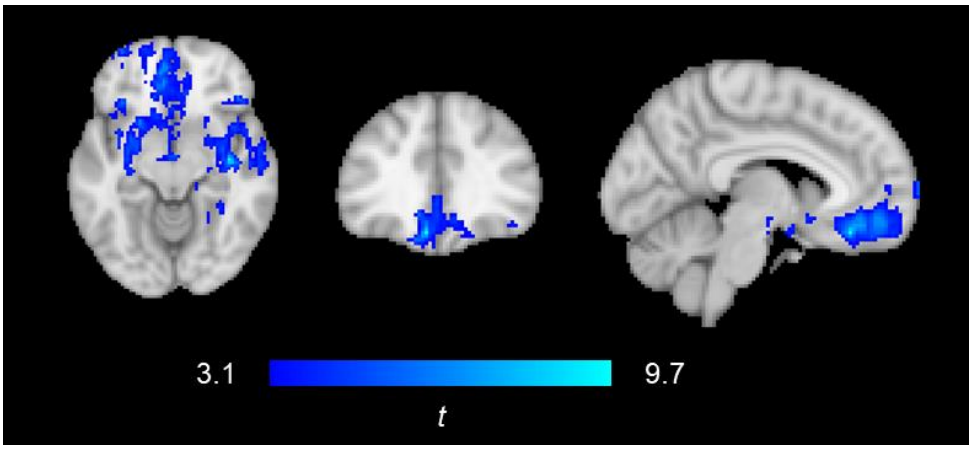

Figure 4.6: Relationship between CBF and slow wave EEG power at the SWAS endpoint. The figure shows the negative correlation between voxel-wise cerebral blood flow and slow wave EEG power (0.5-1.5Hz) at the Fz electrode when participants were held at SWAS. Only t-stat values for statistically significant voxels (TFCE-corrected p<0.05) are plotted. In this analysis, the t statistic is monotonically related to the Pearson's correlation coefficient.

4.4 Discussion

In this study, we used a novel EEG-compatible PASL sequence to show large alterations in grey matter CBF under deep sevoflurane anaesthesia. We standardised the level of deep sevoflurane anaesthesia by identifying maximal slow wave power increase on an individual subject basis using real-time EEG

feedback. We compared changes in cerebral CBF at SWAS to wakefulness when breathing either room air or 100% O_2. To our knowledge, our study is the first to use ASL to quantify the effect of surgical levels of sevoflurane on cerebral blood CBF. Previous ASL studies of sevoflurane used either sub-anaesthetic doses (0.25 MAC) (Qiu et al., 2008; Ramani et al., 2007) or did not include an awake control condition (Venkatraghavan et al., 2016).

During surgical anaesthesia, oxygen is routinely administered alongside the anaesthetic to reduce the risk of hypoxia. We found that inducing hyperoxia during wakefulness by delivering 100% O_2 significantly reduced grey matter CBF overall, particularly in the medial occipital lobe, the parietal lobe, the posterior cingulate gyrus, the thalamus, as well as regions of bilateral lateral frontal cortex including the precentral gyrus. These results are in agreement with previous studies of hyperoxia using both ASL (Bulte et al., 2007) and other methods (Rostrup et al., 1995, 2000; Watson et al., 2000). We did not measure end-tidal CO_2 in the room air condition, and therefore cannot perform a direct comparison to CO_2 levels in the O_2 condition.

At SWAS, when participants were breathing a mix of sevoflurane and O_2, we observed a large increase in grey matter CBF relative to wakeful breathing of either room air or O_2. In other words, the addition of sevoflurane at concentrations sufficient to induce deep sedation not only cancelled out the decrease in CBF due to hyperoxia, but also significantly elevated grey matter CBF well above normoxia levels. Whole-brain CBF maps revealed a global elevation of grey matter CBF in

both cortical and subcortical regions at SWAS compared to wakeful breathing of O_2. When comparing wakeful breathing of room air to SWAS, there were widespread but also more regional increases in grey matter CBF. These were localised to occipital and temporal regions, the medial and inferior frontal cortices, the cerebellum, and subcortical grey matter regions including the thalamus and brainstem.

Previous studies on the effect of sevoflurane anaesthesia on CBF using a range of measurement techniques have yielded inconsistent findings (Table 4.1). Some studies, in agreement with our results, some studies report that sevoflurane increased CBF (Bundgaard et al., 1998; Kolbitsch et al., 2000, 2001; Kondo et al., 2016; Matta et al., 1999). However, a number of other studies have reported unchanged (Ramani et al., 2007) or decreased CBF (Cho et al., 1996; Conti et al., 2006; Kaisti et al., 2002, 2003; Mielck et al., 1999). Furthermore, some studies suggest a non-linear effect, where CBF is reduced at low concentrations of sevoflurane, but then return to near-baseline levels at higher concentrations (Conti et al., 2006; Kaisti et al., 2002). In line with our results, other studies suggest that sevoflurane may have differential effects on CBF across the brain. Kaisti et al., (2002) reported whole-brain reductions in CBF at 2% end-tidal, only frontal cortex, thalamus, and cerebellum exhibited a rebound at higher sevoflurane concentrations. At sub-anaesthetic doses of sevoflurane, Qiu et al., (2008) reported spatial non-uniformity with both regional increases and decreases in CBF. Finally, studies manipulating the level of CO_2 at a steady sevoflurane concentration have reported decreased CBF under hypocapnic and normocapnic

conditions and increased under hypercapnic conditions relative to baseline (Cho et al., 1996; Mielck et al., 1999).

This complex picture is likely due to a combination of factors. Firstly, the effect of sevoflurane on cerebral blood flow is dependent on the balance between vasoconstriction indirectly due to flow-metabolism coupling (Hansen et al., 1989) and vasodilatory effects through direct action on vascular smooth muscles inherent to the agent (Conti et al., 2006; Matta et al., 1995, 1999). Secondly, the effect of the agent can influence other physiological effects, such as the end-tidal CO_2 concentrations.

In our study, we observed a significant increase in end-tidal CO_2 from wakefulness breathing O_2 to SWAS (Figure 4.5A). However, we did not find a significant correlation between end-tidal CO_2 and CBF (Figure 4.5B). Importantly, this analysis did not take into account the concentration of sevoflurane. In the healthy brain, CBF is tightly regulated to meet metabolic demand, primarily through cerebral autoregulation (Armstead, 2016). Even in the absence of an anaesthetic, hypercapnia is a potent vasodilator and causes elevated CBF (Tancredi & Hoge, 2013; Zhou et al., 2015), with 5% CO_2 inhalation causing a 50% increase in CBF (Kety & Schmidt, 1948). The most important mechanism through which CO_2 causes increased CBF appears to be related to extracellular H^+ acting on vascular smooth muscle to cause vasodilation (Kontos et al., 1977). Considering the well-established relationship between CO_2 and CBF, it is possible that a multivariate analysis including both CO_2 and sevoflurane concentrations would show a

significant relationship between CO_2 and CBF in our study. However, the percentage change in CBF in our study was higher than what has previously been found with comparable increases in end-tidal CO_2 in hypercapnic challenges without anaesthesia (Zhou et al., 2015). Therefore, it is likely that the elevated CBF levels we observe in our study is in part driven by hypercapnia secondary to the anaesthetic. Therefore, the whole brain analyses of the effects of sevoflurane on CBF are limited by not including end-tidal CO_2 as a regressor, as we cannot disentangle the contribution of sevoflurane and CO_2 in the overall change in CBF.

Table 4.1: Overview of studies on the effect of sevoflurane on CBF. FIO_2 = fractional inspired oxygen, PaO_2 = partial pressure of oxygen in arterial blood, TCD = Transcranial Doppler ultrasound, Xe113 = Xenon 113 tracer, K-S = Kety-Schmidt technique, ceMRI = contrast enhanced MRI, PET = positron emission tomography, ASL = arterial spin labelling, NIRS = near-infrared spectroscopy.

Study	Method	ET sevo (%)	O_2	CO_2	Principal finding
Cho et al., (1996)	TCD	2	FIO_2 100%	Managed to hypocapnia, normocapnia and hypercapnia for different conditions	CBF ↓ compared to the same capnic condition at baseline. CBF ↑ during hypercapnia anaesthesia compared to awake normocapnia.
Bundgaard et al., (1998)	Xe113	1.5 & 2.5	PaO_2 > 18 kPa	Managed to mild hypocapnia/normocapnia.	CBF ↑ from 1.5 to 2.5% sevoflurane.
Matta et al., (1999)	TCD	0.8-1.0 & 2.4-3.0	FIO_2 50%	Managed to mild hypocapnia (30-35mmHg)	CBF ↑ from baseline to 0.8-1.0% and from 0.8-1.0% to 2.4-3.0%.
Mielck et al., (1999)	K-S	1.7	FIO_2 30%	Managed to hypocapnia, normocapnia, and hypercapnia for different conditions	CBF ↓ at 1.7% compared to baseline when normocapnic and hypocapnic, and CBF ↑ when hypercapnic.
Kolbitsch et al., (2000)	ceMRI	0.8	FIO_2 50%	Managed to 40mmHg (normocapnia)	CBF ↑ in all ROIs (white matter, striatum, thalamus, frontal cortex, parietal cortex, occipital cortex)
Kolbitsch et al., (2001)	ceMRI	0.8	FIO_2 50%	Managed to 40mmHg (normocapnia)	CBF ↑ in all ROIs (white matter, striatum, thalamus, frontal cortex, parietal cortex, occipital cortex)
Kaisti et al., (2002)	PET	2.0, 3.0 & 4.0	FIO_2 100%	Managed to mild hypocapnia	CBF ↓ in all ROIs (frontal love, parietal lobe, temporal lobe, putamen, caudate, thalamus, cerebellum) and whole brain, at all three levels of sevoflurane.CBF ↑ from 2 to 3% in frontal lobe, thalamus, and cerebellum. CBF ↑ from 2 to 4% in thalamus and cerebellum. CBF ↑ from 3 to 4% in cerebellum.
Kaisti et al., (2003)	PET	1.5	FIO_2 100%	Managed to levels measured at baseline (normocapnia)	CBF ↓ in occipital cortex, caudate, thalamus and cerebellum. Not significantly altered in frontal cortex, parietal cortex, temporal cortex or putamen.
Conti et al., (2006)	TCD	1.7 & 2.0-4.0	FIO_2 40%	Maintained to within 10% of pre-induction values (normocapnia)	CBF ↓ at 1.7%, returned to near-baseline levels at 2-4%.
Ramani et al., (2007)	ASL	0.5	FIO_2 100%	Monitored, no change in etCO2 between conditions (normocapnia)	CBF unchanged in all ROIs (primary visual cortex, secondary visual cortex, primary auditory cortex, primary motor cortex, pre-motor area, supplementary motor area, prefrontal cortex, hippocampus, cimulate gyrus, thalamus)
Qiu et al., (2008)	ASL	0.5	FIO_2 100%	Monitored, no change in etCO2 between conditions (normocapnia)	CBF ↑: Anterior cingulate, bilateral insula, bilateral claustra, bilateral parahippocampal gyrus, bilateral amygdala, bilateral anterior cerebrellum (culmen), and bilateral hippocampus. CBF ↓: Posterior cingulate, biateral superior and middle temporal gyrus, bilateral parietal lobule, and bilateral frontal gyrus.
Kondo et al., (2016)	NIRS	8.3	FIO_2 100%	Managed to 35-40mmHg (normocapnia)	CBF ↑ relative to baseline

General anaesthesia is associated with altered EEG power in several frequency bands. Moreover, different anaesthetic agents have different frequency characteristics (Purdon, Sampson, et al., 2015). Understanding the functional significance of anaesthesia-induced EEG changes is an active area of research. Therefore, combining EEG with MRI is often desirable in neuroimaging studies of anaesthesia. However, due to the risk of electrode heating, great care must be taken when combining these techniques, particularly when applied to unconscious subjects. Compared to other labelling standards such as pcASL, PASL sequences have lower power deposition, reducing the risk of electrode heating during simultaneous MRI data acquisition. To further mitigate this risk, the ASL sequence we developed for this study features an extended inversion pulse compared to standard PASL sequences.

Other more generally recommended blood labelling approaches such as pseudo-continuous ASL (pcASL) employ long labelling durations (≈1800ms) to maximise signal-to-noise ratio. However, as a consequence the labelling efficiency is dependent on the blood-water flow rate through the labelling plane (Aslan et al., 2010). This is problematic when an intervention alters the velocity of blood in the feeding arteries, such as the administration of anaesthesia. Conversely, pulsed ASL (PASL) sequences use a very short radiofrequency pulse (≈10ms) to label the blood-water, rendering the effect of flow rate negligible. Consequently, PASL is likely a more appropriate labelling approach when applied to neuroimaging of anaesthesia, despite having some downsides compared to pcASL, particularly lower signal-to-noise ratio.

We found that there was a negative correlation between slow wave power and CBF in the medial prefrontal cortex and temporal lobe when held at SWAS. These regions overlap with regions where CBF has previously been found to be negatively correlated with slow waves during non-REM sleep (Dang-Vu et al., 2005; Tüshaus et al., 2017).

During eyes-closed resting wakefulness, we were unable to detect any significant between subject CBF correlation with any EEG frequency band. This is in contrast to a previous study which found that delta EEG power (1-4Hz) was found to be negatively correlated with CBF (O'Gorman et al., 2013). The reason for this discrepancy is unclear but, while both studies used similar numbers of participants and duration of the ASL recording, there were several other methodological differences. In our study, participants were breathing 100% O_2 and we recorded concurrent EEG and PASL, whereas O'Gorman and colleagues (2013) recorded EEG outside the MRI and employed pcASL.

Furthermore, there is precedent for a negative relationship between CBF and slow wave activity in pathological states. Notably, in ischemic stroke there is a general slowing of the EEG and increases in slow frequencies with reduced CBF (Rabiller et al., 2015). However, it is important to note that while the direction of the correlation was the same, unlike ischemic stroke where CBF levels drop below normal, all participants in our study exhibited CBF levels above baseline.

We note a few limitations to this ASL analysis. Firstly, as we targeted a specific brain state, SWAS, we only measured CBF at one sevoflurane concentration in each subject. Our initial study protocol included a PASL acquisition during the hold at loss of responsiveness, but this had to be taken out because an unacceptably high number of sessions having to be aborted due to hyperexcitability. This was potentially elicited by a change in scanner noise due to the change in MRI data acquisition sequence. Secondly, as ASL is not well suited to estimating white matter CBF, our analyses focus on grey matter CBF. Finally, for the correlation analysis between CBF and slow wave power, we only used slow wave power at a single, frontal electrode.

In conclusion, our results show that sevoflurane anaesthesia delivered to SWAS significantly elevated cerebral blood CBF compared to wakefulness. The brain regions with the highest relative increase in CBF from wakeful breathing of 100% O_2 to SWAS were the thalamus and cerebellum. Additionally, concurrent EEG-ASL revealed that slow wave power at the Fz electrode was negatively correlated with CBF in the prefrontal cortex.

5 Disruption of pain- and auditory processing at SWAS

5.1 Introduction

Pain is the phenomenological, conscious experience of real or perceived noxious input. This is distinct from nociception, i.e., the neural encoding and processing of the noxious stimulus. The International Association for the Study of Pain defines pain as “An unpleasant sensory and emotional experience associated with, or resembling that associated with, actual or potential tissue damage” (Raja et al., 2020). While pain serves an important evolutionary function in promoting avoidance behaviours, in the context of surgery, pain is an undesirable consequence of the surgical intervention. Intense experience of unavoidable pain can be deeply distressing, contributing to the prevalence of long term psychological disorder following instances of intra-operative awareness (Leslie, Chan, et al., 2010). Therefore, preventing awareness of painful surgical stimulation is a primary objective of anaesthesia.

Pain perception is influenced by many factors, including memories, emotions, genetics, and cognition (Tracey & Mantyh, 2007). Consequently, even a simple nociceptive stimulation elicits responses in a distributed network of brain regions involved in different aspects of nociceptive and pain processing. In general, pain perception involves activation in both sensory regions (e.g., the primary somatosensory [S1] cortex, secondary somatosensory [S2] cortex, thalamus) and

higher order regions including the insula, anterior cingulate cortex (ACC) and prefrontal cortex (Kong et al., 2010).

In surgical anaesthesia, the analgesic component of the triad of anaesthesia is usually provided by an opioid (Egan, 2019). Nevertheless, there is some evidence that hypnotic agents have analgesic properties at sub-anaesthetic doses (Toscano et al., 2003; Yeo et al., 2007). Complete anaesthesia-induced unconsciousness would prevent pain perception, though not functioning as an analgesic *per se*. This is supported by neuroimaging during pain stimulation showing attenuated brain responses to pain at surgical doses of anaesthesia (Hofbauer et al., 2004; Lichtner et al., 2018; Mhuircheartaigh et al., 2010, 2013). However, the current human neuroimaging literature on pain and nociception under general anaesthesia is largely restricted to propofol. Propofol is a very common induction agent (Brown et al., 2018) and is sometimes used to maintain anaesthesia during surgery, through a practice known as total intravenous anaesthesia (TIVA) (Al-Rifai & Mulvey, 2016). However, anaesthetic maintenance is most commonly achieved with volatile anaesthetics (Brown et al., 2018; Eger, 2004). Despite their common usage during the surgical intervention itself, there is a marked gap in the neuroimaging literature on how volatile anaesthetic agents, including sevoflurane, affect pain processing.

While preventing pain is a chief concern in surgical anaesthesia, intra-operative awareness has been reported to occur both with and without pain (Ag et al., 2016). It may not be that all sensory modalities are disrupted at the same time or even in

the same way across individuals (Sleigh et al., 2018). Hearing noises and conversations in the operating theatre are experiences are most frequently reported. The less common incidences of intra-operative awareness without pain can still cause distress and long-term psychological illness (Leslie, Chan, et al., 2010; Osterman et al., 2001). As discussed in Chapter 3 (Section 3.1), the isolated forearm test (IFT) is the gold standard for detecting connected consciousness during surgery (Linassi et al., 2018). Furthermore, auditory evoked potentials have been suggested as a method of detecting intra-operative awareness (Mantzaridis & Kenny, 1997; Schneider et al., 2005). Therefore, while preventing perception of surgical pain is a primary purpose of anaesthesia, improving our understanding of how anaesthetic agents affect auditory processing is still of great importance in preventing intra-operative awareness.

As discussed in Chapter 1 (Section 1.4), SWAS may reflect the most refractory way the brain can respond to stimulation and constitute a state of complete perception loss under general anaesthesia (Mhuircheartaigh et al., 2013). Specifically, Mhuircheartaigh et al., (2013) found that under propofol anaesthesia, the thalamocorticial system became isolated from external stimulation, with preserved pain- and auditory-evoked brain responses only in the precuneus, posterior parietal, and prefrontal regions. However, in the initial characterisation of SWAS, all participants were taken to the same propofol effect site concentration (Mhuircheartaigh et al., 2013). Therefore, it could not be conclusively determined that there was complete perception loss at SWAS rather than at concentrations in excess of SWAS.

The analyses presented in this chapter use the findings in the previous chapter to identify ASL-calibrated changes in BOLD FMRI responses at SWAS. Firstly, we were interested in whether pain and auditory responses to these stimuli are disrupted in individuals held at SWAS compared to awake, indicating perception loss to external stimulation in the SWAS state. Secondly, we wanted to investigate whether there is preserved stimulus-evoked activity outside the thalamocortical system at concentrations in excess of SWAS, as previously reported by Warnaby et al., (2013) for propofol. Finally, we wanted to assess whether we could detect pain-evoked changes in non-brain cardiovascular measures.

5.2 Methods

All data analysed in this chapter were acquired as part of Study 2, as outlined in Chapter 3 (Section 3.2.3). The analyses presented here are based on the multiband BOLD-FMRI data that was acquired during the pain stimulation paradigm when participants were awake and held at SWAS. Additionally, analyses of the changes in brain evoked responses to the modified isolated forearm test that was performed as part of the paradigm to assess conscious content will be presented. In essence in the awake state, this involved squeezing an experimenter's hand in response to an auditory command. Based on the offline SWAS curve analyses discussed in Chapter 3 (Section 3.3.2.3), a total of 15 participants were determined to be held at SWAS during the final task FMRI acquisition and were included in the following analyses.

5.2.1 MRI data acquisition

BOLD-FMRI data were acquired with the following sequence parameters: Whole-brain single-shot EPI, multi-band acceleration factor 4, TR = 1170ms, TE = 30.00ms, 500 volumes, R=2 GRAPPA in-plane acceleration, 106 x 106 matrix size, FOV 212mm, 2mm slice thickness, $2mm^3$ voxel size, 72 axial slices with no slice gap, fat saturation, echo spacing = 0.63ms, and anterior-posterior phase encoding, flip angle = 45 degrees. Each acquisition consisted of 500 volumes for a total of 585 seconds of scan time, excluding dummy scans at the beginning of each sequence. A single-band reference image was acquired at the beginning of each acquisition to improve translation between functional and structural space.

T_1-weighted anatomical images and field maps used for the task FMRI analyses were the same as were used for the ASL analyses in Chapter 4 (Section 4.2.1.1). To summarise, the T_1-weighted anatomical image was acquired with the following parameters: $1mm^3$ voxel size, TR = 2500ms, TE = 4.7ms, FOV = 192, 192x192 matrix size. Field maps for distortion correction were acquired when participants were awake and when held at SWAS (TR = 482ms, TE1 = 4.92ms, TE2 = 7.38ms).

5.2.2 Pain stimulation and modified isolated forearm paradigm

The pain stimulation paradigm consisted of 11 trials comprised of a moderate heat pain stimulus followed by two modified IFT tests. The time course of each trial was as follows: Heat pain stimulus (3s), delay (6s), first IFT command (4s), delay (5s), second IFT command (4s) (Figure 5.1). The interstimulus interval (ISI) between

each pain stimulation was pseudo-randomly jittered between 45 and 60 seconds to prevent habituation and expectation of the stimulus onset. The randomisation was performed ahead of time and was the same for all participants. The minimum ISI of 45 seconds was chosen to allow the stimulated skin to cool down to prevent tissue damage. The stimulation presentation timings were controlled by a custom script in Presentation (Neurobehavioural Systems Inc., USA).

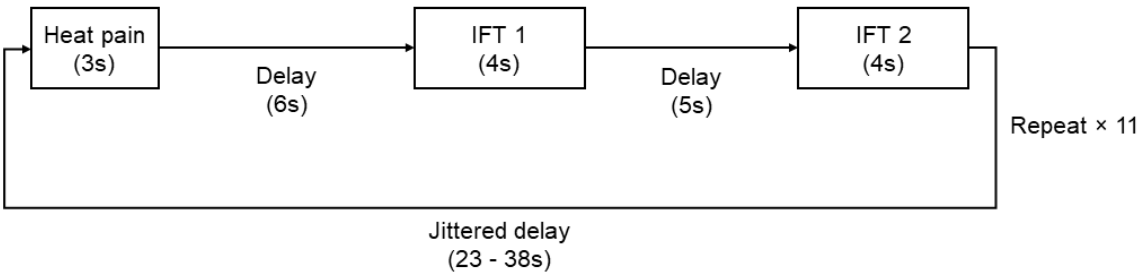

Figure 5.1: Flow chart of the timing and duration of the pain and verbal IFT commands administered during BOLD FMRI acquisition when awake and at SWAS. IFT = modified isolated forearm test.

Heat pain stimuli were generated by a Medoc Pathway contact heat thermode (Medoc, Ramat Yishai, Israel) applied to the lateral side of the right calf. Prior to situating the participant in the scanner, the temperature of the heat pain stimulation was calibrated to an individual rating of 5 on a scale from 0 to 10, where 0 indicated no pain and 10 indicated the worst pain imaginable. Participants were not informed about the target pain rating. The pain calibration was confirmed once the participant was situated in the MRI scanner and further calibration was performed if the pain rating had changed significantly. After the pain FMRI

acquisition during wakefulness, the participants were asked to rate the average pain intensity during the stimulation block.

The modified IFT consisted of two commands that requested the participants respond. The first prompt asked the participants to respond if they felt the stimulation ("[PARTICIPANT NAME], squeeze your hand if you felt something"). The second prompt asked the participants to respond if they felt pain specifically ("[PARTICIPANT NAME], squeeze your hand if you felt pain"). The IFT was modified in the sense that since no neuromuscular blockers were administered there was no need to isolate, i.e., restrict blood flow to, the responding arm. The IFT commands were pre-recorded by a male experimenter and delivered through noise dampening earbuds. The anaesthetist in the scanner room was holding the participant's left hand during these sequences and would digitally record the response or nonresponse to the IFT commands by selecting the appropriate response on a button box.

5.2.3 Physiological data acquisition

Physiological data was continuously recorded for the duration of the anaesthesia session (see Chapter 3 Section 3.2.3.2.2). In brief, we acquired pulse plethysmography and respiration bellows traces using an MP150 system and recorded at 200Hz in Acknowledge (BIOPAC Systems Inc., Goleta, CA, USA). Vital signs and end-tidal gas data were exported from the anaesthesia monitor and recorded by VSCapture v1.005 (Karippacheril & Ho, 2013).

5.2.4 Pre-processing of BOLD-FMRI data

All MRI data processing and analysis was performed using analysis tools in FSL version 6.0 (FMRIB Software Library). Task FMRI-BOLD data for both the awake and SWAS conditions was pre-processed using FEAT (Woolrich et al., 2001). This pre-processing involved automated non-brain tissue removal performed using Brain Extraction Tool (Smith, 2002), motion correction using MCFLIRT (Jenkinson et al., 2002), spatial smoothing with a Gaussian kernel of 5mm full-width half-maximum, and a 50s cut-off temporal high-pass filter to eliminate slow scanner drift. Distortions due to magnetic field inhomogeneities were corrected for using the acquired field maps.

Each of the FMRI datasets was decomposed into linearly mixed spatially independent components using MELODIC (Beckmann & Smith, 2004). For each dataset, components were visually inspected for temporal and spatial signatures that were indicative of artefacts of non-neuronal origin, including movement, physiological, and scanner-related artefacts (Griffanti et al., 2017). Noise components were regressed out and the datasets were reconstructed prior to first-level statistical analyses.

The high-contrast single-band image acquired at the beginning of each BOLD-FMRI acquisition was used to co-register the functional images to individual high-resolution T_1-weighted structural images using FLIRT (Jenkinson et al., 2002) and, subsequently, to standard space (Montreal Neurological Institute 152 [MNI 152] brain) using FNIRT (Andersson et al., 2007).

5.2.5 Whole-brain task FMRI analysis

5.2.5.1 Identifying mean responses to pain

The task BOLD-FMRI data for the awake and SWAS conditions were analysed with the general linear model (GLM) approach as implemented in FEAT (Woolrich et al., 2004).

Firstly, we wanted to assess brain responses to pain and auditory IFT commands when awake and at SWAS separately. We estimated the group mean effect for each stimulus type (i.e., pain and IFT) in separate two-level GLMs for the SWAS and awake conditions. Individual brain responses were modelled on the first level and the mean group effect at the second level. Secondly, in order to make a formal statistical assessment of the difference in brain response to pain and verbal IFT commands at SWAS compared with wakefulness, we performed a three-level GLM. Here, individual brain responses were modelled on the first level, the change in individual brain response between conditions was estimated on the second level, and the mean group difference was estimated on the third level. Individual changes in whole-brain median grey matter CBF, which were estimated from individual ASL images in Chapter 4 (Section 4.2.2.1), were included as a confound regressor to control for inter-individual differences in how CBF was affected by sevoflurane. All group level analyses used FLAME 1 + 2 to account for mixed-effects variance, allowing for greater generalisability from this group to the general population.

All higher-level analyses were based on the same first-level analysis. Here, the stimulus times and durations were convolved with the canonical haemodynamic response function (HRF) to model BOLD signal changes in response to the stimulation. The pain stimulation and each of the two IFT commands were included as separate regressors. Additionally, motion parameters for rotation and translation were included as regressors of no interest. Contrasts were set up to identify positive and negative BOLD responses to the pain stimulation, each IFT command separately, and for both IFT commands combined.

5.2.6 Task FMRI region of interest analysis

As was discussed in Chapter 4, sevoflurane has profound effects on cerebral haemodynamics. As the HRF is inherently tied to cerebral blood flow, we wanted to assess stimulus-evoked brain responses without relying on the HRF. Independent of the whole-brain analysis detailed in Section 5.2.5, we calculated the grand average stimulus-locked BOLD percentage change across individuals for regions of interest (ROIs) in left primary somatosensory cortex (S1; contralateral to the stimulated leg), left posterior insula, bilateral anterior insula, bilateral putamen, and primary auditory cortex (PAC).

Importantly, these ROIs were defined *a priori* from previously published MNI coordinates and brain atlases and were not derived from the whole-brain analysis detailed above. For S1, a combined mask consisting of 10mm spherical ROIs centred at MNI coordinates for peak activation in Broadman areas (BA) 1, 2, and 3B in response to left calf touch from Akselrod et al. (2017). For the left posterior

insula, anterior insula, and putamen ROIs, spherical ROIs were centred on group peak activation to heat pain to the left foot from Brooks et al. (2005). Table 5.1 presents an overview of MNI coordinates used to generate each spherical ROI. Finally, the ROI for the PAC was generated from areas TE 1.0, 1.1, and 1.2 of the Jülich Histological Atlas as implemented in FSL 6.0, and thresholded at 50%.

Table 5.1: MNI coordinates used as centres for spherical ROIs.

ROI		x	y	z	Radius (mm)
S1	BA1	-14.5	-39.5	68.8	10
	BA2	-13.1	-43.9	62.5	10
	BA3B	-12.5	-41.8	62.3	10
Anterior insula	Left	-34.0	22.0	-4.0	10
	Right	38.0	14.0	0.0	10
Posterior insula	Left	-38.0	-18.0	8.0	5
Putamen	Left	-22.0	14.0	-6.0	5
	Right	-26.0	16.0	-2.0	5

Each ROI was translated from MNI 152 space to individual functional space and a mean time-series of all the voxels within each ROI was calculated for each participant. Each mean time-series was epoched around the onset of the pain stimulation (5s pre-stimulus to 45s post-stimulus) and averaged for that ROI and participant.

5.2.7 Heart rate variability analysis

Non-brain physiological monitoring of surgical anaesthesia, including cardiovascular monitoring, remains far more prevalent than brain-based monitoring. We therefore analysed heart rate variability (HRV) changes in response to the pain stimulation as a non-brain physiological readout of potential

pain perception. Peaks in the respiration and pulse waveform data were identified using the FSL tool PNM (Brooks et al., 2008). The output from PNM was visually inspected and corrected for mistakes prior to further analysis. The mean respiration rate and heart rate was calculated for each condition.

HRV was calculated for each condition as the root mean square of successive differences (RMSSD) in time duration between heart beats. Additionally, to investigate pain-evoked changes in HRV, RMSSD was calculated for a five-second interval before and after the onset of each pain stimulus. Average pre-stimulus and post-stimulus HRV was calculated for each condition and participant. Finally, differences in HRV pre- and post-stimulus in each condition were tested for statistical significance with paired t-tests.

5.3 Results

As previously reported, no participants responded to either IFT prompt when held at SWAS. Furthermore, no participants reported any recollection of the experimental procedures when asked upon recovering from the anaesthetic. The end-tidal sevoflurane concentration during the task FMRI acquisition at SWAS was 2.8±0.4 (mean±SD).

5.3.1 Pain- and IFT-evoked brain activity disrupted at SWAS

When participants were awake, the painful stimulation elicited significant activation in areas relevant for nociceptive and pain processing, including primary somatosensory cortex (S1) contralateral to the stimulated leg, bilateral insular cortex, bilateral anterior cingulate cortex (ACC), bilateral caudate, bilateral

supplementary motor cortex, and bilateral opercular cortex (Figure 5.2). At SWAS, there was no significant activation or deactivation in response to the pain stimulation. A statistical comparison of the two conditions confirmed that there was significantly reduced pain-evoked activation in all the aforementioned regions (Figure 5.2 and Table 5.2).

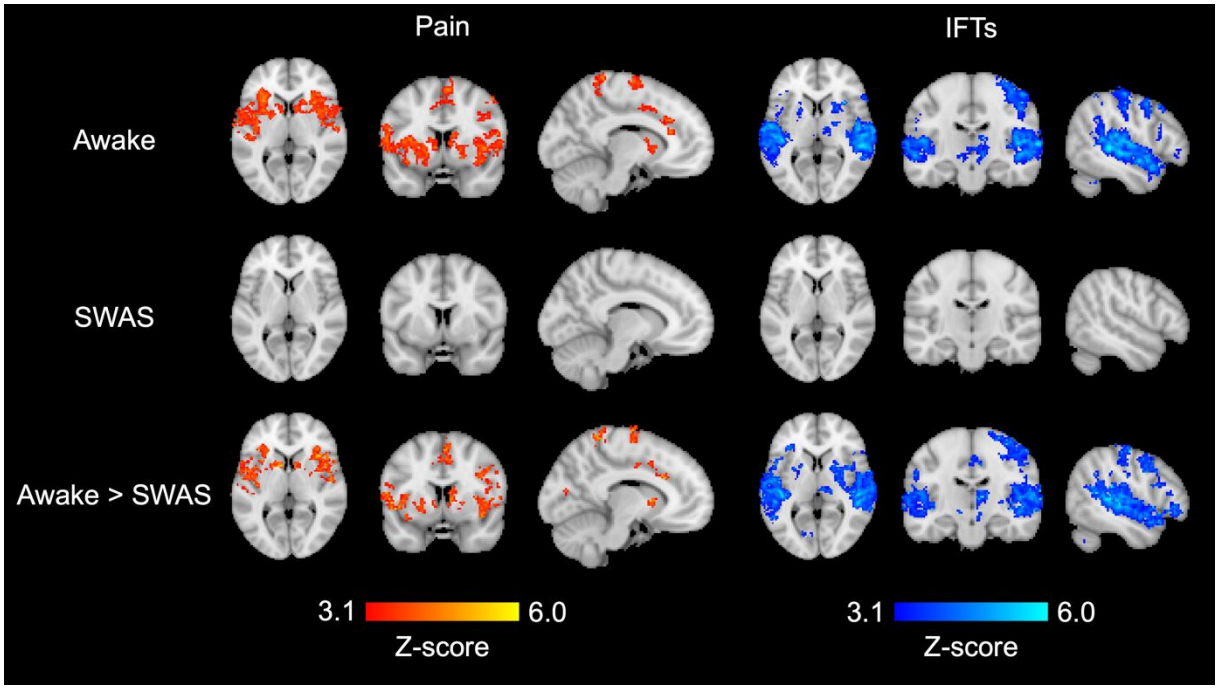

Figure 5.2: Mean BOLD activation maps showing areas of significant responses to pain stimulation (left) and auditory IFT response commands (right) when participants were awake (top) and at SWAS (middle; mixed-effects analysis, cluster-threshold corrected Z>3.1, p<0.05). Bottom: Clusters of significantly reduced brain activation at SWAS compared to wakefulness (paired t-tests, mixed effects analysis, cluster-threshold corrected Z>3.1, p<0.05).

Similarly, when awake the auditory IFT prompts elicited responses both in areas related to auditory and language processing, including bilateral primary auditory cortex (A1), secondary auditory cortex (A2), and Wernicke's area, and areas involved in generating a motor response, including precentral gyrus, right thalamus

(contralateral to the responding hand), and the cerebellum (Figure 5.2). When held at SWAS there was no significant activation or deactivation in response to the IFT prompts. Comparing the two conditions statistically, there were significant reductions in BOLD response in all these regions (Figure 5.2 and Table 5.2).

Table 5.2: Locations of clusters where the BOLD signal was significantly higher when participants were awake compared to when held at SWAS. Paired t-tests, mixed effects analysis, cluster-threshold corrected Z>3.1, p<0.05. COG coord. = Centre of gravity coordinate, R = right, L = left, B = bilateral.

				COG coord. (mm)				
	Size (voxels)	P-value	Z-max	X	Y	Z	Side	Cluster location
Pain	2006	<0.001	6.4	42.3	14.2	7.3	R	Insular cortex, central and frontal operculum, inferior frontal gyrus
	1746	<0.001	5.8	-37.5	7.2	2.2	L	Central operculum, precentral gyrus, temporal pole, caudate, insula
	1065	<0.001	5.3	0.5	5.6	48.7	B	Supplementary motor cortex, paracingulate gyrus, superior frontal gyrus
	607	<0.001	5.3	-53.4	-31.5	22.8	L	Central and parietal operculum, postcentral gyrus, supramarginal gyrus
	203	<0.001	5.1	-13.4	-44.6	67.6	L	Postcentral gyrus, superior parietal lobule
	117	<0.001	4.8	10.1	7.8	7.3	R	Caudate
	113	<0.001	4.7	55.2	-31.3	30.6	R	Supramarginal gyrus, parietal operculum
	110	<0.001	5.9	-35.0	-24.1	17.0	L	Insular cortex, planum temporale, parietal operculum
	75	<0.001	4.9	37.0	-19.3	14.9	R	Insular cortex, central opercular cortex, Heschl's gyrus
	47	0.005	4.5	11.7	-71.3	10.5	R	Intracalcarine cortex
	46	0.006	4.3	10.3	-18.4	-10.8	R	Brainstem
	43	0.009	4.8	-5.9	-76.2	11.0	L	Intracalcarine cortex
	39	0.016	4.3	-35.6	-4.7	48.8	L	Precentral gyrus
	37	0.022	4.8	39.4	-11.7	-4.8	R	Insular cortex
	36	0.026	4.8	-23.7	-66.7	-53.1	L	Cerebellum (VIIb, VIIIa)
	36	0.026	4.5	17.2	-46.6	66.2	R	Superior parietal lobule
IFTs	10975	<0.001	13.1	42.5	-15.1	22.5	R	Superior temporal gyrus, middle temporal gyrus
	6102	<0.001	10.3	-52.5	-26.5	7.7	L	Temporal pole, superior temporal gyrus, central and parietal operculum, posterior supramarginal gyrus
	951	<0.001	7.3	-20.5	-56.2	-21.9	L	Cerebellum (V, VI)
	472	<0.001	5.8	32.9	-57.5	-29.2	R	Cerebellum (Crus I, VI)
	380	<0.001	5.7	-41.6	-2.3	50.4	L	Precentral gyrus, middle frontal gyrus
	325	<0.001	6.1	-18.4	-68.3	-49.5	L	Cerebellum (Crus II, VIIIa, VIIIb)
	278	<0.001	5.1	-47.2	-26.8	39.4	L	Postcentral gyrus
	277	<0.001	5.3	25.3	-65.1	-50.5	R	Cerebellum (Crus II, VIIb, VIIIa)
	259	<0.001	4.9	-2.0	-53.8	39.5	L	Precuneous

210	<0.001	5.1	-38.0	28.1	-2.4	L	Orbitofrontal cortex, inferior frontal gyrus, frontal operculum
139	<0.001	5.1	34.4	43.2	24.2	R	Frontal pole
116	<0.001	4.5	-9.4	-27.2	-9.7	L	Brainstem, thalamus
93	<0.001	4.4	-47.0	13.1	29.5	L	Inferior frontal gyrus, middle frontal gyrus
92	<0.001	4.4	5.7	-19.3	43.4	R	Posterior cingulate cortex
83	<0.001	4.8	-34.8	41.6	26.7	L	Frontal pole, middle frontal gyrus
73	<0.001	4.9	3.5	47.0	41.8	B	Frontal pole, superior frontal gyrus
59	0.001	4.8	2.5	33.4	54.0	B	Superior frontal gyrus
55	0.001	4.4	8.9	-15.1	-8.3	R	Brainstem
55	0.001	4.6	13.5	57.8	18.4	R	Frontal pole
48	0.003	5.5	12.7	56.0	35.3	R	Frontal pole
43	0.007	4.6	40.9	26.0	-1.4	R	Frontal operculum, inferior frontal gyrus, orbitofrontal cortex
37	0.017	4.1	40.5	2.5	-43.7	R	Inferior temporal gyrus, temporal pole
32	0.038	4.5	47.0	29.8	26.6	R	Middle frontal gyrus
32	0.038	4.1	-13.6	-74.7	5.4	L	Intracalcarine cortex, lingual gyrus

There were a few clusters where the BOLD signal was significantly greater at SWAS compared to awake (Table 5.3). When comparing these clusters to clusters of negative BOLD response to pain stimulation and the IFT commands when awake, there was considerable overlap (Figure 5.3). Across the six clusters of significantly greater BOLD signal at SWAS compared to awake, there was 64.2% overlap with clusters of significant negative BOLD response to pain when awake. All six SWAS>awake clusters had some overlap with awake negative BOLD clusters. Similarly, in response to the IFTs, one of two cluster overlapped with negative BOLD response (50.0% overlap). The only SWAS>awake cluster with no overlap with awake negative BOLD clusters was in was in the superior sagittal sinus, an area that is physiologically implausible to represent neuronal activity.

Table 5.3: Locations of clusters where the BOLD signal was significantly higher at SWAS compared to awake. Paired t-tests, mixed effects analysis, cluster-threshold corrected Z>3.1, p<0.05. # indicates the cluster number,

				COG coord. (mm)				
	Size (voxels)	P-value	Z-max	X	Y	Z	Side	Cluster location
Pain	119	<0.001	4.94	58.8	-6.1	28.1	R	Postcentral gyrus, precentral gyrus
	98	<0.001	5.13	46.2	-72.0	27.9	R	Superior lateral occipital cortex
	76	<0.001	4.82	-47.4	-24.7	60.2	L	Postcentral gyrus
	57	0.001	4.53	-42.6	-74.0	28.0	L	Superior lateral occipital cortex
	56	0.001	4.33	-60.5	-5.7	18.9	L	Postcentral gyrus, precentral gyrus
	35	0.030	4.37	24.5	21.9	44.9	R	Middle frontal gyrus, superior frontal gyrus
IFTs	38	0.015	4.14	-28.9	-55.2	10.5	L	Cerebral white matter
	33	0.033	4.56	4.04	-87.8	38.5	R	CSF

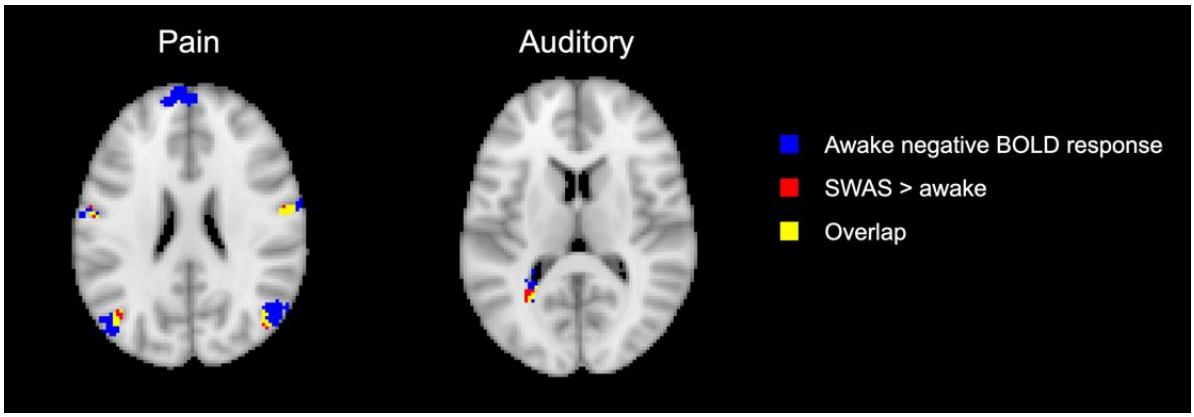

Figure 5.3: Overlap between clusters of significantly higher BOLD signal at SWAS and significant clusters of negative BOLD response to pain stimulation (left) and auditory IFT prompts (right). Clusters from mixed effects analyses, cluster-threshold corrected Z>3.1, p<0.05.

As these whole-brain analyses are dependent on the canonical BOLD response, we conducted a region of interest analysis to explore if the stimulation elicited any BOLD response that might not have been captured in the whole-brain analysis (Figure 5.4). As in the whole-brain analysis, when awake pain elicited a clear response in the S1, right posterior insula, anterior insula, and putamen ROIs.

Unexpectedly, there was also a pain response evident in the auditory ROI. The IFT prompts elicited a response in the auditory, anterior insula, right posterior insula, and putamen ROIs. At SWAS there was no response evident in any of the ROIs to any stimulation.

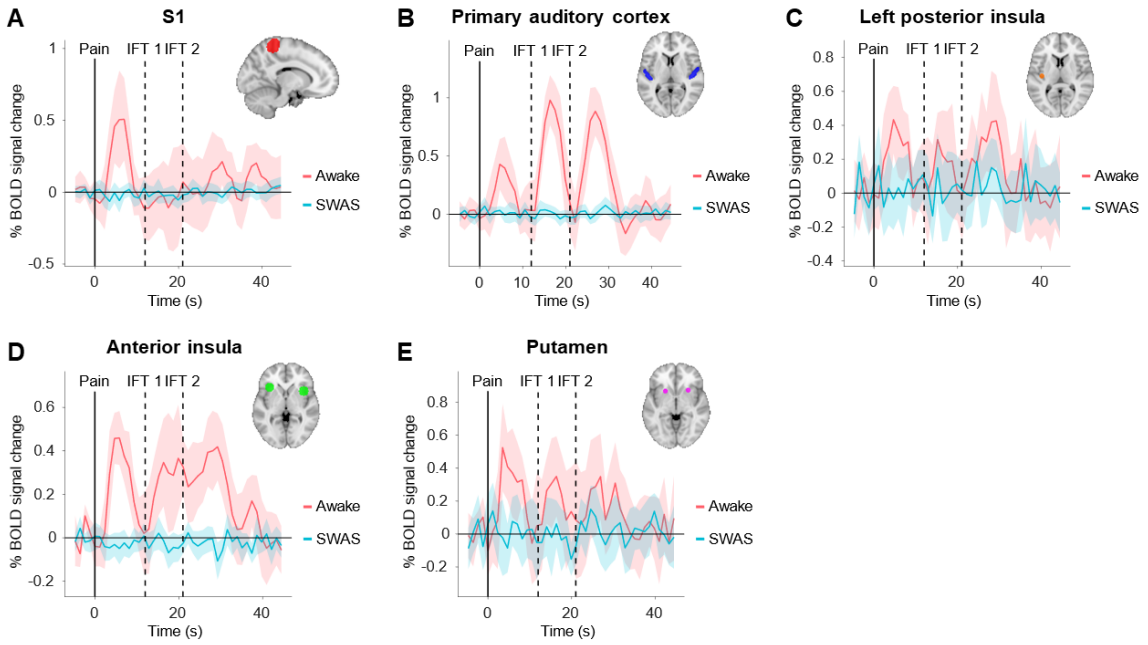

Figure 5.4: Between-subject (N=15) average stimulus-locked BOLD percent signal change within five regions of interest: Left S1 (A), bilateral primary auditory cortex (B), left posterior insula (C), bilateral anterior insula (D), and bilateral putamen (E). when awake (red) and at SWAS (blue). Solid line indicates group mean and shaded area indicates 95% confidence interval.

5.3.2 Heart rate variability reduced at SWAS

While overall heart rate did not change between wakefulness (62.8±14.3) and SWAS (68.0±16.3, $p>0.05$), heart rate variability was significantly reduced at SWAS (38.0±18.0) compared to wakefulness (73.2±26.1, $p<0.001$; Figure 5.5). However, there was no significant difference in heart rate variability in a 5s pre-stimulus and post-stimulus (from the onset of the pain stimulation) in either

condition (awake pre-stim (83.3±67.2) vs. awake post-stim (66.2±38.6, p>0.05) and SWAS pre-stim (42.7±28.2) vs. SWAS post-stim (34.9±14.3), p>0.05).

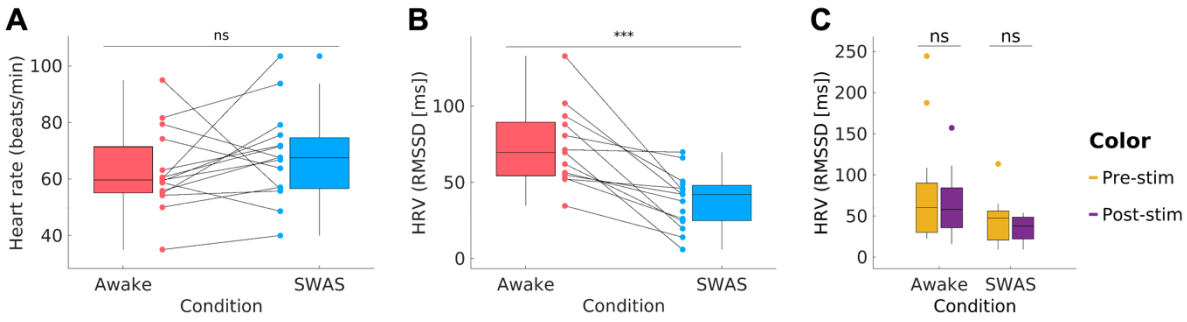

Figure 5.5: Effects of sevoflurane on HR and HRV during pain stimulation. A) Boxplots displaying interindividual heart rate when awake and at SWAS. Dots connected by a line indicate change in individual participants. B) Heart rate variability (HRV) when awake and at SWAS. C) HRV in a 5s interval before and after onset of pain stimulation.

5.4 Discussion

In this study we acquired task FMRI during a heat pain and auditory stimulation paradigm having titrated sevoflurane anaesthesia to SWAS. This approach ensured that all functional images were acquired in the same brain state in all subjects. Our findings show that the brain's ability to process painful and auditory stimulation is severely disrupted at SWAS. The whole-brain analysis of brain activation in response to pain and verbal IFT commands showed a stereotypical modality-specific responses when awake, but no significant brain activation in response to either stimulus type was found at SWAS. Crucially, these results do not conclusively show that there was no activity in the brain in response to pain or the IFT commands at SWAS whatsoever. However, statistically comparing the stimulus-evoked responses at SWAS to awake confirmed that this constituted a

significant reduction in both modality-specific primary and higher-order cortical regions.

5.4.1 Altered CBF cannot explain lack of stimulus-evoked BOLD response

Based on the CBF analyses discussed in Chapter 4, we know that the haemodynamics was altered during the task FMRI acquisition at SWAS compared to wakefulness. We therefore included individual changes in CBF as a confound regressor in the inter-condition comparison to explain the variance that was due to increased CBF. Beyond this, the altered CBF could affect the modelling of the stimulus-evoked responses on the first level (Handwerker et al., 2004). Conventional first-level FMRI analyses involve convolving the stimulus timings with a canonical HRF function to model stimulus-evoked BOLD signal change (Friston et al., 1995; Worsley & Friston, 1995). Even within- and between-subject HRF variability without drug-induced alterations to CBF can cause false-negative results (Handwerker et al., 2004). In all the analyses performed in this chapter, a temporal derivative of the HRF was included in the first level analysis. This is recommended practice to account for the difference in time that slices of each 3D FMRI volume were acquired, but also has the additional benefit of accounting for variations in the HRF delay between subjects and sessions. Therefore, the whole-brain analysis does account for some potential effects of the anaesthetic on the time course of the HRF.

However, temporal derivatives do not account for all HRF variability (Handwerker et al., 2004). Therefore, as the effects of sevoflurane on the HRF is unknown, we performed a region of interest analysis to see what the stimulus-locked time course of the BOLD signal was in regions we *a priori* expect to respond to pain and auditory stimulation. There were expected BOLD signal increases in all the regions of interest when awake. At SWAS, however, there was no BOLD evident signal change, corroborating that the lack of stimulus-evoked activation at SWAS in the whole-brain analysis was not due to assumptions about the HRF having been violated.

It has been postulated that elevated CBF can cause a ceiling effect where neuronal activation does not elicit a change in BOLD signal (Buxton et al., 2004; Haller et al., 2006). This possibility is problematic in interpreting FMRI of anaesthesia (K. Sicard et al., 2003). However, while some early investigations yielded support for this view in rats (K. M. Sicard & Duong, 2005) and humans (Posse et al., 2001), other human imaging studies show a modulation of the BOLD response with elevated CBF rather than a ceiling effect within physiologically relevant ranges (Cohen et al., 2002; Corfield et al., 2001; Whittaker et al., 2016). In particular relevance to the present work, a hypercapnic challenge study that acquired both ASL and event-related BOLD FMRI images found that the BOLD response to visual stimulation was preserved at CBF levels comparable to what was found in the present study at SWAS (Whittaker et al., 2016). Therefore, while the possibility of a ceiling effect in our study cannot be excluded without a formal

control, such as a hypercapnic challenge, the CBF levels at SWAS are within a range where event-related BOLD signal changes are still expected to present.

5.4.2 Negative stimulus-evoked BOLD responses are absent at SWAS

Counter to our expectations, some regions had significantly higher BOLD signal at SWAS compared to wakefulness. However, upon comparing these regions to regions that had significantly negative BOLD response when awake, there was considerable overlap. Combined with the lack of significant activation to either stimulus at SWAS, this indicates that the clusters of significantly higher BOLD signal at SWAS were due to the disappearance of a negative BOLD response. While the functional significance of negative BOLD are still incompletely understood, they are thought to reflect decreased neuronal activity. In particular, the default mode network is frequently found to deactivate during stimulation and task behaviour, including acute heat pain (Kong et al., 2010). In line with this, three of the six overlapping clusters for pain were in the default mode network. The two of the three remaining clusters were also in areas previously been found to have a negative BOLD response to heat pain (Kong et al., 2010). Therefore, upon closer inspection, the clusters of elevated BOLD at SWAS compared to awake are best explained as a lack of stimulus-evoked deactivation at SWAS.

5.4.3 Disruption of pain and auditory processing under general anaesthesia

To our knowledge, no studies have assessed stimulus-evoked responses using BOLD FMRI at sevoflurane concentrations comparable to our study. At concentrations slightly lower than in the present study, semantic auditory cortical

BOLD response have been found to be strongly reduced at 1% and 2% sevoflurane, although not entirely abolished (Kerssens et al., 2005). Similar attenuation in primary sensory regions have been reported for other types of stimulation, including vision (Marcar et al., 2006) and finger flexion (Yamamoto et al., 2019).

Propofol has been explored most extensively with FMRI in the context of acute pain. Early studies indicated that propofol attenuated pain-evoked brain responses in a dose-dependent fashion (Hofbauer et al., 2004; Mhuircheartaigh et al., 2010), though with preserved pain-evoked activation in the precuneus even at concentrations exceeding SWAS (Mhuircheartaigh et al., 2013). This was interpreted to imply that SWAS constitutes the most refractory way the brain can respond to external stimulation. It is noteworthy that we did not find this residual brain stimulus-evoked activation in subjects titrated to SWAS with sevoflurane, highlighting a potential difference in how the two anaesthetic agents affect pain and auditory processing. A recent study found dose-dependent decreases in pain-evoked activity in key pain processing regions including the insula and S2, but that intense, but not moderate, noxious electrical stimulation elicited counter-intuitive increases in pain-evoked responses in ACC, OFC, and putamen at propofol concentrations in far excess of SWAS into burst suppression (Lichtner et al., 2018). In contrast to (Mhuircheartaigh et al., 2013), the precuneus was not among the regions that responded to pain during deep anaesthesia in this study. Lichtner et al., (2018) did not segment the FMRI according to EEG, so there was likely some conflation of different brain states at each target concentration due to inter-

individual differences in susceptibility to anaesthesia. Therefore, the counter-intuitive increases in frontal regions likely reflects various degrees of burst suppression in different individuals. In light of these studies, it is surprising that we observed no significant brain activation to pain at SWAS. This may reflect differences in how sevoflurane and propofol affect nociception and pain processing. Additionally, by targeting SWAS, we ensured that all participants were in the same brain state. Nevertheless, Lichtner et al. (2018) highlight that showing non-responsiveness to moderate pain does not necessarily preclude brain responsiveness to surgical pain levels. This will be important to follow up on in future investigation of pain perception at SWAS.

FMRI studies on auditory processing under propofol anaesthesia have shown a similar attenuation of stimulus-evoked activation. At concentrations at and in excess of SWAS, Mhuircheartaigh et al. (2013) found that auditory-evoked activation was reduced to posterior parietatal regions including the precuneus, similarly to that found for pain-evoked activation. Other studies (Heinke et al., 2004; Plourde et al., 2006) have found that primary auditory activation, while reduced, persists at concentrations comparable to that targeted by Mhuircheartaigh et al. (2013).

While there are few event-related BOLD FMRI studies under sevoflurane anaesthesia, we can to some extent infer cortical activation from evoked potentials. Contact heat evoked potentials (CHEPs) have been found to have increased latency and decreased amplitude at sub-anaesthetic concentrations of

sevoflurane (Untergehrer et al., 2013). The cortical generators of CHEPs have been located to secondary somatosensory cortex and the parietal operculum, with later contributions from the ACC (Chen et al., 2001; Le Pera et al., 2002; Valeriani et al., 2002). As CHEPs amplitudes are more strongly associated with subjective pain ratings than stimulus intensity (Granovsky et al., 2008), this implies an analgesic effect of sevoflurane. This is corroborated by clinical reports in the context of sevoflurane analgesia during labour (Toscano et al., 2003; Yeo et al., 2007), though an earlier study in healthy volunteers found no analgesic effect of sub-anaesthetic concentrations of sevoflurane (Tomi et al., 1993).

Auditory evoked potentials (AEPs) generally reduce in amplitude and increase in latency with increasing depth of anaesthesia (Thornton & Sharpe, 1998). AEPs are generally sub-divided into early (0-10ms), mid (10-100ms), and late latency potentials (100-1000ms), thought to originate in brain stem, primary auditory cortex, and higher order cortices respectively. Early latency AEPs are generally preserved at surgical levels of anaesthesia. For that reason, the lack of significant brain stem BOLD response at SWAS should be interpreted with caution as the FMRI of the brain stem is inherently limited by poor signal-to-noise ratio (Brooks et al., 2013). By contrast, mid latency AEPs have been found to be severely attenuated or completely abolished by surgical levels of volatile anaesthetics, including sevoflurane (Feuerecker et al., 2011; Schwender et al., 1995). Presence of mid-latency AEPs have been found to correlate with recovery of responsiveness during emergence from sevoflurane, isoflurane, and xenon (Goto et al., 2001). As

the cortical origin of mid-latency AEPs is well characterised to the PAC, the lack of PAC activation at SWAS in our study is therefore broadly in line with this research.

Note that the stimulation used in this study was not suitable for analysis of evoked potentials in the concurrently acquired EEG due to the stimulus durations being in the order of multiple seconds.

5.4.4 Inconclusive results on pain-evoked HRV changes

While brain imaging was the primary outcome measure for the pain stimulation, we also assessed the effect of the pain stimulation on heart rate variability as a non-brain physiological outcome measure. While heart rate did not change between awake and SWAS, there was an overall reduction in heart rate variability during the task FMRI acquisition at SWAS compared to awake. This is in line with previous research on the effect of sevoflurane anaesthesia on heart rate and heart rate variability (Mäenpää et al., 2007).

However, there was no detectable difference in heart rate variability before and during the pain stimulation in either condition. Since no effect could be detected during wakefulness, this finding is inconclusive. Acute pain has been found to cause changes in measures of heart rate variability, including RMSSD (J. Koenig et al., 2014). However, as the stimulation paradigm was optimised for FMRI, it may not have been sufficient to elicit detectable stimulus-evoked changes in heart rate variability. Most studies on the effect of pain on heart rate variability employ a sustained period of pain stimulation (≥1min) (J. Koenig et al., 2014), though shorter-duration heat pain stimulation (12s) has also been found to alter heart rate

variability (Aslaksen et al., 2007). Therefore, the lack of detectable pain-evoked alterations in heart rate variability is likely due to the stimulation paradigm not having been optimised for heart rate variability analyses.

While the results in this chapter are promising with respect to SWAS being a state of perception loss under general anaesthesia, these results are limited by the task FMRI being acquired only in steady states during wakefulness and at SWAS. As a consequence, these results cannot show whether the level of disruption of pain and auditory processing observed at SWAS occurs at lower concentrations during the transition to SWAS. This would need to be addressed in future research looking at how sensory processing is altered during the transition to SWAS.

In conclusion, we have demonstrated that brain activation in response to pain and verbal IFT commands was severely disrupted in subjects titrated to SWAS with sevoflurane. Examination of BOLD signal change in regions *a priori* expected to respond to pain and auditory stimulation determined that these results cannot be explained by invalid assumptions about the HRF. Additionally, by measuring and controlling for sevoflurane-induced changes to CBF we can likely exclude a BOLD ceiling effect. These results provide further evidence that SWAS is a state of perception loss to external stimulation under general anaesthesia. Additionally, this study provides rigorous control of factors usually not controlled for in neuroimaging of anaesthesia by targeting a specific brain state as well as incorporating measures of CBF.

6 Breakdown of large-scale brain networks at SWAS

6.1 Introduction

Several converging lines of research suggest that consciousness is supported by communication between different brain regions. Leading theories of consciousness, including the Integrated Information Theory (IIT) (Tononi, 2004, 2012; Tononi et al., 2016) and the Global Workspace Hypothesis (GWH) (Baars, 1997, 2005), postulate that consciousness involves the integration of multiple experiential modalities into a cohesive whole. Consequently, according to these theories, disruption of this integration is accompanied by loss of consciousness.

In line with these general theories of consciousness, disruption of communication between different brain regions is known to be a common effect of a range of anaesthetic agents (Blain-Moraes et al., 2015; Lee et al., 2013). However, precisely how different anaesthetic agents disrupt inter-regional communication is an ongoing subject of study. In particular, the roles of the thalamocortical system and cortico-cortical networks in anaesthesia-induced loss of consciousness remains unclear.

6.1.1 Anaesthetic effects on thalamocortical connectivity

Early studies found depression of thalamic activity as a common effect of both inhalational and intravenous anaesthetics (Alkire et al., 1999, 2000; Fiset et al., 1999), leading to hypotheses regarding a thalamocortical switch serving a causal

role in anaesthetic loss of consciousness (Alkire et al., 2000). Subsequent studies however suggest a less direct role of the thalamus (Hudetz, 2012). Other investigations have found that cortico-cortical functional connectivity is disrupted under general anaesthesia while thalamocortical connectivity is preserved (Boly et al., 2012; Lee et al., 2009) or that thalamocortical connectivity is indirectly disrupted as a consequence of cortico-cortical disconnection (Velly et al., 2007). In propofol specifically, it has been shown that thalamocortical connectivity from nuclei involved in relay of somatosensory signals were relatively preserved compared to other thalamic nuclei groups (Liu et al., 2013).

Effects of anaesthetic agents on the thalamocortical system, whether direct or indirect, has important implications for conscious experience of pain under general anaesthesia. The thalamus plays an important role in transmitting ascending pain signalling from the spinothalamic tract to the cortex, as well as in descending pain modulation (Ab Aziz & Ahmad, 2006; Tracey & Mantyh, 2007). Previous work in our lab has shown that the thalamocortical system became isolated from external pain stimulation under deep propofol anaesthesia (Mhuircheartaigh et al., 2013). Demonstrating disrupted thalamocortical connectivity at SWAS, particularly to somatosensory cortical regions, would therefore provide further evidence that pain perception is disrupted at SWAS.

6.1.2 Anaesthetic effects on connectivity in large-scale brain networks

Resting state networks are sets of brain regions where the BOLD signal covaries during wakefulness and are generally considered to represent large-scale

neuronal networks involved in specific cognitive functions. Despite their prevalence in human FMRI studies and potential clinical utility in inferring brain functionality in unconscious patients (Heine et al., 2012), the roles of particular resting state networks in loss of consciousness under general anaesthesia remain unclear (Palanca et al., 2017). Furthermore, most resting state FMRI studies of anaesthesia have investigated intravenous anaesthetics (Palanca et al., 2015), and while recently more resting state FMRI studies using sevoflurane have been published, many involve secondary analyses of only six unique datasets (Palanca et al., 2017).

Previous FMRI work on SWAS has focused on task-related brain activity (Mhuircheartaigh et al., 2013). Furthermore, most sevoflurane resting state FMRI studies have targeted end-tidal sevoflurane concentrations that were lower than what we found necessary to achieve SWAS on average in a comparable healthy adult sample in Chapter 3. The remaining studies either titrated to burst-suppression before stepping down the concentration (Ranft et al., 2016), introducing potential effects of neural inertia (Friedman et al., 2010; Warnaby et al., 2017), or focusing on a subset of resting state networks (Huang et al., 2014, 2016). No studies have targeted observational end-points past loss of responsiveness, which has been pointed out as a limitation of the current resting state FMRI literature of sevoflurane (Palanca et al., 2017).

To address these outstanding questions regarding functional connectivity in the SWAS state, we analysed resting state FMRI data acquired when awake and at

SWAS in two different ways. Firstly, to investigate whether and how functional connectivity in the thalamocortical system is altered at SWAS, we used a seed-based connectivity analysis from thalamic sub-regions to the cortex. Secondly, to assess functional connectivity changes in large-scale cortical networks due to anaesthesia, we used a data-driven, dual regression approach based on an independent component analysis (ICA). This allowed us to identify brain networks with significant changes of within-network functional connectivity at SWAS.

6.2 Methods

6.2.1 Data acquisition

The data analysed in this chapter was acquired as part of Study 2 that was outlined in Chapter 3. Based on the offline SWAS model fitting reported in Chapter 3, 14 participants were determined to have been held at SWAS during the final resting state FMRI acquisition and were eligible for inclusion in the following analyses.

We acquired 10 minutes closed-eyes resting state BOLD FMRI data during wakefulness and at SWAS. With the exception of the number of volumes acquired, FMRI acquisition parameters were identical to those used for the task FMRI acquisition reported in Chapter 5. In summary, we acquired whole-brain single-shot EPI, multi-band acceleration factor 4, $2mm^3$ voxel size, TR = 1170ms, TE = 30.00ms, 513 volumes, and R=2 GRAPPA in-plane acceleration.

Diffusion weighted EPI imaging was performed during the evening baseline session with the following parameters: TR = 2483ms, TE = 78.2ms, 122 x 122 matrix size, FOV = 214 x 214 mm, 1.75mm slice thickness, 1.75mm^3 voxel size, multi-band acceleration factor 4, 76 axial slices, anterior-posterior phase encoding, flip angle = 80 degrees, refocus flip angle = 180 degrees. Diffusion weighted images were acquired for two *b*-values: 1250s/mm^2 and 2500s/mm^2 distributed over 60 gradient directions each. Additionally, at b = 0 s/mm^2 11 volumes were acquired for the anterior-posterior (AP) phase-encoding direction and 4 volumes for the posterior-anterior (PA) phase-encoding direction.

T1-weighted images and field maps that were used for the following analyses are the same as those in Chapter 4 and 5.

6.2.2 Resting state FMRI preprocessing

Preprocessing of each individual's resting state FMRI data for the awake and SWAS conditions was performed in MELODIC (Beckmann & Smith, 2004). This involved automatic removal of non-brain tissue using BET, motion correction using MCFLIRT, spatial smoothing with a Gaussian kernel of 3mm FWHM, and a 100s cut-off temporal high pass filter to remove scanner drift. Magnetic field inhomogeneity distortions were corrected for using field map images acquired in the conditions as the resting state FMRI acquisitions.

Each dataset was decomposed into linearly mixed spatially independent components. The components of each dataset were visually inspected for spatial or time series characteristics indicative of non-neuronal artefactual origin, such as motion, physiological, or MRI-related artefacts (Griffanti et al., 2017). After regressing out noise components each dataset was reconstructed to provide a cleaned resting state dataset for each condition.

The high-contrast single-band volume acquired at the start of each acquisition was used to register the functional images to individual T1-weighted images using FLIRT (Jenkinson et al., 2002) and to MNI 152 space using FNIRT (Andersson et al., 2007).

6.2.3 Thalamocortical functional connectivity analysis

To assess the question of thalamocortical connectivity at SWAS, we conducted a seed-based correlation analysis (SCA) between sub-regions of the thalamus and the cortex (Figure 6.1). The thalamus was first parcellated into subregions based on structural connectivity to different cortical regions following the methodology by Behrens et al. (2003). These parcellations were then used as seed regions for a seed-based correlation analysis of the resting state FMRI data.

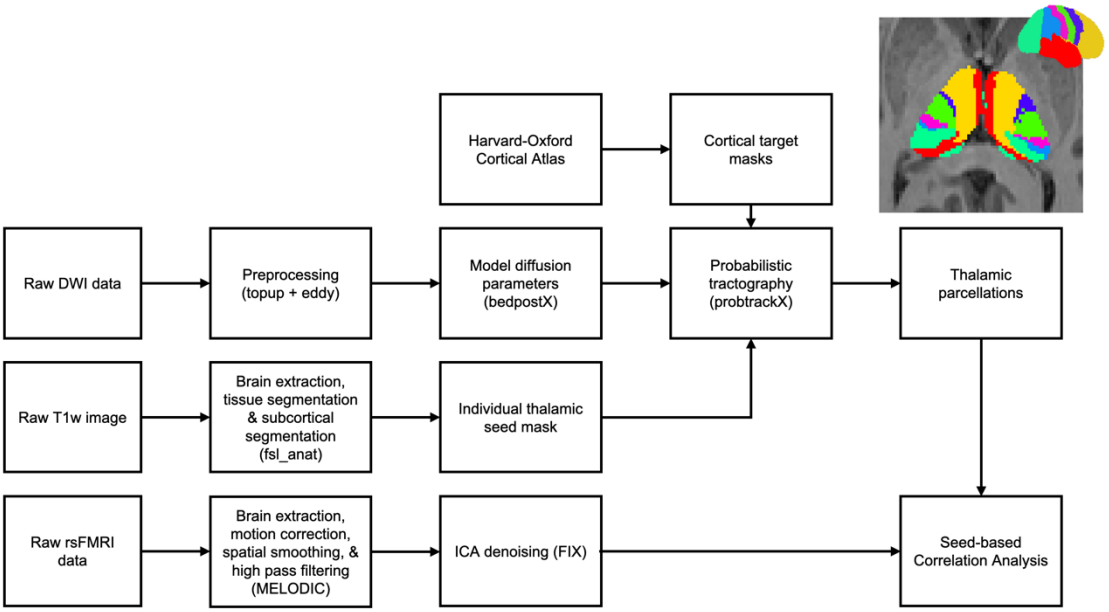

Figure 6.1: Flow chart of the analysis pipeline for the analysis of thalamocortical functional connectivity. Probabilistic tractography was performed on the diffusion MRI data using thalamus masks generated from T_1-weighted images as the seed mask and cortical target masks generated from the Harvard Oxford Cortical Atlas. This yielded thalamic parcellations that were used as seed regions in a seed-based connectivity analysis of the resting state FMRI data. Cortical target masks on a MNI 152 brain and the thalamic parcellation from an example subject is shown in the top right.

6.2.3.1 Diffusion MRI preprocessing

Diffusion-weighted MRI data was preprocessed using tools from FSL v6.0. The topup tool (Andersson et al., 2003) was used on averaged AP and PA b0 volumes to estimate susceptibility-induced off-resonance fields that were input into eddy (Andersson & Sotiropoulos, 2016) to correct for eddy current distortions and subject head motion. Next, a probabilistic diffusion model was fitted to the corrected data using a multi-shell ball and stick model as implemented in bedpostx_gpu (Hernández et al., 2012; Jbabdi et al., 2012). Diffusion weighted

images were translated to structural space using linear registration in FLIRT and to MNI 152 space using non-linear translation in FNIRT.

6.2.3.2 Probabilistic thalamic parcellation

Thalamic seed masks were generated for each subject from individual T1-weighted images using FIRST. Cortical target masks for the frontal lobe, parietal lobe, temporal lobe, occipital lobe, sensory cortex, and motor cortex were generated in 152 MNI space by combining masks from the Harvard-Oxford Cortical Structural Atlas as implemented in FSL, then translated to individual structural space. Probabilistic tractography from the thalamic seed mask to each cortical region of interest was performed in diffusion space using probtrackx (Behrens et al., 2007; Behrens, Woolrich, et al., 2003). Translation of thalamic seed mask and cortical target masks to individual diffusion space was handled within probtrackx using the translation matrices generated previously.

6.2.3.3 Seed-based correlation analysis

The thalamic parcellations were used as the seed regions for a seed-based correlation analysis of functional connectivity. First, the average BOLD time series was calculated from all voxels within each thalamic parcellation. Next, Pearson's correlation analyses were performed between the average signal of each parcellation and all voxels in the corresponding cortical target. Finally, an average of all voxel-wise correlations was calculated for each cortical region. Difference in functional connectivity between conditions was assessed for each cortical region with paired t-tests corrected for Benjamini-Hochberg false discovery rate.

6.2.4 Within-network functional connectivity analysis

In order to identify changes in large-scale brain networks due to anaesthesia, we first needed to identify resting state networks across the awake and SWAS conditions. These resting state networks were estimated from cleaned resting state FMRI datasets for using temporally concatenated group ICA with MELODIC. Data from both the awake and SWAS conditions were included in the ICA to ensure that the extracted networks were not biased to either condition. The number of components was fixed to ensure that extracted networks were comparable to the established literature and nomenclature (Uddin et al., 2019). An initial run with 20 components resulted in networks splitting into multiple parts (e.g., the default mode network was split into an anterior and a posterior component). Therefore, the dimensionality was reduced to 15 to avoid fragmentation of known resting state networks. Components corresponding to previously reported resting state networks in healthy adults were hand-classified, while the remaining components were identified as noise components and not considered in subsequent analyses.

In order to assess functional connectivity changes within the identified resting state networks between awake and SWAS, it is necessary to identify brain activity in the datasets for each individual subject and condition that corresponded to the group components that were common to both conditions. This was achieved by passing both the individual cleaned resting state FMRI datasets and the resting state network components into a dual regression analysis of within-network functional connectivity with the FSL tool dual_regression (Nickerson et al., 2017). Group ICA

spatial maps were regressed into individual FMRI datasets to generate a subject and condition-specific time-courses for each spatial map. Each time course was then regressed into the same resting state FMRI datasets to generate subject and condition-specific spatial maps corresponding to each group-level spatial map. Between-condition difference was tested for statistical significance with paired T-tests using voxel-wise non-parametric permutation testing ($N_{permutations}$ = 5000). Correction for multiple comparisons across voxels was achieved using TFCE and the significance threshold of $p<0.05$ was Bonferroni-corrected to account for testing of multiple networks.

6.3 Results

6.3.1 Thalamocortical connectivity at SWAS

We found that the mean seed-based connectivity between each thalamus parcellation and its primary cortical target was significantly reduced at SWAS for all seed-target pairs (adjusted $p<0.05$; Figure 6.2).

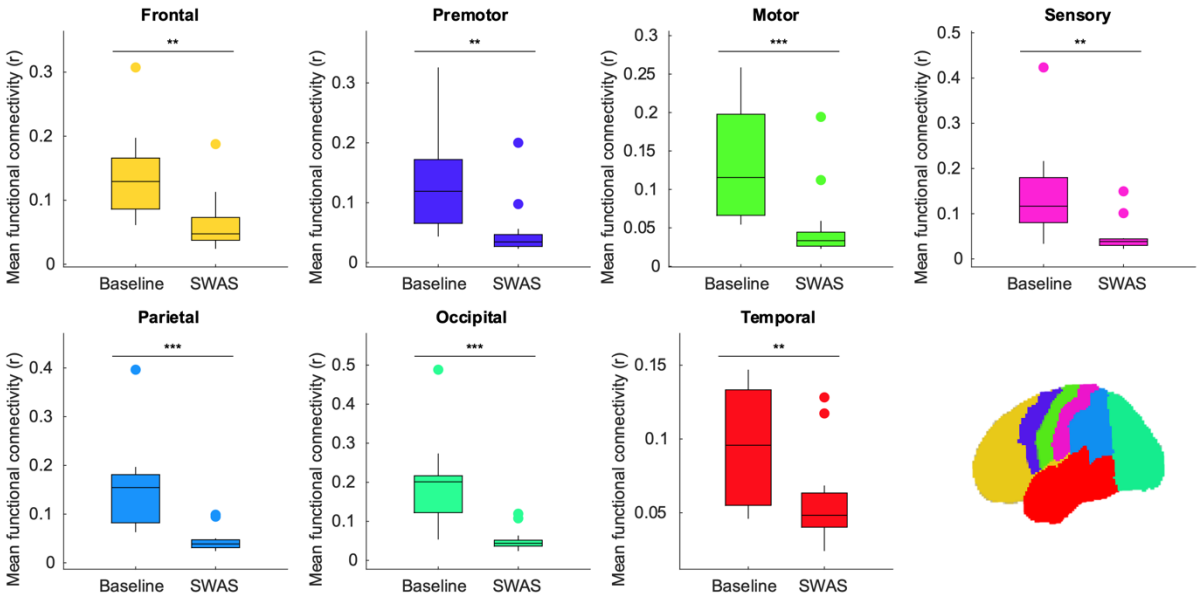

*Figure 6.2: Changes in thalamocortical functional connectivity at SWAS compared to awake. Each plot indicates the between-subject mean functional connectivity between each thalamic parcellation and its primary cortical target as estimated by structural connectivity from diffusion MRI. *** indicates p<0.001 and ** indicates p<0.01 corrected for Benjamini-Hochberg false discovery rate.*

6.3.2 Within-network connectivity at SWAS

Eight components corresponding to known resting state networks could be identified from the 15 independent components produced by the temporal-concatenation group ICA (Figure 6.3). These were the medial visual network, lateral visual network, auditory network, sensorimotor network, default mode network, dorsal attention network, fronto-parietal network, and executive control network.

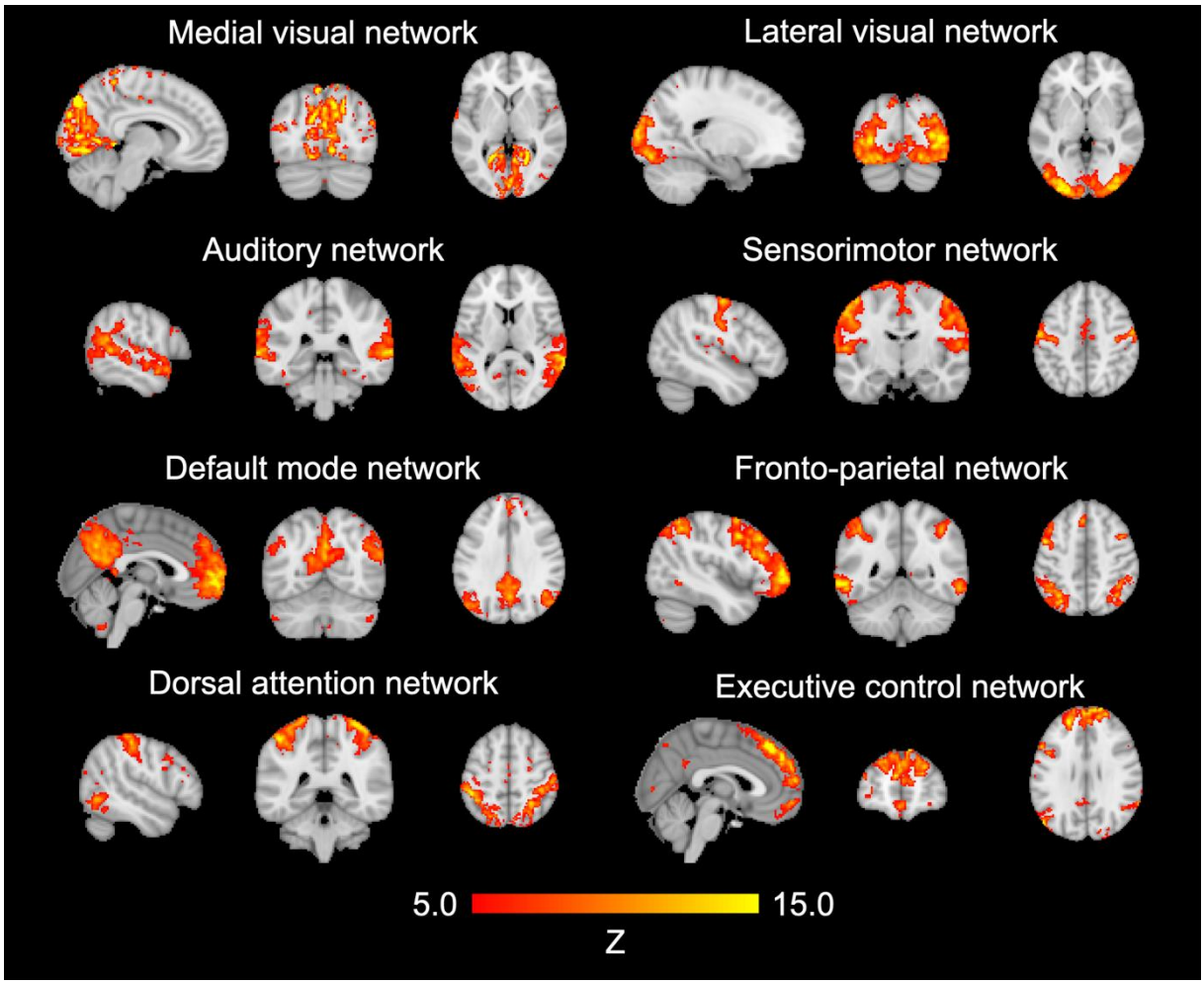

Figure 6.3: Normalised independent component spatial maps from the temporal-concatenation group ICA. These eight large-scale resting state networks were identified from a total of 15 components and used as input to the dual regression analysis. Z-values were arbitrarily thresholded between 5 and 15 for visualisation purposes.

Within-network connectivity was significantly reduced at SWAS compared to awake in all eight resting state networks (Figure 6.4). However, there was some heterogeneities in the spatial extent of the significant reduction. Functional connectivity was reduced in the entirety of the default mode network, lateral visual network, sensorimotor network, and auditory network. Meanwhile, only parts of the medial visual network, executive control network, dorsal attention network, and

frontoparietal network displayed significantly reduced connectivity. Reductions in functional connectivity in the medial visual network was found in parts of the intracalcarine cortex, supercalcarine cortex, and cuneal cortex. In the executive control network, significant reductions were found in the frontal regions of the network. In the frontoparietal network, the reduction in connectivity was primarily in the left hemisphere and in the dorsal attention network the reduction was most pronounced in the right hemisphere. Finally, parts of the thalamus had significantly reduced functional connectivity to the default mode network and the sensorimotor network despite not being part of either network component.

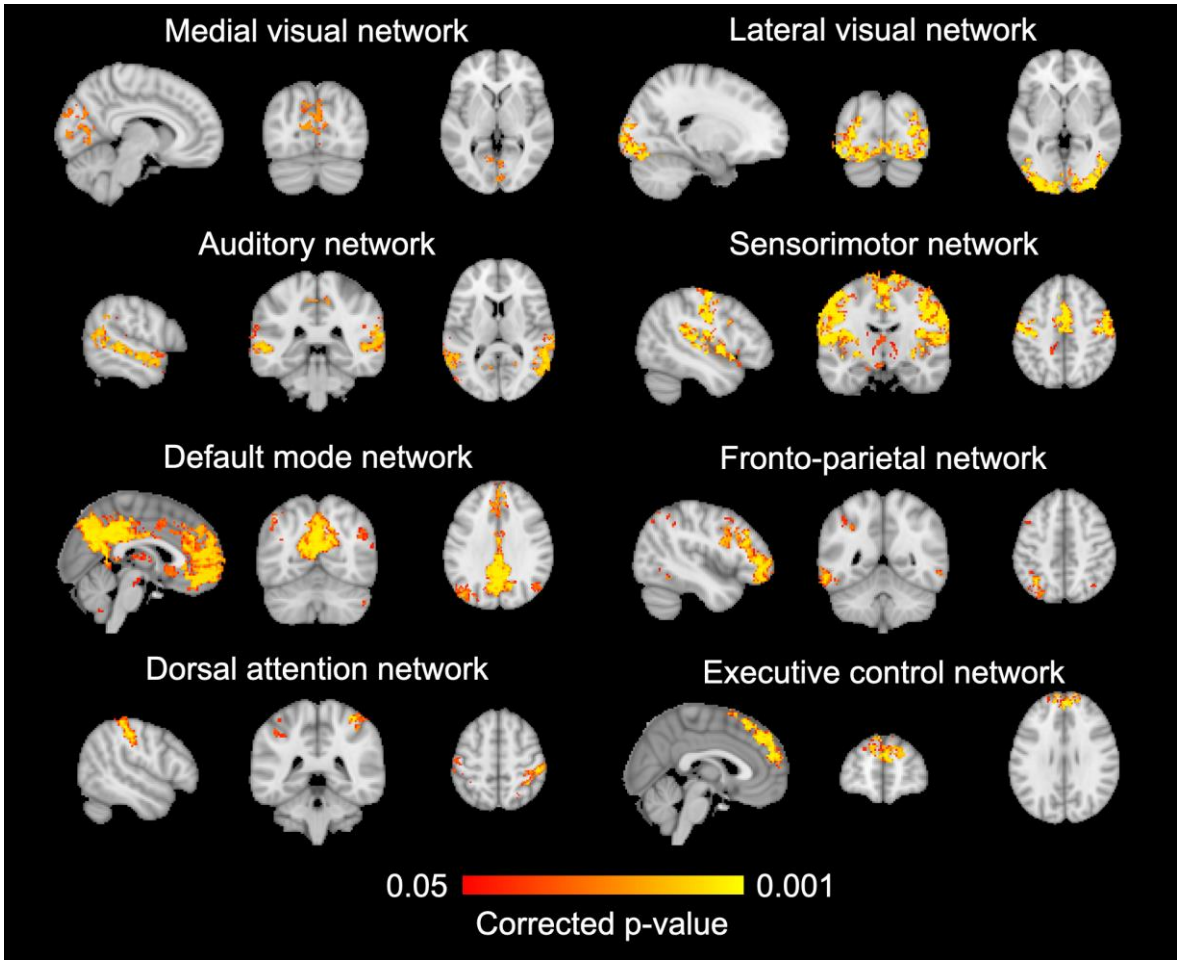

Figure 6.4: Group averaged statistical maps of voxel-wise reduction in within-network connectivity at SWAS compared to awake ($p<0.05$) in eight commonly identified resting state networks. P-value corrected for multiple comparisons across voxels and networks.

6.4 Discussion

6.4.1 Thalamocortical connectivity at SWAS

Our results clearly indicate that the thalamocortical system is severely disrupted in the SWAS state compared to when awake. Our investigation is therefore in line with accounts of anaesthetic-induced loss of consciousness in which the thalamocortical system plays a central role (Ranft et al., 2016; White & Alkire, 2003). However, our results stand in direct contrast to the study by Liu et al. (2013) using a similar methodology of analysing thalamocortical seed-based functional connectivity but using a different thalamic parcellation. They reported that, under propofol anaesthesia, thalamocortical functional connectivity from thalamic nuclei involved in the relay of sensory and motor signals was reduced but still relatively preserved when compared to other thalamic nuclei. Our results stand in contrast to these findings as the degree of reduction in functional thalamocortical connectivity to sensory and motor areas appears to be comparable to with other cortical regions. It is important to note though that this was using a different anaesthetic agent. Additionally, the target effect site concentration targeted by Liu et al. (2013) (2µg/ml) was lower than what has previously been found to be required for most people to achieve SWAS (mean±SD 2.7±0.5 µg/ml; Warnaby et al., 2017). One possibility is therefore that at higher concentrations, including the SWAS endpoint, there is an additional and later disruption of the sensory and motor thalamocortical system.

The thalamic parcellations used as seeds for the seed-based connectivity analysis were generated using a well-established method (Behrens, Johansen-Berg, et al., 2003) that has been validated to produce parcellations that correspond to nuclei and groups of nuclei defined from thalamic cytoarchitecture (Johansen-Berg et al., 2005). Therefore, this method remains a common paradigm for parcellating the thalamus *in-vivo*. Nevertheless, some caution when interpreting these results is warranted, as recent investigations have highlighted the propensity of probabilistic tractography to produce similar parcellations in intentionally corrupted diffusion data (Clayden et al., 2019).

6.4.2 Higher order network connectivity at SWAS

From the 15 group ICA components we identified four components that corresponded to known higher order networks: default mode network, frontoparietal network, dorsal attention network, and executive control network. We found that functional connectivity within the default mode network and the frontoparietal network was significantly reduced at SWAS compared to awake. Higher order cortical networks that link anterior and posterior brain regions, including the default mode and frontoparietal networks, have consistently been found to have reduced functional connectivity under general anaesthesia. This finding also to appears to hold across multiple anaesthetic agents, including propofol (Boveroux et al., 2010; Guldenmund et al., 2013, 2017; S. Wang et al., 2020), dexmedetomidine (Guldenmund et al., 2017), and sevoflurane (Huang et al., 2014; Palanca et al., 2015; Ranft et al., 2016). One notable exception however is Martuzzi et al., (2010), who found no significant reduction in default mode

network functional connectivity, albeit at a sub-anaesthetic concentration of sevoflurane (1% end-tidal).

The default mode and frontoparietal networks that have been suggested to support important functions supporting consciousness. The frontoparietal network plays an important role in control of goal-directed information flow in the brain (Uddin et al., 2019). As leading theories of consciousness emphasise the importance of integrating information from different neuronal networks (Baars, 2005; Tononi et al., 2016), breakdown of the information control functions of the frontoparietal network implies that important functions for sustaining consciousness are disrupted. While a clear consensus on the functions of the default mode network remains outstanding, it is likely involved in formation and maintenance of high-level associative representations (Uddin et al., 2019). Crucially, the default mode network includes the precuneus, which is part of the so-called posterior hot zone that has been suggested as a candidate for full and content-specific neural correlate of consciousness (Koch et al., 2016). Breakdown of connectivity within these networks under general anaesthesia may underlie frontal-parietal disconnects that have been observed electrophysiological functional connectivity measures (Blain-Moraes et al., 2015; Lee et al., 2013).

We also observed reduced functional connectivity in the dorsal attention network and executive control network at SWAS compared to awake. As Palanca et al., (2015) did not find a significant reduction in dorsal attention network functional connectivity at 1.2% end-tidal sevoflurane, this implies that disruption of the dorsal

attention network could occur at higher sevoflurane concentrations than the default mode and frontoparietal networks. A primary function of the dorsal attention network is directing and maintaining visuospatial attention as well as top-down stimulus and response selection (Uddin et al., 2019). Control of external attention is not a necessary condition for consciousness, as illustrated by states of disconnected consciousness such as dreaming. However, in the context of surgery, a breakdown of the dorsal attention network might render the patient unable to attend to external events in the event of intra-operative awareness. However, this remains somewhat speculative as it is not clear from the current literature that functionality of the dorsal attention network persists after loss of consciousness.

Comparatively, less is known the executive control network in the context of anaesthesia. Part of the reason for this is inconsistencies in terminology and spatial definition of the network in neuroimaging studies in general (Uddin et al., 2019). Some studies that have reported decreased executive control network connectivity under general anaesthesia include it as part of the frontoparietal network (e.g., Boveroux et al., 2010), making it difficult to dissociate frontoparietal and executive control network functional connectivity changes. Other studies do not include the executive control network at all (e.g., Palanca et al., 2015; Ranft et al., 2016). At sub-anaesthetic doses of ketamine, an increased functional connectivity in the executive control network has been reported (Mueller et al., 2018), though this might be related to the dissociative effects of sub-anaesthetic doses of ketamine that are unlikely to be transferrable to other anaesthetic agents.

6.4.2.1 Laterality in frontoparietal functional disconnection

Interestingly, we found that the significant reduction in within-network connectivity in the frontoparietal network was primarily, although not exclusively, found in the left hemisphere. Liu et al., (2013) similarly reported stronger disruption of thalamocortical connectivity to the left hemisphere, which they attributed to predominant left-lateralisation of language functions. As the left frontoparietal network has been suggested to be involved in language processing (Laird et al., 2011), our results add some credence to this interpretation. However, this interpretation should be made with some caution. Depending on the methodology used, particularly the number of ICA components, this network is often represented as two separate components lateralised to each hemisphere (Damoiseaux et al., 2006). Therefore, it could be that the laterality in the dual regression statistical maps is driven by the input frontoparietal component being more strongly representative of the left frontoparietal network.

6.4.3 Visual, auditory, and sensorimotor network connectivity at SWAS

We identified four components of the 15 group ICA components that corresponded with early sensory networks: medial visual network, lateral visual network, auditory network, and sensorimotor network. Functional connectivity within early sensory networks has been found to be relatively preserved under propofol anaesthesia compared to higher order networks (Boveroux et al., 2010; Palanca et al., 2015; S. Wang et al., 2020). Our results are partly in line with this, the reduction in within-network functional connectivity was markedly less in the medial compared to the lateral visual network. The medial visual network is comprised of primary visual

processing regions, including V1, whereas the lateral visual network is comprised of regions involved in secondary visual processing. Our finding therefore indicates a relative preservation of regions involved in primary visual processing over secondary visual processing. An important methodological consideration is that the subjects' eyes were closed during both resting state FMRI acquisitions. While neural activity persists in the visual cortices during eyes closed resting, as evident from occipital resting alpha activity in the EEG (Barry et al., 2007; Berger, 1933), the subjects were not processing visual stimuli in either condition.

However, a similar preservation was not evident for the auditory network or sensorimotor network. Disruption in these networks in our subjects is not unexpected given the lack of stimulus-evoked activation to pain and auditory stimulation discussed in the previous chapter. While it is unclear why these networks might differ from the visual networks, one possibility is that unlike the medial visual network, these resting state networks include more than just the primary sensory cortices. One study specifically investigating sevoflurane effects on the motor cortex reports reduced connectivity at 1% and 2% end-tidal sevoflurane (Peltier et al., 2005). In contrast, Palanca et al., (2015) reported no significant reduction in either the auditory or sensorimotor networks under sevoflurane-induced loss of responsiveness (1.2% end-tidal). In light of this, our results imply that disruption of sensorimotor and auditory networks occurs at higher concentrations of sevoflurane. This view is partially supported by Ranft et al., (2016), who found decreased auditory network connectivity at burst suppression, but not at 2% or 3% end-tidal sevoflurane (Ranft et al., 2016).

Crucially, in their study, resting state FMRI was first acquired at burst suppression, followed by the acquisitions at lower doses. As the process of induction to anaesthesia and recovery from anaesthesia is not necessarily symmetrical, this constitutes an important difference in the anaesthetic protocol compared to our study.

6.4.4 Thalamus connectivity to default mode and sensory motor networks

Interestingly, while the thalamus was not part of any of the resting state networks from the temporal-concatenation group ICA, there were significant reductions in functional connectivity between parts of the thalamus and both the default mode and sensorimotor networks. This may mean that the functional connectivity between these thalamic regions with the default mode and sensorimotor networks was significantly reduced at SWAS compared to awake, despite on average not being strongly connected across both conditions. Alternatively, this may be due to an artefact. These results provide further evidence of a disconnection between the thalamus and the cortex at SWAS using a data-driven analysis method. Palanca et al., (2015) found that at 1.2% end-tidal sevoflurane functional connectivity between the thalamus and the default mode network was significantly reduced, while connectivity between the thalamus and the sensorimotor network was preserved. Seen together with our results, this reinforces the idea that sensorimotor network disconnection occurs at higher concentrations of sevoflurane than default mode network disconnection.

As with the task FMRI analyses discussed in Chapter 5, these analyses are limited by the data having been acquired in steady states during wakefulness and at SWAS. Consequently, we cannot determine from these results whether or not the degree of functional disconnection we observed at SWAS occurred at lower concentrations during the transition to SWAS. However, unlike the task FMRI analyses, where we only acquired data during wakefulness and at SWAS, we did acquire continuous resting state FMRI during the transition to SWAS as part of this study. This could enable future analyses that may elucidate how functional disconnection occurs during transitions to the SWAS state.

In conclusion, using SCA and dual regression analysis methods of resting state FMRI data we found that functional connectivity in the thalamocortical system and known resting state networks was significantly disrupted at SWAS. These findings clearly indicate that the brain is in a strongly disconnected state when held at SWAS. In light of leading theories of consciousness emphasising anterior-posterior communication sustaining conscious experience, this implies that SWAS is a state of unconsciousness under general anaesthesia. To the extent conscious experience is possible, disruption of diverse brain networks involved in attending to the external world, performing executive functions, and relaying and processing of sensory information further implies that perception of external stimulation such as surgical pain is precluded at SWAS. Therefore, the present findings provide further support for SWAS as a state of perception loss under general anaesthesia.

7 Concluding remarks

The motivation to embark on this thesis was deeply rooted in curiosity about the phenomenon of subjective, conscious experience that long has intrigued philosophers and scientists. I aimed to build on the foundational work of the SWAS brain state with a view towards improving our understanding of SWAS, as well as anaesthesia-induced loss of consciousness more generally. Crucially, this work was done with a view to translate these advances to clinical practice by developing SWAS as a target for clinical anaesthesia.

In this thesis, I have reported on the development of a prototype system for titrating anaesthesia to SWAS within an individual. Next, I reported on the application of the prototype system in two studies, one focused on the clinical translation of the SWAS end point and another focused on experimental validation of SWAS as a state of perception loss under general anaesthesia. I have shown that cerebral blood flow is profoundly altered in the SWAS state under sevoflurane anaesthesia. Finally, I have shown that processing of external stimulation was severely disrupted in individuals held at SWAS and that this was accompanied by significant breakdown in functional connectivity within the thalamocortical system and resting state networks.

The work reported in this thesis has several innovations over the current neuroimaging literature of anaesthesia. A major challenge when studying

anaesthesia is consolidating findings across studies and anaesthetic agents. Different studies operationalise loss of consciousness in different ways, leading to reported findings about brain activity under loss of consciousness conflating a range of different brain states. The work presented in this thesis addresses this problem by targeting a specific brain state, SWAS, and showed that it is feasible to titrate anaesthesia to this state. Independent of the clinical viability of SWAS, this provides a framework for the investigation of surgical levels of anaesthesia that can allow comparisons between studies and anaesthetic agents.

Another innovation in the work presented in this thesis is the strict control of anaesthetic effects on cerebral blood flow. The potential confounding effects of anaesthesia on BOLD FMRI have been known for some time. Palanca et al., (2015) indirectly accounted for this by controlling for sevoflurane-induced changes to CO_2. However, to our knowledge, ours is the first neuroimaging study of anaesthesia to incorporate CBF changes in analyses of neuronal activity.

Our results provide support for broader theories of consciousness that emphasise the integration of information from distributed neuronal networks, including the integrated information theory and the global workspace hypothesis. The cortical bistability that underlies slow waves across unconscious states has been argued to disrupt causal integration (Pigorini et al., 2015), providing a potential mechanistic explanation for how a diverse range of anaesthetic agents have the common effect of supressing consciousness. We have shown that when held at the SWAS end point, i.e., when cortical bistability is maximal, the brain's ability to

respond to external stimulation is severely disrupted. This implies that conscious perception of external stimulation is not possible in the SWAS state. Our finding that functional connectivity in large-scale brain networks is significantly reduced when held at SWAS further supports this interpretation. Crucially, however, our data cannot demonstrate a causal relationship between the reduction in functional connectivity and disruption of sensory processing observed at SWAS.

Recently, it has been argued that slow waves are not a universal indicator of loss of consciousness (Frohlich et al., 2021). The authors point to counter examples where slow waves are observable in conscious states, such as delirium and certain neurodevelopmental disorders. The authors conclude that clinicians should not infer consciousness in patients from slow wave power alone. The hypothesis that SWAS is a state of perception loss under general anaesthesia is entirely in line with this position. The potential neurophysiological underpinning of SWAS implies that increasing slow wave power during anaesthetic induction stems from an increasing number of cortical neurons being recruited into the slow oscillation. This further implies that simply observing slow waves under general anaesthesia may not be sufficient to establish loss of consciousness, as it is when the slow waves power reaches saturation that the full consciousness-supressing effect of the anaesthetic has been achieved. Furthermore, it may be overly reductive to argue that high power in the slow wave frequency band is indicative of the same underlying neural processes across all.

Finally, the work in this thesis has important clinical implications. We have demonstrated that it is feasible to titrate anaesthesia to SWAS within an individual with good accuracy within a time frame that is clinically viable. Furthermore, by analysing stimulus-evoked and resting brain activity having titrated anaesthesia to SWAS, we have provided validation that SWAS is a state of perception loss under general anaesthesia. The prototype system for titrating anaesthesia to SWAS provides a foundation for the development of an individualised depth of anaesthesia system. While large scale clinical trials are necessary to establish the clinical efficacy of the SWAS end point as a target, it is noteworthy that in the limited samples analysed to date, there have been no positive IFT responses at SWAS and no post-recovery recall of external events.

A limitation of the work presented in this thesis is that the ASL, task and resting state FMRI analyses have focused on steady state acquisitions at SWAS. While this allows for detailed investigation of SWAS, which is useful for clinical validation of SWAS, it does not tell us how the brain transitions from wakefulness to SWAS. Furthermore, this work does not provide evidence that SWAS specifically is a state of complete unconsciousness compared to other points along the transition to SWAS (e.g., at 70%, 80%, or 90% slow wave power compared to SWAS). As part of Study 2, FMRI was acquired during transition from wakefulness, through LOBR, to SWAS. I was not able to analyse this data within the scope of my thesis, but future work on this data may elucidate how this transition occurs, as well as whether neural correlates of consciousness cease completely at SWAS or earlier in the transition to SWAS.

The phenomenon of consciousness has intrigued and perplexed philosophers and scientists for centuries, but only in the past few decades has modern neuroimaging techniques allowed for a true science of consciousness to emerge. In this thesis I have leveraged advanced multimodal neuroimaging techniques to overcome key challenges in the study of anaesthesia-induced loss of consciousness. By doing so, I have been able to provide validation that SWAS is a state of perception loss under general anaesthesia and a promising target for clinical anaesthesia.

8 Bibliography

Ab Aziz, C. B., & Ahmad, A. H. (2006). The role of the thalamus in modulating pain. *Malaysian Journal of Medical Sciences*, *13*(2), 11–18.

Abbott, J., & Abbott, P. (1995). Psychological and cardiovascular predictors of anaesthesia induction, operative and post-operative complications in minor gynaecological surgery. *British Journal of Clinical Psychology*, *34*(4), 613–625. https://doi.org/10.1111/j.2044-8260.1995.tb01495.x

Ag, M., Wang, M., Ward, M., Wilker, C., Smith, B., Vezina, D., & Pace, N. (2016). Anaesthetic interventions for prevention of awareness during surgery. *Cochrane Database of Systematic Reviews*, *10*, 1–367. https://doi.org/10.1002/14651858.CD007272.pub2

Akeju, O., Westover, B., Pavone, K. J., Sampson, A. L., Hartnack, K. E., Brown, E. N., & Purdon, P. L. (2014). Effects of sevoflurane and propofol on frontal electroencephalogram power and coherence. *Anesthesiology*, *121*(5), 990–998. https://doi.org/10.1097/ALN.0000000000000436

Akselrod, M., Martuzzi, R., Serino, A., van der Zwaag, W., Gassert, R., & Blanke, O. (2017). Anatomical and functional properties of the foot and leg representation in areas 3b, 1 and 2 of primary somatosensory cortex in humans: A 7T fMRI study. *NeuroImage*, *159*, 473–487. https://doi.org/10.1016/j.neuroimage.2017.06.021

Aksenov, D. P., Li, L., Miller, M. J., Iordanescu, G., & Wyrwicz, A. M. (2015). Effects of anesthesia on BOLD signal and neuronal activity in the

somatosensory cortex. *Journal of Cerebral Blood Flow & Metabolism*, *35*(11), 1819–1826. https://doi.org/10.1038/jcbfm.2015.130

Alkire, M. T., Haier, R. J., & Fallon, J. H. (2000). Toward a unified theory of narcosis: Brain imaging evidence for a thalamocortical switch as the neurophysiologic basis of anesthetic-induced unconsciousness. *Consciousness and Cognition*, *9*(3), 370–386. https://doi.org/10.1006/ccog.1999.0423

Alkire, M. T., Pomfrett, C. J. D., Haier, R. J., Gianzero, M. V., Chan, C. M., Jacobsen, B. P., & Fallon, J. H. (1999). Functional brain imaging during anesthesia in humans: Effects of halothane on global and regional cerebral glucose metabolism. *Anesthesiology*, *90*(3), 701–709. https://doi.org/10.1097/00000542-199903000-00011

Allen, P. J., Josephs, O., & Turner, R. (2000). A method for removing imaging artifact from continuous EEG recorded during functional MRI. *NeuroImage*, *12*(2), 230–239. https://doi.org/10.1006/nimg.2000.0599

Allen, P. J., Polizzi, G., Krakow, K., Fish, D. R., & Lemieux, L. (1998). Identification of EEG events in the MR scanner: The problem of pulse artifact and a method for its subtraction. *NeuroImage*, *8*(3), 229–239. https://doi.org/10.1006/nimg.1998.0361

Al-Rifai, Z., & Mulvey, D. (2016). Principles of total intravenous anaesthesia: Practical aspects of using total intravenous anaesthesia. *BJA Education*, *16*(8), 276–280. https://doi.org/10.1093/bjaed/mkv074

Alsop, D. C., Detre, J. A., Golay, X., Günther, M., Hendrikse, J., Hernandez-Garcia, L., Lu, H., MacIntosh, B. J., Parkes, L. M., Smits, M., van Osch, M.

J. P., Wang, D. J., Wong, E. C., & Zaharchuk, G. (2015). Recommended implementation of arterial spin labeled perfusion MRI for clinical applications: A consensus of the ISMRM perfusion study group and the European consortium for ASL in dementia. *Magnetic Resonance in Medicine*, *73*(1), 102–116. https://doi.org/10.1002/mrm.25197

Andersson, J. L. R., Jenkinson, M., & Smith, S. (2007). *Non-linear registration, aka spatial normalisation. FMRIB technical report TR07JA2* [Technical Report]. https://www.fmrib.ox.ac.uk/datasets/techrep/tr07ja2/tr07ja2.pdf

Andersson, J. L. R., Skare, S., & Ashburner, J. (2003). How to correct susceptibility distortions in spin-echo echo-planar images: Application to diffusion tensor imaging. *NeuroImage*, *20*(2), 870–888. https://doi.org/10.1016/S1053-8119(03)00336-7

Andersson, J. L. R., & Sotiropoulos, S. N. (2016). An integrated approach to correction for off-resonance effects and subject movement in diffusion MR imaging. *NeuroImage*, *125*, 1063–1078. https://doi.org/10.1016/j.neuroimage.2015.10.019

Aranake, A., Mashour, G. M., & Avidan, M. S. (2013). Minimum alveolar concentration: Ongoing relevance and clinical utility. *Anaesthesia*, *68*(5), 512–522. https://doi.org/10.1111/anae.12168

Armstead, W. M. (2016). Cerebral Blood Flow Autoregulation and Dysautoregulation. *Anesthesiology Clinics*, *34*(3), 465–477. https://doi.org/10.1016/j.anclin.2016.04.002

Asai, T., Kanayama, N., Imaizumi, S., Koyama, S., & Kaganoi, S. (2016). Development of Embodied Sense of Self Scale (ESSS): Exploring everyday

experiences induced by anomalous self-representation. *Frontiers in Psychology*, *7*, 1005. https://doi.org/10.3389/fpsyg.2016.01005

Aslaksen, P. M., Myrbakk, I. N., Høifødt, R. S., & Flaten, M. A. (2007). The effect of experimenter gender on autonomic and subjective responses to pain stimuli. *PAIN*, *129*(3), 260–268. https://doi.org/10.1016/j.pain.2006.10.011

Aslan, S., Xu, F., Wang, P. L., Uh, J., Yezhuvath, U. S., Osch, M. van, & Lu, H. (2010). Estimation of labeling efficiency in pseudocontinuous arterial spin labeling. *Magnetic Resonance in Medicine*, *63*(3), 765–771. https://doi.org/10.1002/mrm.22245

Austin, V. C., Blamire, A. M., Allers, K. A., Sharp, T., Styles, P., Matthews, P. M., & Sibson, N. R. (2005). Confounding effects of anesthesia on functional activation in rodent brain: A study of halothane and α-chloralose anesthesia. *NeuroImage*, *24*(1), 92–100. https://doi.org/10.1016/j.neuroimage.2004.08.011

Avidan, M. S., Jacobsohn, E., Glick, D., Burnside, B. A., Zhang, L., Villafranca, A., Karl, L., Kamal, S., Torres, B., O'Connor, M., Evers, A. S., Gradwohl, S., Lin, N., Palanca, B. J., & Mashour, G. A. (2011). Prevention of Intraoperative Awareness in a High-Risk Surgical Population. *New England Journal of Medicine*, *365*(7), 591–600. https://doi.org/10.1056/NEJMoa1100403

Baars, B. J. (1997). In the theatre of consciousness. Global Workspace Theory, a rigorous scientific theory of consciousness. *Journal of Consciousness Studies*, *4*(4), 292–309.

Baars, B. J. (2005). Global workspace theory of consciousness: Toward a cognitive neuroscience of human experience. In *Progress in Brain Research* (Vol. 150, pp. 45–53). Elsevier. https://doi.org/10.1016/S0079-6123(05)50004-9

Barry, R. J., Clarke, A. R., Johnstone, S. J., Magee, C. A., & Rushby, J. A. (2007). EEG differences between eyes-closed and eyes-open resting conditions. *Clinical Neurophysiology*, *118*(12), 2765–2773. https://doi.org/10.1016/j.clinph.2007.07.028

Beckmann, C. F., & Smith, S. M. (2004). Probabilistic independent component analysis for functional magnetic resonance imaging. *IEEE Transactions on Medical Imaging*, *23*(2), 137–152. https://doi.org/10.1109/TMI.2003.822821

Behrens, T. E. J., Berg, H. J., Jbabdi, S., Rushworth, M. F. S., & Woolrich, M. W. (2007). Probabilistic diffusion tractography with multiple fibre orientations: What can we gain? *NeuroImage*, *34*(1), 144–155. https://doi.org/10.1016/j.neuroimage.2006.09.018

Behrens, T. E. J., Johansen-Berg, H., Woolrich, M. W., Smith, S. M., Wheeler-Kingshott, C. A. M., Boulby, P. A., Barker, G. J., Sillery, E. L., Sheehan, K., Ciccarelli, O., Thompson, A. J., Brady, J. M., & Matthews, P. M. (2003). Non-invasive mapping of connections between human thalamus and cortex using diffusion imaging. *Nature Neuroscience*, *6*(7), 750–757. https://doi.org/10.1038/nn1075

Behrens, T. E. J., Woolrich, M. W., Jenkinson, M., Johansen-Berg, H., Nunes, R. G., Clare, S., Matthews, P. M., Brady, J. M., & Smith, S. M. (2003). Characterization and propagation of uncertainty in diffusion-weighted MR

imaging. *Magnetic Resonance in Medicine*, *50*(5), 1077–1088. https://doi.org/10.1002/mrm.10609

Berger, H. (1933). Über das Elektrenkephalogramm des Menschen: Fünfte Mitteilung. *Archiv für Psychiatrie und Nervenkrankheiten*, *98*(1), 231–254. https://doi.org/10.1007/BF01814645

Blain-Moraes, S., Tarnal, V., Vanini, G., Alexander, A., Rosen, D., Shortal, B., Janke, E., & Mashour, G. A. (2015). Neurophysiological correlates of sevoflurane-induced unconsciousness. *Anesthesiology*, *122*(2), 307–316. https://doi.org/10.1097/ALN.0000000000000482

Bloor, B. C., Ward, D. S., Belleville, J. P., & Maze, M. (1992). Effects of intravenous dexmedetomidine in humans. II. Hemodynamic changes. *Anesthesiology*, *77*(6), 1134–1142. https://doi.org/10.1097/00000542-199212000-00014

Boly, M., Moran, R., Murphy, M., Boveroux, P., Bruno, M.-A., Noirhomme, Q., Ledoux, D., Bonhomme, V., Brichant, J.-F., Tononi, G., Laureys, S., & Friston, K. (2012). Connectivity Changes Underlying Spectral EEG Changes during Propofol-Induced Loss of Consciousness. *Journal of Neuroscience*, *32*(20), 7082–7090. https://doi.org/10.1523/JNEUROSCI.3769-11.2012

Bouillon, T. (2008). Hypnotic and opioid anesthetic drug interactions on the CNS, focus on response surface modeling. In *Handbook of Experimental Pharmacology* (pp. 471–487). Springer.

Boveroux, P., Vanhaudenhuyse, A., Bruno, M.-A., Noirhomme, Q., Lauwick, S., Luxen, A., Degueldre, C., Plenevaux, A., Schnakers, C., Phillips, C.,

Brichant, J.-F., Bonhomme, V., Maquet, P., Greicius, M. D., Laureys, S., & Boly, M. (2010). Breakdown of within- and between-network Resting State Functional Magnetic Resonance Imaging Connectivity during Propofol-induced Loss of Consciousness. *Anesthesiology*, *113*(5), 1038–1053. https://doi.org/10.1097/ALN.0b013e3181f697f5

Brice, D. D., Hetherington, R. R., & Utting, J. E. (1970). A simple study of awareness and dreaming during anaesthesia. *British Journal of Anaesthesia*, *42*(6), 535–542. https://doi.org/10.1093/bja/42.6.535

Brooks, J. C. W., Beckmann, C. F., Miller, K. L., Wise, R. G., Porro, C. A., Tracey, I., & Jenkinson, M. (2008). Physiological noise modelling for spinal functional magnetic resonance imaging studies. *NeuroImage*, *39*(2), 680–692. https://doi.org/10.1016/j.neuroimage.2007.09.018

Brooks, J. C. W., Faull, O., Pattinson, K., & Jenkinson, M. (2013). Physiological noise in brainstem fMRI. *Frontiers in Human Neuroscience*, *7*, 623. https://doi.org/10.3389/fnhum.2013.00623

Brooks, J. C. W., Zambreanu, L., Godinez, A., Craig, A. D. (Bud), & Tracey, I. (2005). Somatotopic organisation of the human insula to painful heat studied with high resolution functional imaging. *NeuroImage*, *27*(1), 201–209. https://doi.org/10.1016/j.neuroimage.2005.03.041

Brown, E. N., Lydic, R., & Schiff, N. D. (2010). General anesthesia, sleep, and coma. *New England Journal of Medicine*, *363*(27), 2638–2650. https://doi.org/10.1056/NEJMra0808281

Brown, E. N., Pavone, K. J., & Naranjo, M. (2018). Multimodal general anesthesia: Theory and practice. *Anesthesia & Analgesia*, *127*(5), 1246–1258. https://doi.org/10.1213/ANE.0000000000003668

Brown, E. N., Purdon, P. L., & Van Dort, C. J. (2011). General Anesthesia and Altered States of Arousal: A Systems Neuroscience Analysis. *Annual Review of Neuroscience*, *34*(1), 601–628. https://doi.org/10.1146/annurev-neuro-060909-153200

Bruhn, J., Bouillon, T., & Shafer, S. L. (2000). Bispectral Index (BIS) and burst suppression: Revealing a part of the BIS algorithm. *Journal of Clinical Monitoring and Computing*, *16*, 593–596. https://doi.org/10.1023/A:1012216600170

Bulte, D. P., Chiarelli, P. A., Wise, R. G., & Jezzard, P. (2007). Cerebral perfusion response to hyperoxia. *Journal of Cerebral Blood Flow & Metabolism*, *27*(1), 69–75. https://doi.org/10.1038/sj.jcbfm.9600319

Bundgaard, H., Oettingen, G. von, Larsen, K. M., Landsfeldt, U., Jensen, K. A., Nielsen, E., & Cold, G. E. (1998). Effects of sevoflurane on intracranial pressure, cerebral blood flow and cerebral metabolism: A dose-response study in patients subjected to craniotomy for cerebral tumours. *Acta Anaesthesiologica Scandinavica*, *42*(6), 621–627. https://doi.org/10.1111/j.1399-6576.1998.tb05292.x

Buxton, R. B., Uludağ, K., Dubowitz, D. J., & Liu, T. T. (2004). Modeling the hemodynamic response to brain activation. *NeuroImage*, *23*, S220–S233. https://doi.org/10.1016/j.neuroimage.2004.07.013

Buysse, D. J., Reynolds, C. F., Monk, T. H., Berman, S. R., & Kupfer, D. J. (1989). The Pittsburgh Sleep Quality Index: A new instrument for psychiatric practice and research. *Psychiatry Research*, *28*(2), 193–213. https://doi.org/10.1016/0165-1781(89)90047-4

Chalmers, D. (1995). Facing up to the problem of consciousness. *Journal of Consciousness Studies*, *2*(3), 200–219.

Chappell, M. A., Groves, A. R., MacIntosh, B. J., Donahue, M. J., Jezzard, P., & Woolrich, M. W. (2011). Partial volume correction of multiple inversion time arterial spin labeling MRI data. *Magnetic Resonance in Medicine*, *65*(4), 1173–1183. https://doi.org/10.1002/mrm.22641

Chappell, M. A., Groves, A. R., Whitcher, B., & Woolrich, M. W. (2009). Variational Bayesian inference for a nonlinear forward model. *IEEE Transactions on Signal Processing*, *57*(1), 223–236. https://doi.org/10.1109/TSP.2008.2005752

Chen, A. C. N., Niddam, D. M., & Arendt-Nielsen, L. (2001). Contact heat evoked potentials as a valid means to study nociceptive pathways in human subjects. *Neuroscience Letters*, *316*(2), 79–82. https://doi.org/10.1016/S0304-3940(01)02374-6

Cho, S., Fujigaki, T., Uchiyama, Y., Fukusaki, M., Shibata, O., & Sumikawa, K. (1996). Effects of sevoflurane with and without nitrous oxide on human cerebral circulation: Transcranial Doppler study. *Anesthesiology*, *85*(4), 755–760. https://doi.org/10.1097/00000542-199610000-00010

Clayden, J. D., Thomas, D. L., & Kraskov, A. (2019). Tractography-based parcellation does not provide strong evidence of anatomical organisation

within the thalamus. *NeuroImage*, *199*, 418–426. https://doi.org/10.1016/j.neuroimage.2019.06.019

Cohen, E. R., Ugurbil, K., & Kim, S.-G. (2002). Effect of basal conditions on the magnitude and dynamics of the Blood Oxygenation Level-Dependent fMRI response. *Journal of Cerebral Blood Flow & Metabolism*, *22*(9), 1042–1053. https://doi.org/10.1097/00004647-200209000-00002

Conti, A., Iacopino, D. G., Fodale, V., Micalizzi, S., Penna, O., & Santamaria, L. B. (2006). Cerebral haemodynamic changes during propofol–remifentanil or sevoflurane anaesthesia: Transcranial Doppler study under Bispectral Index monitoring. *British Journal of Anaesthesia*, *97*(3), 333–339. https://doi.org/10.1093/bja/ael169

Corfield, D. R., Murphy, K., Josephs, O., Adams, L., & Turner, R. (2001). Does hypercapnia-induced cerebral vasodilation modulate the hemodynamic response to neural activation? *NeuroImage*, *13*(6), 1207–1211. https://doi.org/10.1006/nimg.2001.0760

Damoiseaux, J. S., Rombouts, S. A. R. B., Barkhof, F., Scheltens, P., Stam, C. J., Smith, S. M., & Beckmann, C. F. (2006). Consistent resting-state networks across healthy subjects. *Proceedings of the National Academy of Sciences*, *103*(37), 13848–13853. https://doi.org/10.1073/pnas.0601417103

Dang-Vu, T. T., Desseilles, M., Laureys, S., Degueldre, C., Perrin, F., Phillips, C., Maquet, P., & Peigneux, P. (2005). Cerebral correlates of delta waves during non-REM sleep revisited. *NeuroImage*, *28*(1), 14–21. https://doi.org/10.1016/j.neuroimage.2005.05.028

Dexter, F., Macario, A., Manberg, P. J., & Lubarsky, D. A. (1999). Computer simulation to determine how rapid anesthetic recovery protocols to decrease the time for emergence or increase the phase I postanesthesia care unit bypass rate affect staffing of an ambulatory surgery center. *Anesthesia & Analgesia*, *88*(5), 1053–1063. https://doi.org/10.1213/00000539-199905000-00016

Dexter, F., & Wachtel, R. E. (2006). Economic, educational, and policy perspectives on the preincision operating room period. *Anesthesia & Analgesia*, *103*(4), 919–921. https://doi.org/10.1213/01.ANE.0000240236.66105.A9

Egan, T. D. (2019). Are opioids indispensable for general anaesthesia? *British Journal of Anaesthesia*, *122*(6), e127–e135. https://doi.org/10.1016/j.bja.2019.02.018

Eger, E. I. (2004). Characteristics of anesthetic agents used for induction and maintenance of general anesthesia. *American Journal of Health-System Pharmacy*, *61*(Suppl 4), S3–S10. https://doi.org/10.1093/ajhp/61.suppl_4.S3

Eger, E. I., Saidman, L. J., & Brandstater, B. (1965). Minimum alveolar anesthetic concentration: A standard of anesthetic potency. *Anesthesiology*, *26*(6), 756–763. https://doi.org/10.1097/00000542-196511000-00010

Feuerecker, M., Lenk, M., Flake, G., Edelmann-Gahr, V., Wiepcke, D., Hornuss, C., Daunderer, M., Müller, H.-H., & Kuhnle, G. E. (2011). Effects of increasing sevoflurane MAC levels on mid-latency auditory evoked

potentials in infants, schoolchildren, and the elderly. *British Journal of Anaesthesia*, *107*(5), 726–734. https://doi.org/10.1093/bja/aer226

Fiset, P., Paus, T., Daloze, T., Plourde, G., Meuret, P., Bonhomme, V., Hajj-Ali, N., Backman, S. B., & Evans, A. C. (1999). Brain mechanisms of propofol-induced loss of consciousness in humans: A positron emission tomographic study. *Journal of Neuroscience*, *19*(13), 5506–5513. https://doi.org/10.1523/JNEUROSCI.19-13-05506.1999

Forrest, F. C., Tooley, M. A., Saunders, P. R., & Prys-Roberts, C. (1994). Propofol infusion and the suppression of consciousness: The EEG and dose requirements. *British Journal of Anaesthesia*, *72*(1), 35–41. https://doi.org/10.1093/bja/72.1.35

Franks, N. P. (2008). General anaesthesia: From molecular targets to neuronal pathways of sleep and arousal. *Nature Reviews Neuroscience*, *9*(5), 370–386. https://doi.org/10.1038/nrn2372

Franks, N. P., Dickinson, R., de Sousa, S. L. M., Hall, A. C., & Lieb, W. R. (1998). How does xenon produce anaesthesia? *Nature*, *396*(6709), 324–324. https://doi.org/10.1038/24525

Friedman, E. B., Sun, Y., Moore, J. T., Hung, H.-T., Meng, Q. C., Perera, P., Joiner, W. J., Thomas, S. A., Eckenhoff, R. G., Sehgal, A., & Kelz, M. B. (2010). A conserved behavioral state barrier impedes transitions between anesthetic-induced unconsciousness and wakefulness: Evidence for neural inertia. *PLOS ONE*, *5*(7), e11903. https://doi.org/10.1371/journal.pone.0011903

Friston, K. J., Holmes, A. P., Poline, J.-B., Grasby, P. J., Williams, S. C. R., Frackowiak, R. S. J., & Turner, R. (1995). Analysis of fMRI time-series revisited. *NeuroImage*, *2*(1), 45–53. https://doi.org/10.1006/nimg.1995.1007

Frohlich, J., Toker, D., & Monti, M. M. (2021). Consciousness among delta waves: A paradox? *Brain*, *144*(8), 2257–2277. https://doi.org/10.1093/brain/awab095

Garcia, P. S., Kolesky, S. E., & Jenkins, A. (2010). General anesthetic actions on $GABA_A$ receptors. *Current Neuropharmacology*, *8*(1), 2–9. https://doi.org/10.2174/157015910790909502

Glisky, M. L., Tataryn, D. J., Tobias, B. A., Kihlstrom, J. F., & McConkey, K. M. (1991). Absorption, openness to experience, and hypnotizability. *Journal of Personality and Social Psychology*, *60*(2), 263. https://doi.org/10.1037/0022-3514.60.2.263

Goto, T., Nakata, Y., Saito, H., Ishiguro, Y., Niimi, Y., & Morita, S. (2001). The midlatency auditory evoked potentials predict responsiveness to verbal commands in patients emerging from anesthesia with xenon, isoflurane, and sevoflurane but not with nitrous oxide. *Anesthesiology*, *94*(5), 782–789. https://doi.org/10.1097/00000542-200105000-00015

Granovsky, Y., Granot, M., Nir, R.-R., & Yarnitsky, D. (2008). Objective correlate of subjective pain perception by contact heat-evoked potentials. *The Journal of Pain*, *9*(1), 53–63. https://doi.org/10.1016/j.jpain.2007.08.010

Griffanti, L., Douaud, G., Bijsterbosch, J., Evangelisti, S., Alfaro-Almagro, F., Glasser, M. F., Duff, E. P., Fitzgibbon, S., Westphal, R., Carone, D., Beckmann, C. F., & Smith, S. M. (2017). Hand classification of fMRI ICA

noise components. *NeuroImage*, *154*, 188–205. https://doi.org/10.1016/j.neuroimage.2016.12.036

Guldenmund, P., Demertzi, A., Boveroux, P., Boly, M., Vanhaudenhuyse, A., Bruno, M.-A., Gosseries, O., Noirhomme, Q., Brichant, J.-F., Bonhomme, V., Laureys, S., & Soddu, A. (2013). Thalamus, brainstem and salience network connectivity changes during propofol-induced sedation and unconsciousness. *Brain Connectivity*, *3*(3), 273–285. https://doi.org/10.1089/brain.2012.0117

Guldenmund, P., Vanhaudenhuyse, A., Sanders, R. D., Sleigh, J. W., Bruno, M. A., Demertzi, A., Bahri, M. A., Jaquet, O., Sanfilippo, J., Baquero, K., Boly, M., Brichant, J. F., Laureys, S., & Bonhomme, V. (2017). Brain functional connectivity differentiates dexmedetomidine from propofol and natural sleep. *BJA: British Journal of Anaesthesia*, *119*(4), 674–684. https://doi.org/10.1093/bja/aex257

Haller, S., Wetzel, S. G., Radue, E. W., & Bilecen, D. (2006). Mapping continuous neuronal activation without an ON–OFF paradigm: Initial results of BOLD ceiling fMRI. *European Journal of Neuroscience*, *24*(9), 2672–2678. https://doi.org/10.1111/j.1460-9568.2006.05147.x

Handwerker, D. A., Ollinger, J. M., & D'Esposito, M. (2004). Variation of BOLD hemodynamic responses across subjects and brain regions and their effects on statistical analyses. *NeuroImage*, *21*(4), 1639–1651. https://doi.org/10.1016/j.neuroimage.2003.11.029

Hansen, T. D., Warner, D. S., Todd, M. M., & Vust, L. J. (1989). The role of cerebral metabolism in determining the local cerebral blood dlow effects of

volatile anesthetics: Evidence for persistent flow-metabolism coupling. *Journal of Cerebral Blood Flow & Metabolism*, *9*(3), 323–328. https://doi.org/10.1038/jcbfm.1989.50

Harris, R. S., Lazar, O., Johansen, J. W., & Sebel, P. S. (2006). Interaction of propofol and sevoflurane on loss of consciousness and movement to skin incision during general anesthesia. *Anesthesiology*, *104*(6), 1170–1175. https://doi.org/10.1097/00000542-200606000-00011

Heine, L., Soddu, A., Gomez, F., Vanhaudenhuyse, A., Tshibanda, L., Thonnard, M., Charland-Verville, V., Kirsch, M., Laureys, S., & Demertzi, A. (2012). Resting State Networks and Consciousness. *Frontiers in Psychology*, *3*, 295. https://doi.org/10.3389/fpsyg.2012.00295

Heinke, W., Kenntner, R., Gunter, T. C., Sammler, D., Olthoff, D., & Koelsch, S. (2004). Sequential effects of increasing propofol sedation on frontal and temporal cortices as indexed by auditory event-related potentials. *Anesthesiology*, *100*(3), 617–625. https://doi.org/10.1097/00000542-200403000-00023

Hendrickx, J. F. A., Eger, E. I. I., Sonner, J. M., & Shafer, S. L. (2008). Is synergy the rule? A review of anesthetic interactions producing hypnosis and immobility. *Anesthesia & Analgesia*, *107*(2), 494–506. https://doi.org/10.1213/ane.0b013e31817b859e

Hernández, M., Guerrero, G. D., Cecilia, J. M., Garcia, J. M., Inuggi, A., & Sotiropoulos, S. N. (2012). Accelerating fibre orientation estimation from diffusion weighted magnetic resonance imaging using GPUs. *2012 20th*

Euromicro International Conference on Parallel, Distributed and Network-Based Processing, 622–626. https://doi.org/10.1109/PDP.2012.46

Hofbauer, R. K., Fiset, P., Plourde, G., Backman, S. B., & Bushnell, M. C. (2004). Dose-dependent effects of propofol on the central processing of thermal pain. *Anesthesiology*, *100*(2), 386–394. https://doi.org/10.1097/00000542-200402000-00031

Huang, Z., Liu, X., Mashour, G. A., & Hudetz, A. G. (2018). Timescales of intrinsic BOLDsignal dynamics and functional connectivity in pharmacologic and neuropathologic states of unconsciousness. *Journal of Neuroscience*, *38*(9), 2304–2317. https://doi.org/10.1523/JNEUROSCI.2545-17.2018

Huang, Z., Wang, Z., Zhang, J., Dai, R., Wu, J., Li, Y., Liang, W., Mao, Y., Yang, Z., Holland, G., Zhang, J., & Northoff, G. (2014). Altered temporal variance and neural synchronization of spontaneous brain activity in anesthesia. *Human Brain Mapping*, *35*(11), 5368–5378. https://doi.org/10.1002/hbm.22556

Huang, Z., Zhang, J., Wu, J., Qin, P., Wu, X., Wang, Z., Dai, R., Li, Y., Liang, W., Mao, Y., Yang, Z., Zhang, J., Wolff, A., & Northoff, G. (2016). Decoupled temporal variability and signal synchronization of spontaneous brain activity in loss of consciousness: An fMRI study in anesthesia. *NeuroImage*, *124*, 693–703. https://doi.org/10.1016/j.neuroimage.2015.08.062

Hudetz, A. G. (2012). General anesthesia and human brain connectivity. *Brain Connectivity*, *2*(6), 291–302. https://doi.org/10.1089/brain.2012.0107

Husain, A. M. (2006). Electroencephalographic assessment of coma. *Journal of Clinical Neurophysiology*, *23*(3), 208–220. https://doi.org/10.1097/01.wnp.0000220094.60482.b5

Huupponen, E., Maksimow, A., Lapinlampi, P., Särkelä, M., Saastamoinen, A., Snapir, A., Scheinin, H., Scheinin, M., Meriläinen, P., Himanen, S. L., & Jääskeläinen, S. (2008). Electroencephalogram spindle activity during dexmedetomidine sedation and physiological sleep. *Acta Anaesthesiologica Scandinavica*, *52*(2), 289–294. https://doi.org/10.1111/j.1399-6576.2007.01537.x

Jang, H.-S., Jung, J.-Y., Jang, K.-H., & Lee, M.-G. (2010). Effects of isoflurane anesthesia on post-anesthetic sleep-wake architectures in rats. *The Korean Journal of Physiology & Pharmacology*, *14*(5), 291–297. https://doi.org/10.4196/kjpp.2010.14.5.291

Jawaid, M., Mushtaq, A., Mukhtar, S., & Khan, Z. (2007). Preoperative anxiety before elective surgery. *Neurosciences Journal*, *12*(2), 145–148.

Jbabdi, S., Sotiropoulos, S. N., Savio, A. M., Graña, M., & Behrens, T. E. J. (2012). Model-based analysis of multishell diffusion MR data for tractography: How to get over fitting problems. *Magnetic Resonance in Medicine*, *68*(6), 1846–1855. https://doi.org/10.1002/mrm.24204

Jenkinson, M., Bannister, P., Brady, M., & Smith, S. (2002). Improved optimization for the robust and accurate linear registration and motion correction of brain images. *NeuroImage*, *17*(2), 825–841. https://doi.org/10.1006/nimg.2002.1132

Jevtović-Todorović, V., Todorovć, S. M., Mennerick, S., Powell, S., Dikranian, K., Benshoff, N., Zorumski, C. F., & Olney, J. W. (1998). Nitrous oxide (laughing gas) is an NMDA antagonist, neuroprotectant and neurotoxin. *Nature Medicine*, *4*(4), 460–463. https://doi.org/10.1038/nm0498-460

Johansen-Berg, H., Behrens, T. E. J., Sillery, E., Ciccarelli, O., Thompson, A. J., Smith, S. M., & Matthews, P. M. (2005). Functional–anatomical validation and individual variation of diffusion tractography-based segmentation of the human thalamus. *Cerebral Cortex*, *15*(1), 31–39. https://doi.org/10.1093/cercor/bhh105

Jordan, D., Ilg, R., Riedl, V., Schorer, A., Grimberg, S., Neufang, S., Omerovic, A., Berger, S., Untergehrer, G., Preibisch, C., Schulz, E., Schuster, T., Schröter, M., Spoormaker, V., Zimmer, C., Hemmer, B., Wohlschläger, A., Kochs, E. F., & Schneider, G. (2013). Simultaneous electroencephalographic and functional magnetic resonance imaging indicate impaired cortical top–down processing in association with anesthetic-induced unconsciousness. *Anesthesiology*, *119*(5), 1031–1042. https://doi.org/10.1097/ALN.0b013e3182a7ca92

Kaisti, K. K., Långsjö, J. W., Aalto, S., Oikonen, V., Sipilä, H., Teräs, M., Hinkka, S., Metsähonkala, L., & Scheinin, H. (2003). Effects of sevoflurane, propofol, and adjunct nitrous oxide on regional cerebral blood flow, oxygen consumption, and blood volume in humans. *Anesthesiology*, *99*(3), 603–613. https://doi.org/10.1097/00000542-200309000-00015

Kaisti, K. K., Metsähonkala, L., Teräs, M., Oikonen, V., Aalto, S., Jääskeläinen, S., Hinkka, S., & Scheinin, H. (2002). Effects of surgical levels of propofol and

sevoflurane anesthesia on cerebral blood flow in healthy subjects studied with positron emission tomography. *Anesthesiology*, *96*(6), 1358–1370. https://doi.org/10.1097/00000542-200206000-00015

Kaplan, P. W. (2004). The EEG in metabolic encephalopathy and coma. *Journal of Clinical Neurophysiology*, *21*(5), 307–318. https://doi.org/10.1097/01.WNP.0000145004.22230.D5

Karippacheril, J. G., & Ho, T. Y. (2013). Data acquisition from S/5 GE Datex anesthesia monitor using VSCapture: An open source.NET/Mono tool. *Journal of Anaesthesiology, Clinical Pharmacology*, *29*(3), 423–424. https://doi.org/10.4103/0970-9185.117096

Kerssens, C., Hamann, S., Peltier, S., Hu, X. P., Byas-Smith, M. G., & Sebel, P. S. (2005). Attenuated brain response to auditory word stimulation with sevoflurane: A functional magnetic resonance imaging study in humans. *Anesthesiology*, *103*(1), 11–19. https://doi.org/10.1097/00000542-200507000-00006

Kety, S. S., & Schmidt, C. F. (1948). The effects of altered arterial tensions of carbon dioxide and oxygen on cerebral blood flow and cerebral oxygen consumption of normal young men. *Journal of Clinical Investigation*, *27*(4), 484–492. https://doi.org/10.1172/JCI101995

Kiang, T. K. L., Sherwin, C. M. T., Spigarelli, M. G., & Ensom, M. H. H. (2012). Fundamentals of population pharmacokinetic modelling. *Clinical Pharmacokinetics*, *51*(8), 515–525. https://doi.org/10.1007/BF03261928

Koch, C., Massimini, M., Boly, M., & Tononi, G. (2016). Neural correlates of consciousness: Progress and problems. *Nature Reviews Neuroscience*, *17*(5), 307–321. https://doi.org/10.1038/nrn.2016.22

Koenig, J., Jarczok, M. N., Ellis, R. J., Hillecke, T. K., & Thayer, J. F. (2014). Heart rate variability and experimentally induced pain in healthy adults: A systematic review. *European Journal of Pain*, *18*(3), 301–314. https://doi.org/10.1002/j.1532-2149.2013.00379.x

Koenig, T., Neumann, C., Ocker, T., Kramer, S., Spies, C., & Schuster, M. (2011). Estimating the time needed for induction of anaesthesia and its importance in balancing anaesthetists' and surgeons' waiting times around the start of surgery. *Anaesthesia*, *66*(7), 556–562. https://doi.org/10.1111/j.1365-2044.2011.06661.x

Kolbitsch, C., Lorenz, I. H., Hörmann, C., Kremser, C., Schocke, M., Felber, S., Moser, P. L., Hinteregger, M., Pfeiffer, K. P., & Benzer, A. (2001). Sevoflurane and nitrous oxide increase regional cerebral blood flow (rCBF) and regional cerebral blood volume (rCBV) in a drug-specific manner in human volunteers. *Magnetic Resonance Imaging*, *19*(10), 1253–1260. https://doi.org/10.1016/S0730-725X(01)00465-9

Kolbitsch, C., Lorenz, I. H., Hörmann, C., Schocke, M., Kremser, C., Zschiegner, F., Löckinger, A., Pfeiffer, K. P., Felber, S., & Benzer, A. (2000). A subanesthetic concentration of sevoflurane increases regional cerebral blood flow and regional cerebral blood volume and decreases regional mean transit time and regional cerebrovascular resistance in volunteers.

Anesthesia & Analgesia, *91*(1), 156–162. https://doi.org/10.1213/00000539-200007000-00029

Kondo, Y., Hirose, N., Maeda, T., Suzuki, T., Yoshino, A., & Katayama, Y. (2016). Changes in cerebral blood flow and oxygenation during induction of general anesthesia with sevoflurane versus propofol. In C. E. Elwell, T. S. Leung, & D. K. Harrison (Eds.), *Oxygen Transport to Tissue XXXVII* (pp. 479–484). Springer New York. https://doi.org/10.1007/978-1-4939-3023-4_60

Kong, J., Loggia, M. L., Zyloney, C., Tu, P., LaViolette, P., & Gollub, R. L. (2010). Exploring the brain in pain: Activations, deactivations and their relation. *PAIN*, *148*(2), 257–267. https://doi.org/10.1016/j.pain.2009.11.008

Kontos, H. A., Raper, A. J., & Patterson, J. L. (1977). Analysis of vasoactivity of local pH, PCO2 and bicarbonate on pial vessels. *Stroke*, *8*(3), 358–360. https://doi.org/10.1161/01.STR.8.3.358

Kreuer, S., & Wilhelm, W. (2006). The Narcotrend monitor. *Best Practice & Research Clinical Anaesthesiology*, *20*(1), 111–119. https://doi.org/10.1016/j.bpa.2005.08.010

Laird, A. R., Fox, P. M., Eickhoff, S. B., Turner, J. A., Ray, K. L., McKay, D. R., Glahn, D. C., Beckmann, C. F., Smith, S. M., & Fox, P. T. (2011). Behavioral interpretations of intrinsic connectivity networks. *Journal of Cognitive Neuroscience*, *23*(12), 4022–4037. https://doi.org/10.1162/jocn_a_00077

Law, C. J., Jacobson, G. M., Kluger, M., Chaddock, M., Scott, M., & Sleigh, J. W. (2014). Randomized controlled trial of the effect of depth of anaesthesia on

postoperative pain. *British Journal of Anaesthesia*, *112*(4), 675–680. https://doi.org/10.1093/bja/aet419

Le Pera, D., Valeriani, M., Niddam, D., Chen, A. C. N., & Arendt-Nielsen, L. (2002). Contact heat evoked potentials to painful and non-painful stimuli: Effect of attention towards stimulus properties. *Brain Topography*, *15*(2), 115–123. https://doi.org/10.1023/A:1021472524739

Lee, U., Kim, S., Noh, G.-J., Choi, B.-M., Hwang, E., & Mashour, G. A. (2009). The directionality and functional organization of frontoparietal connectivity during consciousness and anesthesia in humans. *Consciousness and Cognition*, *18*(4), 1069–1078. https://doi.org/10.1016/j.concog.2009.04.004

Lee, U., Ku, S., Noh, G., Baek, S., Choi, B., & Mashour, G. A. (2013). Disruption of frontal–parietal communication by ketamine, propofol, and sevoflurane. *Anesthesiology*, *118*(6), 1264–1275. https://doi.org/10.1097/ALN.0b013e31829103f5

Leistritz, L., Jäger, H., Schelenz, C., Witte, H., Putsche, P., Specht, M., & Reinhart, K. (1999). New approaches for the detection and analysis of electroencephalographic burst-suppression patterns in patients under sedation. *Journal of Clinical Monitoring and Computing*, *15*(6), 357–367. https://doi.org/10.1023/A:1009990629797

Leslie, K., Chan, M. T. V., Myles, P. S., Forbes, A., & McCulloch, T. J. (2010). Posttraumatic stress disorder in aware patients from the B-aware trial. *Anesthesia & Analgesia*, *110*(3), 823–828. https://doi.org/10.1213/ANE.0b013e3181b8b6ca

Leslie, K., Myles, P. S., Forbes, A., & Chan, M. T. V. (2010). The effect of Bispectral Index monitoring on long-term survival in the B-aware trial. *Anesthesia & Analgesia*, *110*(3), 816–822. https://doi.org/10.1213/ANE.0b013e3181c3bfb2

Levenson, H. (1973). Multidimensional locus of control in psychiatric patients. *Journal of Consulting and Clinical Psychology*, *41*(3), 397–404. https://doi.org/10.1037/h0035357

Lichtner, G., Auksztulewicz, R., Kirilina, E., Velten, H., Mavrodis, D., Scheel, M., Blankenburg, F., & von Dincklage, F. (2018). Effects of propofol anesthesia on the processing of noxious stimuli in the spinal cord and the brain. *NeuroImage*, *172*, 642–653. https://doi.org/10.1016/j.neuroimage.2018.02.003

Linassi, F., Zanatta, P., Tellaroli, P., Ori, C., & Carron, M. (2018). Isolated forearm technique: A meta-analysis of connected consciousness during different general anaesthesia regimens. *British Journal of Anaesthesia*, *121*(1), 198–209. https://doi.org/10.1016/j.bja.2018.02.019

Lipping, T., Ferenets, R., Mortier, E. P., & Struys, M. M. R. F. (2007). A new method for evaluating the performance of depth-of-hypnosis indices—The D-value. *2007 29th Annual International Conference of the IEEE Engineering in Medicine and Biology Society*, 6487–6490. https://doi.org/10.1109/IEMBS.2007.4353845

Lipping, T., Loula, P., Jäntti, V., & Yli-Hankala, A. (1994). DC-level detection of burst-suppression EEG. *Methods of Information in Medicine*, *33*(1), 35–38. https://doi.org/10.1055/s-0038-1634968

Liu, X., Lauer, K. K., Ward, B. D., Li, S.-J., & Hudetz, A. G. (2013). Differential effects of deep sedation with propofol on the specific and nonspecific thalamocortical systems: A functional magnetic resonance imaging study. *Anesthesiology*, *118*(1), 59–69. https://doi.org/10.1097/ALN.0b013e318277a801

Logothetis, N. K., & Wandell, B. A. (2004). Interpreting the BOLD signal. *Annual Review of Physiology*, *66*(1), 735–769. https://doi.org/10.1146/annurev.physiol.66.082602.092845

Macario, A., Vitez, T. S., Dunn, B., & McDonald, T. (1995). Where are the costs in perioperative care? Analysis of hospital costs and charges for inpatient surgical care. *Anesthesiology*, *83*(6), 1138–1144. https://doi.org/10.1097/00000542-199512000-00002

MacDonald, J. F., Miljkovic, Z., & Pennefather, P. (1987). Use-dependent block of excitatory amino acid currents in cultured neurons by ketamine. *Journal of Neurophysiology*, *58*(2), 251–266. https://doi.org/10.1152/jn.1987.58.2.251

Mäenpää, M., Penttilä, J., Laitio, T., Kaisti, K., Kuusela, T., Hinkka, S., & Scheinin, H. (2007). The effects of surgical levels of sevoflurane and propofol anaesthesia on heart rate variability. *European Journal of Anaesthesiology*, *24*(7), 626–633. https://doi.org/10.1017/S0265021507000129

Makki, M. I., O'Gorman, R. L., Buhler, P., Baledent, O., Kellenberger, C. J., Sabandal, C., Weiss, M., Scheer, I., & Schmitz, A. (2019). Total cerebrovascular blood flow and whole brain perfusion in children sedated using propofol with or without ketamine at induction: An investigation with

2D-Cine PC and ASL. *Journal of Magnetic Resonance Imaging*, *50*(5), 1433–1440. https://doi.org/10.1002/jmri.26725

Mantzaridis, H., & Kenny, G. N. C. (1997). Auditory evoked potential index: A quantitative measure of changes in auditory evoked potentials during general anaesthesia. *Anaesthesia*, *52*(11), 1030–1036. https://doi.org/10.1111/j.1365-2044.1997.185-az0327.x

Mapleson, W. W. (1996). Effect of age on MAC in humans: A meta-analysis. *British Journal of Anaesthesia*, *76*(2), 179–185. https://doi.org/10.1093/bja/76.2.179

Marcar, V. L., Schwarz, U., Martin, E., & Loenneker, T. (2006). How depth of anesthesia influences the Blood Oxygenation Level–Dependent signal from the visual cortex of children. *American Journal of Neuroradiology*, *27*(4), 799–805.

Marsh, B., White, M., Morton, N., & Kenny, G. N. C. (1991). Pharmacokinetic model driven infusion of propofol in children. *BJA: British Journal of Anaesthesia*, *67*(1), 41–48. https://doi.org/10.1093/bja/67.1.41

Martuzzi, R., Ramani, R., Qiu, M., Rajeevan, N., & Constable, R. T. (2010). Functional connectivity and alterations in baseline brain state in humans. *NeuroImage*, *49*(1), 823–834. https://doi.org/10.1016/j.neuroimage.2009.07.028

Mashour, G. A., & Avidan, M. S. (2015). Intraoperative awareness: Controversies and non-controversies. *British Journal of Anaesthesia*, *115*, i20–i26. https://doi.org/10.1093/bja/aev034

Mashour, G. A., & Hudetz, A. G. (2018). Neural correlates of unconsciousness in large-scale brain networks. *Trends in Neurosciences*, *41*(3), 150–160. https://doi.org/10.1016/j.tins.2018.01.003

Mashour, G. A., Kent, C., Picton, P., Ramachandran, S. K., Tremper, K. K., Turner, C. R., Shanks, A., & Avidan, M. S. (2013). Assessment of intraoperative awareness with explicit recall: A comparison of 2 methods. *Anesthesia & Analgesia*, *116*(4), 889–891. https://doi.org/10.1213/ANE.0b013e318281e9ad

Massimini, M., Huber, R., Ferrarelli, F., Hill, S., & Tononi, G. (2004). The sleep slow oscillation as a traveling wave. *Journal of Neuroscience*, *24*(31), 6862–6870. https://doi.org/10.1523/JNEUROSCI.1318-04.2004

Matta, B. F., Heath, K. J., Tipping, K., & Summors, A. C. (1999). Direct cerebral vasodilatory effects of sevoflurane and isoflurane. *Anesthesiology*, *91*(3), 677–677. https://doi.org/10.1097/00000542-199909000-00019

Matta, B. F., Mayberg, T., & Lam, A. (1995). Direct cerebrovasodilatory effects of halothane, isoflurane, and desflurane during propofol-induced isoelectric electroencephalogram in humans. *Anesthesiology*, *83*(5), 980–985. https://doi.org/10.1097/00000542-199511000-00011

Messner, M., Beese, U., Romstöck, J., Dinkel, M., & Tschaikowsky, K. (2003). The Bispectral Index declines during neuromuscular block in fully awake persons. *Anesthesia & Analgesia*, *97*(2), 488–491. https://doi.org/10.1213/01.ANE.0000072741.78244.C0

Mhuircheartaigh, R. N., Rosenorn-Lanng, D., Wise, R., Jbabdi, S., Rogers, R., & Tracey, I. (2010). Cortical and subcortical connectivity changes during

decreasing levels of consciousness in humans: A functional magnetic resonance imaging study using propofol. *The Journal of Neuroscience*, *30*(27), 9095–9102. https://doi.org/10.1523/JNEUROSCI.5516-09.2010

Mhuircheartaigh, R. N., Warnaby, C., Rogers, R., Jbabdi, S., & Tracey, I. (2013). Slow-wave activity saturation and thalamocortical isolation during propofol anesthesia in humans. *Science Translational Medicine*, *5*(208), 208ra148-208ra148. https://doi.org/10.1126/scitranslmed.3006007

Mielck, F., Stephan, H., Weyland, A., & Sonntag, H. (1999). Effects of one minimum alveolar anesthetic concentration sevoflurane on cerebral metabolism, blood flow, and CO_2 reactivity in cardiac patients. *Anesthesia & Analgesia*, *89*(2), 364–369. https://doi.org/10.1213/00000539-199908000-00022

Mirkheshti, A., Vishteh, M., Tajbakhsh, A., Abtahi, D., Falahinejadghajari, R., & Memary, E. (2020). The difference between induction and maintenance dosages of propofol for general anesthesia in patients with and without sleep quality disorder. *Perioperative Care and Operating Room Management*, *21*, 100125. https://doi.org/10.1016/j.pcorm.2020.100125

Moerman, N., van Dam, F. S. A. M., Muller, M. J., & Oosting, H. (1996). The Amsterdam Preoperative Anxiety and Information Scale (APAIS). *Anesthesia & Analgesia*, *82*(3), 445–451.

Monk, T. G., Saini, V., Weldon, B. C., & Sigl, J. C. (2005). Anesthetic management and one-year mortality after noncardiac surgery. *Anesthesia and Analgesia*, *100*(1), 4–10. https://doi.org/10.1213/01.ANE.0000147519.82841.5E

Moote, C. A., & Knill, R. L. (1988). Isoflurane anesthesia causes a transient alteration in nocturnal sleep. *Anesthesiology*, *69*(3), 327–331. https://doi.org/10.1097/00000542-198809000-00007

Mueller, F., Musso, F., London, M., de Boer, P., Zacharias, N., & Winterer, G. (2018). Pharmacological fMRI: Effects of subanesthetic ketamine on resting-state functional connectivity in the default mode network, salience network, dorsal attention network and executive control network. *NeuroImage: Clinical*, *19*, 745–757. https://doi.org/10.1016/j.nicl.2018.05.037

Mullinger, K. J., Castellone, P., & Bowtell, R. (2013). Best current practice for obtaining high quality EEG data during simultaneous fMRI. *Journal of Visualized Experiments*, *76*, 1–10. https://doi.org/10.3791/50283

Murphy, M., Bruno, M. A., Riedner, B. A., Boveroux, P., Noirhomme, Q., Landsness, E. C., Brichant, J. F., Phillips, C., Massimini, M., Laureys, S., Tononi, G., & Boly, M. (2011). Propofol anesthesia and sleep: A high-density EEG study. *Sleep*, *34*(3), 283–291. https://doi.org/10.1093/sleep/34.3.283

Myles, P., Leslie, K., McNeil, J., Forbes, A., & Chan, M. (2004). Bispectral index monitoring to prevent awareness during anaesthesia: The B-Aware randomised controlled trial. *The Lancet*, *363*(9423), 1757–1763. https://doi.org/10.1016/S0140-6736(04)16300-9

Nelson, A. B., Faraguna, U., Tononi, G., & Cirelli, C. (2010). Effects of anesthesia on the response to sleep deprivation. *Sleep*, *33*(12), 1659–1667. https://doi.org/10.1093/sleep.33.12.1659

Neske, G. T. (2016). The slow oscillation in cortical and thalamic networks: Mechanisms and functions. *Frontiers in Neural Circuits*, *9*. https://doi.org/10.3389/fncir.2015.00088

Nickerson, L. D., Smith, S. M., Öngür, D., & Beckmann, C. F. (2017). Using dual regression to investigate network shape and amplitude in functional connectivity analyses. *Frontiers in Neuroscience*, *11*, 115. https://doi.org/10.3389/fnins.2017.00115

O'Gorman, R. L., Poil, S.-S., Brandeis, D., Klaver, P., Bollmann, S., Ghisleni, C., Lüchinger, R., Martin, E., Shankaranarayanan, A., Alsop, D. C., & Michels, L. (2013). Coupling Between Resting Cerebral Perfusion and EEG. *Brain Topography*, *26*(3), 442–457. https://doi.org/10.1007/s10548-012-0265-7

Oostenveld, R., Fries, P., Maris, E., & Schoffelen, J.-M. (2011). FieldTrip: Open source software for advanced analysis of MEG, EEG, and invasive electrophysiological data. *Computational Intelligence and Neuroscience*, *2011*, 1:1-1:9. https://doi.org/10.1155/2011/156869

Osterman, J. E., Hopper, J., Heran, W. J., Keane, T. M., & van der Kolk, B. A. (2001). Awareness under anesthesia and the development of posttraumatic stress disorder. *General Hospital Psychiatry*, *23*(4), 198–204. https://doi.org/10.1016/S0163-8343(01)00142-6

Overdyk, F. J., Harvey, S. C., Fishman, R. L., & Shippey, F. (1998). Successful strategies for improving operating room efficiency at academic institutions. *Anesthesia & Analgesia*, *86*(4), 896–906. https://doi.org/10.1213/00000539-199804000-00039

Pak, D. J., Yong, R. J., Kaye, A. D., & Urman, R. D. (2018). Chronification of Pain: Mechanisms, Current Understanding, and Clinical Implications. *Current Pain and Headache Reports*, *22*(2), 9. https://doi.org/10.1007/s11916-018-0666-8

Palanca, B. J. A., Avidan, M. S., & Mashour, G. A. (2017). Human neural correlates of sevoflurane-induced unconsciousness. *BJA: British Journal of Anaesthesia*, *119*(4), 573–582. https://doi.org/10.1093/bja/aex244

Palanca, B. J. A., Mitra, A., Larson-Prior, L., Snyder, A. Z., Avidan, M. S., & Raichle, M. E. (2015). Resting-state functional magnetic resonance imaging correlates of sevoflurane-induced unconsciousness. *Anesthesiology*, *123*(2), 346–356. https://doi.org/10.1097/ALN.0000000000000731

Pandit, J. J. (2013). Isolated forearm – or isolated brain? Interpreting responses during anaesthesia – or 'dysanaesthesia'. *Anaesthesia*, *68*(10), 995–1000. https://doi.org/10.1111/anae.12361

Pandit, J. J. (2014). Acceptably aware during general anaesthesia: 'Dysanaesthesia' – The uncoupling of perception from sensory inputs. *Consciousness and Cognition*, *27*, 194–212. https://doi.org/10.1016/j.concog.2014.05.007

Pandit, J. J., Andrade, J., Bogod, D. G., Hitchman, J. M., Jonker, W. R., Lucas, N., Mackay, J. H., Nimmo, A. F., O'Connor, K., O'Sullivan, E. P., Paul, R. G., Palmer, J. H. M. G., Plaat, F., Radcliffe, J. J., Sury, M. R. J., Torevell, H. E., Wang, M., Hainsworth, J., Cook, T. M., … Rangasami, J. (2014). 5th National Audit Project (NAP5) on accidental awareness during general anaesthesia: Summary of main findings and risk factors. *BJA: British*

Journal of Anaesthesia, *113*(4), 549–559. https://doi.org/10.1093/bja/aeu313

Pandit, J. J., Russell, I. F., & Wang, M. (2015). Interpretations of responses using the isolated forearm technique in general anaesthesia: A debate. *British Journal of Anaesthesia*, *115*(suppl_1), i32–i45. https://doi.org/10.1093/bja/aev106

Peltier, S. J., Kerssens, C., Hamann, S. B., Sebel, P. S., Byas-Smith, M., & Hu, X. (2005). Functional connectivity changes with concentration of sevoflurane anesthesia. *NeuroReport*, *16*(3), 285–288.

Pick, J., Chen, Y., Moore, J. T., Sun, Y., Wyner, A. J., Friedman, E. B., & Kelz, M. B. (2011). Rapid eye movement sleep debt accrues in mice exposed to volatile anesthetics. *Anesthesiology*, *115*(4), 702–712. https://doi.org/10.1097/ALN.0b013e31822ddd72

Pigorini, A., Sarasso, S., Proserpio, P., Szymanski, C., Arnulfo, G., Casarotto, S., Fecchio, M., Rosanova, M., Mariotti, M., Lo Russo, G., Palva, J. M., Nobili, L., & Massimini, M. (2015). Bistability breaks-off deterministic responses to intracortical stimulation during non-REM sleep. *NeuroImage*, *112*, 105–113. https://doi.org/10.1016/j.neuroimage.2015.02.056

Plourde, G., Belin, P., Chartrand, D., Fiset, P., Backman, S. B., Xie, G., & Zatorre, R. J. (2006). Cortical processing of complex auditory stimuli during alterations of consciousness with the general anesthetic propofol. *Anesthesiology*, *104*(3), 448–457. https://doi.org/10.1097/00000542-200603000-00011

Posse, S., Kemna, L. J., Elghahwagi, B., Wiese, S., & Kiselev, V. G. (2001). Effect of graded hypo- and hypercapnia on fMRI contrast in visual cortex: Quantification of T^*_2 changes by multiecho EPI. *Magnetic Resonance in Medicine*, *46*(2), 264–271. https://doi.org/10.1002/mrm.1187

Price, C. C., Pereira, D. B., Andre, R., Garvan, C. W., Nguyen, P., Herman, M., & Seubert, C. (2015). Prospective pilot investigation: Presurgical depressive symptom severity and anesthesia response in women undergoing surgery for gynecologic mass removal. *International Journal of Behavioral Medicine*, *22*(4), 521–529. https://doi.org/10.1007/s12529-014-9451-1

Purdon, P. L., Pavone, K. J., Akeju, O., Smith, A. C., Sampson, A. L., Lee, J., Zhou, D. W., Solt, K., & Brown, E. N. (2015). The ageing brain: Age-dependent changes in the electroencephalogram during propofol and sevoflurane general anaesthesia. *British Journal of Anaesthesia*, *115*, i46–i57. https://doi.org/10.1093/bja/aev213

Purdon, P. L., Pierce, E. T., Mukamel, E. A., Prerau, M. J., Walsh, J. L., Wong, K. F. K., Salazar-Gomez, A. F., Harrell, P. G., Sampson, A. L., Cimenser, A., Ching, S., Kopell, N. J., Tavares-Stoeckel, C., Habeeb, K., Merhar, R., & Brown, E. N. (2013). Electroencephalogram signatures of loss and recovery of consciousness from propofol. *Proceedings of the National Academy of Sciences*, 1–10. https://doi.org/10.1073/pnas.1221180110

Purdon, P. L., Sampson, A., Pavone, K. J., & Brown, E. N. (2015). Clinical electroencephalography for anesthesiologists part I: Background and basic signatures. *Anesthesiology*, *123*(4), 937–960. https://doi.org/10.1097/ALN.0000000000000841

Qiu, M., Ramani, R., Swetye, M., & Constable, R. T. (2008). Spatial nonuniformity of the resting CBF and BOLD responses to sevoflurane: In vivo study of normal human subjects with magnetic resonance imaging. *Human Brain Mapping*, *29*(12), 1390–1399. https://doi.org/10.1002/hbm.20472

Qiu, M., Scheinost, D., Ramani, R., & Constable, R. T. (2017). Multi-modal analysis of functional connectivity and cerebral blood flow reveals shared and unique effects of propofol in large-scale brain networks. *NeuroImage*, *148*, 130–140. https://doi.org/10.1016/j.neuroimage.2016.12.080

Quasha, A. L., Eger, E. I., & Tinker, J. H. (1980). Determination and applications of MAC. *Anesthesiology*, *53*(4), 315–334. https://doi.org/10.1097/00000542-198010000-00008

Rabiller, G., He, J.-W., Nishijima, Y., Wong, A., & Liu, J. (2015). Perturbation of brain oscillations after ischemic stroke: A potential biomarker for post-stroke function and therapy. *International Journal of Molecular Sciences*, *16*(10), 25605–25640. https://doi.org/10.3390/ijms161025605

Raja, S. N., Carr, D. B., Cohen, M., Finnerup, N. B., Flor, H., Gibson, S., Keefe, F. J., Mogil, J. S., Ringkamp, M., Sluka, K. A., Song, X.-J., Stevens, B., Sullivan, M. D., Tutelman, P. R., Ushida, T., & Vader, K. (2020). The revised International Association for the Study of Pain definition of pain: Concepts, challenges, and compromises. *PAIN*, *161*(9), 1976–1982. https://doi.org/10.1097/j.pain.0000000000001939

Ramani, R., Qiu, M., & Constable, R. T. (2007). Sevoflurane 0.25 MAC preferentially affects higher order association areas: A functional magnetic

resonance imaging study in volunteers. *Anesthesia & Analgesia*, *105*(3), 648–655. https://doi.org/10.1213/01.ane.0000277496.12747.29

Rampil, I. J. (1998). A primer for EEG signal processing in anesthesia. *Anesthesiology*, *89*, 980–1002. https://doi.org/10.1167/8.5.1.

Rampil, I. J., & Laster, M. J. (1992). No correlation between quantitative electroencephalographic measurements and movement response to noxious stimuli during isoflurane anesthesia in rats. *Anesthesiology*, *77*(5), 920–925. https://doi.org/10.1097/00000542-199211000-00014

Ranft, A., Golkowski, D., Kiel, T., Riedl, V., Kohl, P., Rohrer, G., Pientka, J., Berger, S., Thul, A., Maurer, M., Preibisch, C., Zimmer, C., Mashour, G. A., Kochs, E. F., Jordan, D., & Ilg, R. (2016). Neural correlates of sevoflurane-induced unconsciousness identified by simultaneous functional magnetic resonance imaging and electroencephalography. *Anesthesiology*, *125*(5), 861–872. https://doi.org/10.1097/ALN.0000000000001322

Rees, G. J., & Gray, T. C. (1950). Methyl-N-Propyl Ether. *British Journal of Anaesthesia*, *22*(2), 83–91.

Ringli, M., & Huber, R. (2011). Developmental aspects of sleep slow waves: Linking sleep, brain maturation and behavior. *Progress in Brain Research*, *193*, 63–82. https://doi.org/10.1016/B978-0-444-53839-0.00005-3

Rostrup, E., Larsson, H. B., Toft, P. B., Garde, K., & Henriksen, O. (1995). Signal changes in gradient echo images of human brain induced by hypo- and hyperoxia. *NMR in Biomedicine*, *8*(1), 41–47. https://doi.org/10.1002/nbm.1940080109

Rostrup, E., Law, I., Blinkenberg, M., Larsson, H. B., Born, A. P., Holm, S., & Paulson, O. B. (2000). Regional differences in the CBF and BOLD responses to hypercapnia: A combined PET and fMRI study. *NeuroImage*, *11*(2), 87–97. https://doi.org/10.1006/nimg.1999.0526

Sanchez-Vives, M. V., & McCormick, D. A. (2000). Cellular and network mechanisms of rhythmic recurrent activity in neocortex. *Nature Neuroscience*, *3*(10), 1027–1034. https://doi.org/10.1038/79848

Sanders, R. D., Tononi, G., Laureys, S., & Sleigh, J. W. (2012). Unresponsiveness ≠ unconsciousness. *Anesthesiology: The Journal of the American Society of Anesthesiologists*, *116*(4), 946–959. https://doi.org/10.1097/ALN.0b013e318249d0a7

Särkelä, M., Mustola, S., Seppänen, T., Koskinen, M., Lepola, P., Suominen, K., Juvonen, T., Tolvanen-Laakso, H., & Jäntti, V. (2002). Automatic analysis and monitoring of burst suppression in anesthesia. *Journal of Clinical Monitoring and Computing*, *17*(2), 125–134. https://doi.org/10.1023/A:1016393904439

Saxena, N., Gili, T., Diukova, A., Huckle, D., Hall, J. E., & Wise, R. G. (2019). Mild propofol sedation reduces frontal lobe and thalamic cerebral blood flow: An arterial spin labeling study. *Frontiers in Physiology*, *10*, 1541. https://doi.org/10.3389/fphys.2019.01541

Schneider, G., Hollweck, R., Ningler, M., Stockmanns, G., & Kochs, E. F. (2005). Detection of consciousness by electroencephalogram and auditory evoked potentials. *Anesthesiology*, *103*(5), 934–943. https://doi.org/10.1097/00000542-200511000-00006

Schneider, T. W., Minto, C. F., Gambus, P. L., Andresen, C., Goodale, D. B., Shafer, S. L., & Youngs, E. J. (1998). The influence of method of administration and covariates on the pharmacokinetics of propofol in adult volunteers. *Anesthesiology*, *88*(5), 1170–1182. https://doi.org/10.1097/00000542-199805000-00006

Schuller, P. J., Newell, S., Strickland, P. A., & Barry, J. J. (2015). Response of Bispectral Index to neuromuscular block in awake volunteers. *BJA: British Journal of Anaesthesia*, *115*(suppl_1), i95–i103. https://doi.org/10.1093/bja/aev072

Schuster, M., Kotjan, T., Fiege, M., & Goetz, A. E. (2008). Influence of resident training on anaesthesia induction times. *BJA: British Journal of Anaesthesia*, *101*(5), 640–647. https://doi.org/10.1093/bja/aen239

Schwender, D., Conzen, P., Klasing, S., Finsterer, U., Poppel, E., & Peter, K. (1995). The effects of anesthesia with increasing end-expiratory concentrations of sevoflurane on midlatency auditory evoked potentials. *Anesthesia & Analgesia*, *81*(4), 817–822.

Sessler, D. I., Sigl, J. C., Kelley, S. D., Chamoun, N. G., Manberg, P. J., Saager, L., Kurz, A., & Greenwald, S. (2012). Hospital stay and mortality are increased in patients having a “triple low” of low blood pressure, low bispectral index, and low minimum alveolar concentration of volatile anesthesia. *Anesthesiology*, *116*(6), 1195–1203. https://doi.org/10.1097/ALN.0b013e31825683dc

Seth, A. (2010). The grand challenge of consciousness. *Frontiers in Psychology*, *1*, 5. https://doi.org/10.3389/fpsyg.2010.00005

Shanker, A., Abel, J. H., Schamberg, G., & Brown, E. N. (2021). Etiology of burst suppression EEG patterns. *Frontiers in Psychology*, *12*, 2207. https://doi.org/10.3389/fpsyg.2021.673529

Shepherd, J., Jones, J., Frampton, G. K., Bryant, J., Baxter, L., & Cooper, K. (2013). Clinical effectiveness and cost-effectiveness of depth of anaesthesia monitoring (E-Entropy, Bispectral Index and Narcotrend): A systematic review and economic evaluation. *Health Technology Assessment*, *17*(34), 1–264. https://doi.org/10.3310/hta17340

Sicard, K. M., & Duong, T. Q. (2005). Effects of hypoxia, hyperoxia, and hypercapnia on baseline and stimulus-evoked BOLD, CBF, and $CMRO_2$ in spontaneously breathing animals. *NeuroImage*, *25*(3), 850–858. https://doi.org/10.1016/j.neuroimage.2004.12.010

Sicard, K., Shen, Q., Brevard, M. E., Sullivan, R., Ferris, C. F., King, J. A., & Duong, T. Q. (2003). Regional cerebral blood flow and BOLD responses in conscious and anesthetized rats under basal and hypercapnic conditions: Implications for functional MRI studies. *Journal of Cerebral Blood Flow & Metabolism*, *23*(4), 472–481. https://doi.org/10.1097/01.WCB.0000054755.93668.20

Siero, J. C. W., Strother, M. K., Faraco, C. C., Hoogduin, H., Hendrikse, J., & Donahue, M. J. (2015). In vivo quantification of hyperoxic arterial blood water T1. *NMR in Biomedicine*, *28*(11), 1518–1525. https://doi.org/10.1002/nbm.3411

Sigtermans, M., Dahan, A., Mooren, R., Bauer, M., Kest, B., Sarton, E., & Olofsen, E. (2009). S(+)-ketamine effect on experimental pain and cardiac output: A

population pharmacokinetic-pharmacodynamic modeling study in healthy volunteers. *Anesthesiology*, *111*(4), 892–903. https://doi.org/10.1097/ALN.0b013e3181b437b1

Sleigh, J. W., Pullon, R. M., Vlisides, P. E., & Warnaby, C. E. (2019). Electroencephalographic slow wave dynamics and loss of behavioural responsiveness induced by ketamine in human volunteers. *British Journal of Anaesthesia*, *123*(5), 592–600. https://doi.org/10.1016/j.bja.2019.07.021

Sleigh, J. W., Scheib, C. M., & Sanders, R. D. (2011). General anaesthesia and electroencephalographic spindles. *Trends in Anaesthesia and Critical Care*, *1*(5), 263–269. https://doi.org/10.1016/j.tacc.2011.10.001

Sleigh, J. W., Warnaby, C., & Tracey, I. (2018). General anaesthesia as fragmentation of selfhood: Insights from electroencephalography and neuroimaging. *British Journal of Anaesthesia*, *121*(1), 233–240. https://doi.org/10.1016/j.bja.2017.12.038

Smith, S. M. (2002). Fast robust automated brain extraction. *Human Brain Mapping*, *17*(3), 143–155. https://doi.org/10.1002/hbm.10062

Spielberger, C., Gorsuch, R., Lushene, R., Vagg, P., & Jacobs, G. (1983). *Manual for the State-Trait Anxiety Inventory*. Consulting Psychologists Press.

Steriade, M., Nuiiez, A., & Amzica, F. (1993). Intracellular analysis of relations between the slow (<1 Hz) neocortical oscillation and other sleep rhythms of the electroencephalogram. *The Journal of Neuroscience*, *13*(8), 3266–3283. https://doi.org/10.1523/JNEUROSCI.13-08-03266.1993

Steriade, M., Nuñez, A., & Amzica, F. (1993). A novel slow (< 1 Hz) oscillation of neocortical neurons in vivo: Depolarizing and hyperpolarizing components. *The Journal of Neuroscience*, *13*(8), 3252–3265. https://doi.org/3252-3265

Sutter, R., & Kaplan, P. (2012). Electroencephalographic patterns in coma: When things slow down. *Epileptologie*, *29*, 201–209.

Tancredi, F. B., & Hoge, R. D. (2013). Comparison of cerebral vascular reactivity measures obtained using breath-holding and CO_2 inhalation. *Journal of Cerebral Blood Flow & Metabolism*, *33*(7), 1066–1074. https://doi.org/10.1038/jcbfm.2013.48

Tasbihgou, S. R., Vogels, M. F., & Absalom, A. R. (2018). Accidental awareness during general anaesthesia – a narrative review. *Anaesthesia*, *73*(1), 112–122. https://doi.org/10.1111/anae.14124

Tellegen, A., & Atkinson, G. (1974). Openness to absorbing and self-altering experiences ('absorption'), a trait related to hypnotic susceptibility. *Journal of Abnormal Psychology*, *83*(3), 268–277. https://doi.org/10.1037/h0036681

Thornton, C., & Sharpe, R. M. (1998). Evoked responses in anaesthesia. *British Journal of Anaesthesia*, *81*, 771–781. https://doi.org/10.1093/bja/81.5.771

Timofeev, I., Grenier, F., Bazhenov, M., Sejnowski, T. J., & Steriade, M. (2000). Origin of slow cortical oscillations in deafferented cortical slabs. *Cerebral Cortex*, *10*(12), 1185–1199. https://doi.org/10.1093/cercor/10.12.1185

Tomi, K., Mashimo, T., Tashiro, C., Yagi, M., Pak, M., Nishimura, S., Nishimura, M., & Yoshiya, I. (1993). Alterations in pain threshold and psychomotor response associated with subanaesthetic concentrations of inhalation

anaesthetics in humans. *BJA: British Journal of Anaesthesia*, *70*(6), 684–686. https://doi.org/10.1093/bja/70.6.684

Tononi, G. (2004). An information integration theory of consciousness. *BMC Neuroscience*, *5*(1), 42. https://doi.org/10.1186/1471-2202-5-42

Tononi, G. (2012). The integrated information theory of consciousness: An updated account. *Archives Italiennes de Biologie*, *150*(2/3), 56–90. https://doi.org/10.4449/aib.v149i5.1388

Tononi, G., Boly, M., Massimini, M., & Koch, C. (2016). Integrated information theory: From consciousness to its physical substrate. *Nature Reviews Neuroscience*, *17*(7), 450–461. https://doi.org/10.1038/nrn.2016.44

Toscano, A., Pancaro, C., Giovannoni, S., Minelli, G., Baldi, C., Guerrieri, G., Crowhurst, J. A., & Peduto, V. A. (2003). Sevoflurane analgesia in obstetrics: A pilot study. *International Journal of Obstetric Anesthesia*, *12*(2), 79–82. https://doi.org/10.1016/S0959-289X(02)00195-4

Tracey, I., & Mantyh, P. W. (2007). The cerebral signature for pain perception and its modulation. *Neuron*, *55*(3), 377–391. https://doi.org/10.1016/j.neuron.2007.07.012

Tung, A., Bergmann, B. M., Herrera, S., Cao, D., & Mendelson, W. B. (2004). Recovery from sleep deprivation occurs during propofol anesthesia. *Anesthesiology*, *100*(6), 1419–1426. https://doi.org/10.1097/00000542-200406000-00014

Tüshaus, L., Omlin, X., Tuura, R. O., Federspiel, A., Luechinger, R., Staempfli, P., Koenig, T., & Achermann, P. (2017). In human non-REM sleep, more slow-

wave activity leads to less blood flow in the prefrontal cortex. *Scientific Reports*, *7*. https://doi.org/10.1038/s41598-017-12890-7

Uddin, L. Q., Yeo, B. T. T., & Spreng, R. N. (2019). Towards a universal taxonomy of macro-scale functional human brain networks. *Brain Topography*, *32*(6), 926–942. https://doi.org/10.1007/s10548-019-00744-6

Untergehrer, G., Jordan, D., Eyl, S., & Schneider, G. (2013). Effects of propofol, sevoflurane, remifentanil, and (S)-ketamine in subanesthetic concentrations on visceral and somatosensory pain-evoked potentials. *Anesthesiology*, *118*(2), 308–317. https://doi.org/10.1097/ALN.0b013e318279fb21

Valeriani, M., Le Pera, D., Niddam, D., Chen, A. C. N., & Arendt-Nielsen, L. (2002). Dipolar modelling of the scalp evoked potentials to painful contact heat stimulation of the human skin. *Neuroscience Letters*, *318*(1), 44–48. https://doi.org/10.1016/S0304-3940(01)02466-1

van Alst, T. M., Wachsmuth, L., Datunashvili, M., Albers, F., Just, N., Budde, T., & Faber, C. (2019). Anesthesia differentially modulates neuronal and vascular contributions to the BOLD signal. *NeuroImage*, *195*, 89–103. https://doi.org/10.1016/j.neuroimage.2019.03.057

Velly, L. J., Rey, M. F., Bruder, N. J., Gouvitsos, F. A., Witjas, T., Regis, J. M., Peragut, J. C., & Gouin, F. M. (2007). Differential dynamic of action on cortical and subcortical structures of anesthetic agents during induction of anesthesia. *Anesthesiology*, *107*(2), 202–212. https://doi.org/10.1097/01.anes.0000270734.99298.b4

Venkatraghavan, L., Poublanc, J., Bharadwaj, S., Sobczyk, O., Crawley, A. P., Mandell, D. M., Mikulis, D. J., & Fisher, J. A. (2016). Noninvasive

measurement of cerebral blood flow under anesthesia using arterial spin labeling MRI: A pilot study. *Journal of Neurosurgical Anesthesiology*, *28*(4), 331. https://doi.org/10.1097/ANA.0000000000000231

Voss, L., & Sleigh, J. W. (2007). Monitoring consciousness: The current status of EEG-based depth of anaesthesia monitors. *Best Practice & Research Clinical Anaesthesiology*, *21*(3), 313–325. https://doi.org/10.1016/j.bpa.2007.04.003

Wallston, K. A., Strudler Wallston, B., & DeVellis, R. (1978). Development of the Multidimensional Health Locus of Control (MHLC) scales. *Health Education Monographs*, *6*(1), 160–170. https://doi.org/10.1177/109019817800600107

Wang, M., Messina, A. G., & Russell, I. F. (2012). The topography of awareness: A classification of intra-operative cognitive states. *Anaesthesia*, *67*(11), 1197–1201. https://doi.org/10.1111/anae.12041

Wang, S., Li, Y., Qiu, S., Zhang, C., Wang, G., Xian, J., Li, T., & He, H. (2020). Reorganization of rich-clubs in functional brain networks during propofol-induced unconsciousness and natural sleep. *NeuroImage: Clinical*, *25*, 102188. https://doi.org/10.1016/j.nicl.2020.102188

Wang, Y., & Agarwal, R. (2007). Automatic detection of burst suppression. *2007 29th Annual International Conference of the IEEE Engineering in Medicine and Biology Society*, 553–556. https://doi.org/10.1109/IEMBS.2007.4352350

Warnaby, C. E., Seretny, M., Mhuircheartaigh, R. N., Rogers, R., Jbabdi, S., Sleigh, J. W., & Tracey, I. (2016). Anesthesia-induced suppression of human dorsal anterior insula responsivity at loss of volitional behavioral

response. *Anesthesiology*, *124*(4), 766–778. https://doi.org/10.1097/ALN.0000000000001027

Warnaby, C. E., Sleigh, J. W., Hight, D., Jbabdi, S., & Tracey, I. (2017). Investigation of slow-wave activity saturation during surgical anesthesia reveals a signature of neural inertia in humans. *Anesthesiology*, *127*(4), 645–657. https://doi.org/10.1097/ALN.0000000000001759

Watson, N. A., Beards, S. C., Altaf, N., Kassner, A., & Jackson, A. (2000). The effect of hyperoxia on cerebral blood flow: A study in healthy volunteers using magnetic resonance phase-contrast angiography. *European Journal of Anaesthesiology*, *17*(3), 152–159. https://doi.org/10.1046/j.1365-2346.2000.00640.x

White, N. S., & Alkire, M. T. (2003). Impaired thalamocortical connectivity in humans during general-anesthetic-induced unconsciousness. *NeuroImage*, *19*(2), 402–411. https://doi.org/10.1016/S1053-8119(03)00103-4

Whittaker, J. R., Driver, I. D., Bright, M. G., & Murphy, K. (2016). The absolute CBF response to activation is preserved during elevated perfusion: Implications for neurovascular coupling measures. *NeuroImage*, *125*, 198–207. https://doi.org/10.1016/j.neuroimage.2015.10.023

Wiczling, P., Bienert, A., Sobczyński, P., Hartmann-Sobczyńska, R., Bieda, K., Marcinkowska, A., Malatyńska, M., Kaliszan, R., & Grześkowiak, E. (2012). Pharmacokinetics and pharmacodynamics of propofol in patients undergoing abdominal aortic surgery. *Pharmacological Reports*, *64*(1), 113–122. https://doi.org/10.1016/s1734-1140(12)70737-5

Woolf, C. J., & Chong, M.-S. (1993). Preemptive Analgesia—Treating Postoperative Pain by Preventing the Establishment of Central Sensitization. *Anesthesia & Analgesia*, *77*(2), 362–379.

Woolrich, M. W., Behrens, T. E. J., Beckmann, C. F., Jenkinson, M., & Smith, S. M. (2004). Multilevel linear modelling for FMRI group analysis using Bayesian inference. *NeuroImage*, *21*(4), 1732–1747. https://doi.org/10.1016/j.neuroimage.2003.12.023

Woolrich, M. W., Jbabdi, S., Patenaude, B., Chappell, M., Makni, S., Behrens, T., Beckmann, C., Jenkinson, M., & Smith, S. M. (2009). Bayesian analysis of neuroimaging data in FSL. *NeuroImage*, *45*, S173–S186. https://doi.org/10.1016/j.neuroimage.2008.10.055

Woolrich, M. W., Ripley, B. D., Brady, M., & Smith, S. M. (2001). Temporal autocorrelation in univariate linear modeling of FMRI data. *NeuroImage*, *14*(6), 1370–1386. https://doi.org/10.1006/nimg.2001.0931

Worsley, K. J., & Friston, K. J. (1995). Analysis of fMRI time-series revisited—Again. *NeuroImage*, *2*(3), 173–181. https://doi.org/10.1006/nimg.1995.1023

Yamamoto, A. K., Magerkurth, J., Mancini, L., White, M. J., Miserocchi, A., McEvoy, A. W., Appleby, I., Micallef, C., Thornton, J. S., Price, C. J., Weiskopf, N., & Yousry, T. A. (2019). Acquisition of sensorimotor fMRI under general anaesthesia: Assessment of feasibility, the BOLD response and clinical utility. *NeuroImage: Clinical*, *23*, 101923. https://doi.org/10.1016/j.nicl.2019.101923

Yeo, S. T., Holdcroft, A., Yentis, S. M., Stewart, A., & Bassett, P. (2007). Analgesia with sevoflurane during labour: II. Sevoflurane compared with

Entonox for labour analgesia. *British Journal of Anaesthesia*, *98*(1), 110–115. https://doi.org/10.1093/bja/ael327

Zand, F., Hadavi, S. M. R., Chohedri, A., & Sabetian, P. (2014). Survey on the adequacy of depth of anaesthesia with bispectral index and isolated forearm technique in elective Caesarean section under general anaesthesia with sevoflurane†. *BJA: British Journal of Anaesthesia*, *112*(5), 871–878. https://doi.org/10.1093/bja/aet483

Zhang, X., Petersen, E. T., Ghariq, E., Vis, J. B. D., Webb, A. G., Teeuwisse, W. M., Hendrikse, J., & Osch, M. J. P. van. (2013). In vivo blood T1 measurements at 1.5 T, 3 T, and 7 T. *Magnetic Resonance in Medicine*, *70*(4), 1082–1086. https://doi.org/10.1002/mrm.24550

Zhou, Y., Rodgers, Z. B., & Kuo, A. H. (2015). Cerebrovascular reactivity measured with arterial spin labeling and Blood Oxygen Level Dependent techniques. *Magnetic Resonance Imaging*, *33*(5), 566–576. https://doi.org/10.1016/j.mri.2015.02.018